THE EUROPEAN
PHYSICAL JOURNAL C

Regular Article - Experimental Physics

Measurement of high-Q^2 neutral current deep inelastic $e^- p$ scattering cross sections with a longitudinally polarised electron beam at HERA

The ZEUS Collaboration

S. Chekanov[1], M. Derrick[1], S. Magill[1], B. Musgrave[1], D. Nicholass[1,b], J. Repond[1], R. Yoshida[1], M.C.K. Mattingly[2], P. Antonioli[3], G. Bari[3], L. Bellagamba[3], D. Boscherini[3], A. Bruni[3], G. Bruni[3], F. Cindolo[3], M. Corradi[3], G. Iacobucci[3], A. Margotti[3], R. Nania[3], A. Polini[3], S. Antonelli[4], M. Basile[4], M. Bindi[4], L. Cifarelli[4], A. Contin[4], S. De Pasquale[4,c], G. Sartorelli[4], A. Zichichi[4], D. Bartsch[5], I. Brock[5], H. Hartmann[5], E. Hilger[5], H.P. Jakob[5], M. Jüngst[5], A.E. Nuncio-Quiroz[5], E. Paul[5], U. Samson[5], V. Schönberg[5], R. Shehzadi[5], M. Wlasenko[5], N.H. Brook[6], G.P. Heath[6], J.D. Morris[6], M. Kaur[7], P. Kaur[7,d], I. Singh[7,d], M. Capua[8], S. Fazio[8], A. Mastroberardino[8], M. Schioppa[8], G. Susinno[8], E. Tassi[8], J.Y. Kim[9], Z.A. Ibrahim[10], F. Mohamad Idris[10], B. Kamaluddin[10], W.A.T. Wan Abdullah[10], Y. Ning[11], Z. Ren[11], F. Sciulli[11], J. Chwastowski[12], A. Eskreys[12], J. Figiel[12], A. Galas[12], K. Olkiewicz[12], B. Pawlik[12], P. Stopa[12], L. Zawiejski[12], L. Adamczyk[13], T. Bołd[13], I. Grabowska-Bołd[13], D. Kisielewska[13], J. Łukasik[13,e], M. Przybycień[13], L. Suszycki[13], A. Kotański[14,f], W. Słomiński[14,g], O. Behnke[15], U. Behrens[15], C. Blohm[15], A. Bonato[15], K. Borras[15], D. Bot[15], R. Ciesielski[15], N. Coppola[15], S. Fang[15], J. Fourletova[15,h], A. Geiser[15], P. Göttlicher[15,i], J. Grebenyuk[15], I. Gregor[15], T. Haas[15,a], W. Hain[15], A. Hüttmann[15], F. Januschek[15], B. Kahle[15], I.I. Katkov[15,j], U. Klein[15,k], U. Kötz[15], H. Kowalski[15], M. Lisovyi[15], E. Lobodzinska[15], B. Löhr[15], R. Mankel[15,l], I.-A. Melzer-Pellmann[15], S. Miglioranzi[15,m], A. Montanari[15], T. Namsoo[15], D. Notz[15,l], A. Parenti[15], L. Rinaldi[15,n], P. Roloff[15], I. Rubinsky[15], U. Schneekloth[15], A. Spiridonov[15,o], D. Szuba[15,p], J. Szuba[15,q], T. Theedt[15], J. Ukleja[15,r], G. Wolf[15], K. Wrona[15], A.G. Yagües Molina[15], C. Youngman[15], W. Zeuner[15,l], V. Drugakov[16], W. Lohmann[16], S. Schlenstedt[16], G. Barbagli[17], E. Gallo[17], P.G. Pelfer[18], A. Bamberger[19], D. Dobur[19], F. Karstens[19], N.N. Vlasov[19,s], P.J. Bussey[20,t], A.T. Doyle[20], W. Dunne[20], M. Forrest[20], M. Rosin[20], D.H. Saxon[20], I.O. Skillicorn[20], I. Gialas[21,u], K. Papageorgiu[21], U. Holm[22], R. Klanner[22], E. Lohrmann[22], H. Perrey[22], P. Schleper[22], T. Schörner-Sadenius[22], J. Sztuk[22], H. Stadie[22], M. Turcato[22], C. Foudas[23], C. Fry[23], K.R. Long[23], A.D. Tapper[23], T. Matsumoto[24], K. Nagano[24], K. Tokushuku[24,v], S. Yamada[24], Y. Yamazaki[24,w], A.N. Barakbaev[25], E.G. Boos[25], N.S. Pokrovskiy[25], B.O. Zhautykov[25], V. Aushev[26,x], O. Bachynska[26], M. Borodin[26], I. Kadenko[26], A. Kozulia[26], V. Libov[26], D. Lontkovskyi[26], I. Makarenko[26], Iu. Sorokin[26], A. Verbytskyi[26], O. Volynets[26], D. Son[27], J. de Favereau[28], K. Piotrzkowski[28], F. Barreiro[29], C. Glasman[29], M. Jimenez[29], L. Labarga[29], J. del Peso[29], E. Ron[29], M. Soares[29], J. Terrón[29], C. Uribe-Estrada[29], M. Zambrana[29], F. Corriveau[30], C. Liu[30], J. Schwartz[30], R. Walsh[30], C. Zhou[30], T. Tsurugai[31], A. Antonov[32], B.A. Dolgoshein[32], D. Gladkov[32], V. Sosnovtsev[32], A. Stifutkin[32], S. Suchkov[32], R.K. Dementiev[33], P.F. Ermolov[33,an], L.K. Gladilin[33], Yu.A. Golubkov[33], L.A. Khein[33], I.A. Korzhavina[33], V.A. Kuzmin[33], B.B. Levchenko[33,y], O.Yu. Lukina[33], A.S. Proskuryakov[33], L.M. Shcheglova[33], D.S. Zotkin[33], I. Abt[34], A. Caldwell[34], D. Kollar[34], B. Reisert[34], W.B. Schmidke[34], G. Grigorescu[35], A. Keramidas[35], E. Koffeman[35], P. Kooijman[35], A. Pellegrino[35], H. Tiecke[35], M. Vázquez[35,m], L. Wiggers[35], N. Brümmer[36], B. Bylsma[36], L.S. Durkin[36], A. Lee[36], T.Y. Ling[36], P.D. Allfrey[37], M.A. Bell[37], A.M. Cooper-Sarkar[37], R.C.E. Devenish[37], J. Ferrando[37], B. Foster[37], C. Gwenlan[37,z], K. Horton[37,aa], K. Oliver[37], A. Robertson[37], R. Walczak[37], A. Bertolin[38], F. Dal Corso[38], S. Dusini[38], A. Longhin[38], L. Stanco[38], P. Bellan[39], R. Brugnera[39], R. Carlin[39], A. Garfagnini[39], S. Limentani[39], B.Y. Oh[40], A. Raval[40], J.J. Whitmore[40,ab], Y. Iga[41], G. D'Agostini[42], G. Marini[42], A. Nigro[42], J.E. Cole[43,ac], J.C. Hart[43], H. Abramowicz[44,ad], R. Ingbir[44], S. Kananov[44], A. Levy[44], A. Stern[44], M. Kuze[45], J. Maeda[45], R. Hori[46], S. Kagawa[46,ae], N. Okazaki[46], S. Shimizu[46], T. Tawara[46], R. Hamatsu[47], H. Kaji[47,af], S. Kitamura[47,ag], O. Ota[47,ah], Y.D. Ri[47], M. Costa[48], M.I. Ferrero[48], V. Monaco[48], R. Sacchi[48], V. Sola[48], A. Solano[48], M. Arneodo[49], M. Ruspa[49], S. Fourletov[50,h], J.F. Martin[50], T.P. Stewart[50], S.K. Boutle[51,u], J.M. Butterworth[51], T.W. Jones[51], J.H. Loizides[51], M. Wing[51,ai], B. Brzozowska[52], J. Ciborowski[52,aj], G. Grzelak[52], P. Kulinski[52], P. Łużniak[52,ak], J. Malka[52,ak], R.J. Nowak[52], J.M. Pawlak[52], W. Perlanski[52,ak], T. Tymieniecka[52,al], A.F. Żarnecki[52], M. Adamus[53], P. Plucinski[53,am], A. Ukleja[53], Y. Eisenberg[54],

D. Hochman[54]**, U. Karshon**[54]**, E. Brownson**[55]**, D.D. Reeder**[55]**, A.A. Savin**[55]**, W.H. Smith**[55]**, H. Wolfe**[55]**, S. Bhadra**[56]**, C.D. Catterall**[56]**, Y. Cui**[56]**, G. Hartner**[56]**, S. Menary**[56]**, U. Noor**[56]**, J. Standage**[56]**, J. Whyte**[56]

[1]Argonne National Laboratory, Argonne, IL 60439-4815, USA[bb]
[2]Andrews University, Berrien Springs, MI 49104-0380, USA
[3]INFN Bologna, Bologna, Italy[as]
[4]University and INFN Bologna, Bologna, Italy[as]
[5]Physikalisches Institut der Universität Bonn, Bonn, Germany[ap]
[6]H.H. Wills Physics Laboratory, University of Bristol, Bristol, UK[ba]
[7]Department of Physics, Panjab University, Chandigarh, India
[8]Physics Department and INFN, Calabria University, Cosenza, Italy[as]
[9]Chonnam National University, Kwangju, South Korea
[10]Jabatan Fizik, Universiti Malaya, 50603 Kuala Lumpur, Malaysia[bf]
[11]Nevis Laboratories, Columbia University, Irvington on Hudson, NY 10027, USA[bc]
[12]The Henryk Niewodniczanski Institute of Nuclear Physics, Polish Academy of Sciences, Cracow, Poland[aw]
[13]Faculty of Physics and Applied Computer Science, AGH-University of Science and Technology, Cracow, Poland[bd]
[14]Department of Physics, Jagellonian University, Cracow, Poland
[15]Deutsches Elektronen-Synchrotron DESY, Hamburg, Germany
[16]Deutsches Elektronen-Synchrotron DESY, Zeuthen, Germany
[17]INFN Florence, Florence, Italy[as]
[18]University and INFN Florence, Florence, Italy[as]
[19]Fakultät für Physik, Universität Freiburg i.Br., Freiburg i.Br., Germany[ap]
[20]Department of Physics and Astronomy, University of Glasgow, Glasgow, UK[ba]
[21]Department of Engineering in Management and Finance, University of Aegean, Chios, Greece
[22]Institute of Experimental Physics, Hamburg University, Hamburg, Germany[ap]
[23]High Energy Nuclear Physics Group, Imperial College London, London, UK[ba]
[24]Institute of Particle and Nuclear Studies, KEK, Tsukuba, Japan[at]
[25]Institute of Physics and Technology of Ministry of Education and Science of Kazakhstan, Almaty, Kazakhstan
[26]Institute for Nuclear Research, National Academy of Sciences, Kiev and Kiev National University, Kiev, Ukraine
[27]Center for High Energy Physics, Kyungpook National University, Daegu, South Korea[au]
[28]Institut de Physique Nucléaire, Université Catholique de Louvain, Louvain-la-Neuve, Belgium[be]
[29]Departamento de Física Teórica, Universidad Autónoma de Madrid, Madrid, Spain[az]
[30]Department of Physics, McGill University, Montréal, Québec H3A 2T8, Canada[ao]
[31]Faculty of General Education, Meiji Gakuin University, Yokohama, Japan[at]
[32]Moscow Engineering Physics Institute, Moscow, Russia[ax]
[33]Institute of Nuclear Physics, Moscow State University, Moscow, Russia[ay]
[34]Max-Planck-Institut für Physik, München, Germany
[35]NIKHEF and University of Amsterdam, Amsterdam, Netherlands[av]
[36]Physics Department, Ohio State University, Columbus, OH 43210, USA[bb]
[37]Department of Physics, University of Oxford, Oxford, UK[ba]
[38]INFN Padova, Padova, Italy[as]
[39]Dipartimento di Fisica, Università and INFN, Padova, Italy[as]
[40]Department of Physics, Pennsylvania State University, University Park, PA 16802, USA[bc]
[41]Polytechnic University, Sagamihara, Japan[at]
[42]Dipartimento di Fisica, Università 'La Sapienza' and INFN, Rome, Italy[as]
[43]Rutherford Appleton Laboratory, Chilton, Didcot, Oxon, UK[ba]
[44]Raymond and Beverly Sackler Faculty of Exact Sciences, School of Physics, Tel Aviv University, Tel Aviv, Israel[ar]
[45]Department of Physics, Tokyo Institute of Technology, Tokyo, Japan[at]
[46]Department of Physics, University of Tokyo, Tokyo, Japan[at]
[47]Department of Physics, Tokyo Metropolitan University, Tokyo, Japan[at]
[48]Università di Torino and INFN, Torino, Italy[as]
[49]Università del Piemonte Orientale, Novara, and INFN, Torino, Italy[as]
[50]Department of Physics, University of Toronto, Toronto, Ontario M5S 1A7, Canada[ao]
[51]Physics and Astronomy Department, University College London, London, UK[ba]
[52]Institute of Experimental Physics, Warsaw University, Warsaw, Poland
[53]Institute for Nuclear Studies, Warsaw, Poland
[54]Department of Particle Physics, Weizmann Institute, Rehovot, Israel[aq]
[55]Department of Physics, University of Wisconsin, Madison, WI 53706, USA[bb]
[56]Department of Physics, York University, Ontario M3J 1P3, Canada[ao]

Eur. Phys. J. C (2009) 62: 625–658

627

Abstract Measurements of the neutral current cross sections for deep inelastic scattering in $e^- p$ collisions at HERA with a longitudinally polarised electron beam are presented. The single-differential cross-sections $d\sigma/dQ^2$, $d\sigma/dx$ and $d\sigma/dy$ and the double-differential cross sections in Q^2 and x are measured in the kinematic region $y < 0.9$ and $Q^2 > 185\,\text{GeV}^2$ for both positively and negatively polarised electron beams and for each polarisation state separately.

The measurements are based on an integrated luminosity of $169.9\,\text{pb}^{-1}$ taken with the ZEUS detector in 2005 and 2006 at a centre-of-mass energy of 318 GeV. The structure functions $x\tilde{F}_3$ and $xF_3^{\gamma Z}$ are determined by combining the $e^- p$ results presented in this paper with previously measured $e^+ p$ neutral current data. The asymmetry parameter A^- is used to demonstrate the parity violating effects of electroweak interactions at large spacelike photon virtuality. The measurements agree well with the predictions of the Standard Model.

[a] e-mail: tobias.haas@desy.de

[b] Also affiliated with University College London, UK.

[c] Now at University of Salerno, Italy.

[d] Also working at Max Planck Institute, Munich, Germany.

[e] Now at Institute of Aviation, Warsaw, Poland.

[f] Supported by the research grant No. 1 P03B 04529 (2005–2008).

[g] This work was supported in part by the Marie Curie Actions Transfer of Knowledge project COCOS (contract MTKD-CT-2004-517186).

[h] Now at University of Bonn, Germany.

[i] Now at DESY group FEB, Hamburg, Germany.

[j] Also at Moscow State University, Russia.

[k] Now at University of Liverpool, UK.

[l] On leave of absence at CERN, Geneva, Switzerland.

[m] Now at CERN, Geneva, Switzerland.

[n] Now at Bologna University, Bologna, Italy.

[o] Also at Institut of Theoretical and Experimental Physics, Moscow, Russia.

[p] Also at INP, Cracow, Poland.

[q] Also at FPACS, AGH-UST, Cracow, Poland.

[r] Partially supported by Warsaw University, Poland.

[s] Partially supported by Moscow State University, Russia.

[t] Royal Society of Edinburgh, Scottish Executive Support Research Fellow.

[u] Also affiliated with DESY, Germany.

[v] Also at University of Tokyo, Japan.

[w] Now at Kobe University, Japan.

[x] Supported by DESY, Germany.

[y] Partially supported by Russian Foundation for Basic Research grant No. 05-02-39028-NSFC-a.

[z] STFC Advanced Fellow.

[aa] Nee Korcsak-Gorzo.

[ab] This material was based on work supported by the National Science Foundation, while working at the Foundation.

[ac] Now at University of Kansas, Lawrence, USA.

[ad] Also at Max Planck Institute, Munich, Germany, Alexander von Humboldt Research Award.

[ae] Now at KEK, Tsukuba, Japan.

[af] Now at Nagoya University, Japan.

[ag] Member of Department of Radiological Science, Tokyo Metropolitan University, Japan.

[ah] Now at SunMelx Co. Ltd., Tokyo, Japan.

[ai] Also at Hamburg University, Inst. of Exp. Physics, Alexander von Humboldt Research Award and partially supported by DESY, Hamburg, Germany.

[aj] Also at Łódź University, Poland.

[ak] Member of Łódź University, Poland.

[al] Also at University of Podlasie, Siedlce, Poland.

[am] Now at Lund Universtiy, Lund, Sweden.

[an] Deceased.

[ao] Supported by the Natural Sciences and Engineering Council of Canada (NSERC).

[ap] Supported by the German Federal Ministry for Education and Research (BMBF), under contract numbers 05 HZ6PDA, 05 HZ6GUA, 05 HZ6VFA and 05 HZ4KHA.

[aq] Supported in part by the MINERVA Gesellschaft für Forschung GmbH, the Israel Science Foundation (grant No. 293/02-11.2) and the U.S.–Israel Binational Science Foundation.

[ar] Supported by the Israel Science Foundation.

[as] Supported by the Italian National Institute for Nuclear Physics (INFN).

[at] Supported by the Japanese Ministry of Education, Culture, Sports, Science and Technology (MEXT) and its grants for Scientific Research.

[au] Supported by the Korean Ministry of Education and Korea Science and Engineering Foundation.

[av] Supported by the Netherlands Foundation for Research on Matter (FOM).

[aw] Supported by the Polish State Committee for Scientific Research, project No. DESY/256/2006-154/DES/2006/03.

[ax] Partially supported by the German Federal Ministry for Education and Research (BMBF).

[ay] Supported by RF Presidential grant No. 1456.2008.2 for the leading scientific schools and by the Russian Ministry of Education and Science through its grant for Scientific Research on High Energy Physics.

[az] Supported by the Spanish Ministry of Education and Science through funds provided by CICYT.

[ba] Supported by the Science and Technology Facilities Council, UK.

[bb] Supported by the US Department of Energy.

[bc] Supported by the US National Science Foundation. Any opinion, findings and conclusions or recommendations expressed in this material are those of the authors and do not necessarily reflect the views of the National Science Foundation.

[bd] Supported by the Polish Ministry of Science and Higher Education as a scientific project (2006–2008).

[be] Supported by FNRS and its associated funds (IISN and FRIA) and by an Inter-University Attraction Poles Programme subsidised by the Belgian Federal Science Policy Office.

[bf] Supported by an FRGS grant from the Malaysian government.

628

Eur. Phys. J. C (2009) 62: 625–658

1 Introduction

The study of deep inelastic scattering (DIS) of leptons off nucleons has been instrumental in establishing not only the structure of nucleons but also many other aspects of the Standard Model (SM). The HERA ep collider with a centre-of-mass energy of 318 GeV has expanded the accessible kinematic region for DIS measurements allowing for direct observation of the effects of the weak interaction at high values of the negative four-momentum transfer squared, Q^2. In particular, the structure function $x\tilde{F}_3$ can be obtained from the difference of cross sections in e^+p and e^-p scattering. At HERA $x\tilde{F}_3$ is dominated by the interference of photon and Z-exchange and can be extracted from data on a pure proton target with no complications due to target mass or higher twist effects. This furnishes not only a precise test of the electroweak sector of the standard model but also provides direct information on the valence quark distributions in the nucleon.

The data samples collected from 1992–2000 by the H1 and ZEUS collaborations were used for determinations of the neutral current (NC) cross sections up to values of $Q^2 \approx 30\,000$ GeV^2 [1–10]. A first extraction of $x\tilde{F}_3$ clearly demonstrated the effect of Z-exchange. A measurement of e^+p NC DIS cross sections for a longitudinally polarised positron beam using a limited sample of data collected during 2004 has also been published by the ZEUS collaboration [11].

In this paper, measurements of the cross sections and the asymmetry parameter, representing the difference in the behaviour of negatively and positively polarised electrons, are presented. The measurement is made using data collected during 2005 and 2006 when HERA collided both positively and negatively polarised electron beams of 27.5 GeV with protons of 920 GeV. The integrated luminosity amounts to 169.9 pb^{-1} with mean luminosity-weighted polarisations of $+0.29$ and -0.27. This is a ten-fold increase over the previously available e^-p sample. This allows a detailed and direct probe of electro-weak effects at high Q^2 and a more precise measurement of the structure function $x\tilde{F}_3$.

2 Standard Model predictions

Inclusive deep inelastic lepton-proton scattering can be described in terms of the kinematic variables x, y, and Q^2. The variable Q^2 is defined as $Q^2 = -q^2 = -(k - k')^2$, where k and k' are the four-momenta of the incoming and scattered lepton, respectively. Bjorken x is defined as $x = Q^2/2P \cdot q$, where P is the four-momentum of the incoming proton. The fraction of the lepton energy transferred to the proton in its rest frame is given by $y = P \cdot q/P \cdot k$. The variables x, y and Q^2 are related by $Q^2 = sxy$, where s, the centre-of-mass energy is approximately given by $s = 4E_e E_p$, and E_e

and E_p are the initial energies of the electron and proton, respectively.

The electroweak Born-level cross section for the $e^\pm p$ NC interaction is given by [12, 13]

$$\frac{d^2\sigma(e^\pm p)}{dx\,dQ^2} = \frac{2\pi\alpha^2}{xQ^4}[Y_+\tilde{F}_2(x, Q^2) \mp Y_- x\tilde{F}_3(x, Q^2)$$
$$- y^2\tilde{F}_L(x, Q^2)], \quad (1)$$

where α is the fine-structure constant, $Y_\pm = 1 \pm (1 - y)^2$, and $\tilde{F}_2(x, Q^2)$, $\tilde{F}_3(x, Q^2)$ and $\tilde{F}_L(x, Q^2)$ are generalised structure functions. Next-to-leading order (NLO) QCD calculations predict that the contribution of the longitudinal structure function $\tilde{F}_L$ to $d^2\sigma/dx\,dQ^2$ is approximately 1.5%, averaged over the kinematic range considered, and therefore neglected in the discussion in this section. However, this term is included in SM calculations which are compared to the measurements presented in this paper.

The generalised structure functions depend on the longitudinal polarisation of the lepton beam which is defined as

$$P_e = \frac{N_R - N_L}{N_R + N_L},$$

where N_R and N_L are the numbers of right- and left-handed leptons in the beam.[1]

Photon exchange dominates the cross section at low Q^2 and is described by $\tilde{F}_2$. It is only at Q^2 values comparable to M_Z^2 that the γ/Z interference and pure Z exchange terms become important and the $\tilde{F}_3$ term contributes significantly to the cross section. The sign of the $\tilde{F}_3$ term in (1) shows that electroweak effects increase (decrease) the e^-p (e^+p) cross sections.

Reduced cross sections, $\tilde{\sigma}$, for e^-p and e^+p scattering are defined as

$$\tilde{\sigma}^{e^\pm p} = \frac{xQ^4}{2\pi\alpha^2}\frac{1}{Y_+}\frac{d^2\sigma(e^\pm p)}{dx\,dQ^2}$$
$$= \tilde{F}_2(x, Q^2) \mp \frac{Y_-}{Y_+}x\tilde{F}_3(x, Q^2). \quad (2)$$

The difference in the e^-p and e^+p reduced cross sections yields

$$x\tilde{F}_3 = \frac{Y_+}{2Y_-}(\tilde{\sigma}^{e^-p} - \tilde{\sigma}^{e^+p}). \quad (3)$$

The generalised structure functions can be split into terms depending on γ exchange (F_2^γ), Z exchange (F_2^Z, xF_3^Z) and

---

[1] At HERA beam energies the mass of the incoming leptons may be neglected, and therefore the difference between handedness and helicity may also be neglected.

Eur. Phys. J. C (2009) 62: 625–658

629

γ/Z interference ($F_2^{\gamma Z}$, $xF_3^{\gamma Z}$) as

$$\tilde{F}_2 = F_2^{\gamma} - (v_e - P_e a_e)\chi_Z F_2^{\gamma Z}$$
$$+ (v_e^2 + a_e^2 - 2P_e v_e a_e)\chi_Z^2 F_2^Z, \tag{4}$$

$$x\tilde{F}_3 = -(a_e - P_e v_e)\chi_Z x F_3^{\gamma Z}$$
$$+ (2v_e a_e - P_e(v_e^2 + a_e^2))\chi_Z^2 x F_3^Z. \tag{5}$$

In these equations, the respective vector and axial couplings of the electron to the Z boson in the SM are given by $v_e = -1/2 + 2\sin^2\theta_W$ and $a_e = -1/2$, where θ_W is the Weinberg angle. The relative contribution of Z and γ exchange is given by $\chi_Z = \frac{1}{\sin^2 2\theta_W}\frac{Q^2}{M_Z^2 + Q^2}$ and varies between 0.2 and 1.1 over the range $1\,500 < Q^2 < 30\,000$ GeV^2. For the unpolarised case ($P_e = 0$), the interference structure function $xF_3^{\gamma Z}$ is the dominant term in $x\tilde{F}_3$ as v_e is small (≈ -0.04) and thus terms containing v_e in (5) can be ignored, so that

$$x\tilde{F}_3 \simeq -a_e \chi_Z x F_3^{\gamma Z}. \tag{6}$$

In this paper, measurements of $x\tilde{F}_3$ and $xF_3^{\gamma Z}$ are presented using the full $e^- p$ dataset collected during 2005 and 2006.

The structure functions can be written in terms of the sums and differences of the quark and anti-quark momentum distributions. In leading order (LO) QCD

$$[F_2^{\gamma}, F_2^{\gamma Z}, F_2^Z] = \sum_q [e_q^2, 2e_q v_q, v_q^2 + a_q^2]x(q + \bar{q}), \tag{7}$$

$$[xF_3^{\gamma Z}, xF_3^Z] = \sum_q [e_q a_q, v_q a_q]2x(q - \bar{q}), \tag{8}$$

where v_q and a_q are the vector and axial couplings of the quark q to the Z boson, and e_q is the electric charge of the quark. The densities of the quarks and anti-quarks are given by parton distribution functions (PDFs) q and $\bar{q}$, respectively. The sums run over all quark flavours except the top quark.

The sensitivity of $xF_3^{\gamma Z}$ to u_v and d_v, the valence quark momentum distributions, is demonstrated in LO QCD through

$$xF_3^{\gamma Z} = 2x[e_u a_u u_v + e_d a_d d_v] = \frac{x}{3}(2u_v + d_v). \tag{9}$$

In addition, the integral of $xF_3^{\gamma Z}$ should obey the sum rule [14] :

$$\int_0^1 xF_3^{\gamma Z}\frac{dx}{x} = \frac{1}{3}\int_0^1 (2u_v + d_v)dx = \frac{5}{3}. \tag{10}$$

The charge-dependent polarisation asymmetry, A^-, is defined in terms of pure right-handed ($P_e = +1$) and left-handed ($P_e = -1$) electron beams as

$$A^- \equiv \frac{\sigma^-(P_e = +1) - \sigma^-(P_e = -1)}{\sigma^-(P_e = +1) + \sigma^-(P_e = -1)}, \tag{11}$$

where $\sigma^-(P_e = +1)$ and $\sigma^-(P_e = -1)$ are the cross sections at P_e values of $+1$ and -1, respectively. When the beam polarisation is not unity A^- is given by

$$A^- = \frac{\sigma^-(P_{e,+}) - \sigma^-(P_{e,-})}{P_{e,+}\sigma^-(P_{e,-}) - P_{e,-}\sigma^-(P_{e,+})}, \tag{12}$$

where $\sigma^-(P_{e,+})$ and $\sigma^-(P_{e,-})$ are the cross sections evaluated at positive and negative electron polarisation values. To a good approximation the asymmetry is the ratio of the $F_2^{\gamma Z}$ and F_2^{γ} structure functions, and is proportional to the combination $a_e v_q$:

$$A^- \simeq \chi_Z a_e \frac{F_2^{\gamma Z}}{F_2^{\gamma}}$$
$$= \chi_Z \sum_q [2a_e v_q e_q (q + \bar{q})]/\sum_q [e_q^2(q + \bar{q})]. \tag{13}$$

Thus a measurement of A^- can give direct evidence of parity violation with minimal sensitivity to the proton PDFs, and a comparison to SM predictions provides a test of the electroweak sector of the SM.

3 Experimental apparatus

A detailed description of the ZEUS detector can be found elsewhere [15]. A brief outline of the components most relevant for this analysis is given below.

Charged particles were tracked in the central tracking detector (CTD) [16–18], which operated in a magnetic field of 1.43 T provided by a thin superconducting solenoid. The CTD consisted of 72 cylindrical drift chamber layers, organised in nine superlayers covering the polar-angle[2] region $15° < \theta < 164°$. A silicon microvertex detector (MVD) [19] was installed between the beampipe and the inner radius of the CTD. The MVD was organised into a barrel with 3 cylindrical layers and a forward section with four planar layers perpendicular to the HERA beam direction. Charged-particle tracks were reconstructed using information from the CTD and MVD.

The high-resolution uranium–scintillator calorimeter (CAL) [20–23] consisted of three parts: the forward (FCAL),

---

[2]The ZEUS coordinate system is a right-handed Cartesian system, with the Z axis pointing in the proton beam direction, referred to as the "forward direction", and the X axis pointing left towards the centre of HERA. The coordinate origin is at the nominal interaction point.

630

Eur. Phys. J. C (2009) 62: 625–658

the barrel (BCAL) and the rear (RCAL) calorimeters, covering 99.7% of the solid angle around the nominal interaction point. Each part was subdivided transversely into towers and longitudinally into one electromagnetic section (EMC) and either one (RCAL) or two (BCAL and FCAL) hadronic sections (HAC). The smallest subdivision of the calorimeter was called a cell. The CAL relative energy resolutions, as measured under test-beam conditions, were $\sigma(E)/E = 0.18/\sqrt{E}$ for electrons and $\sigma(E)/E = 0.35/\sqrt{E}$ for hadrons, with E in GeV. The timing resolution of the CAL was better than 1 ns for energy deposits exceeding 4.5 GeV.

An iron structure that surrounded the CAL was instrumented as a backing calorimeter (BAC) [24] to measure energy leakage from the CAL. Muon chambers in the forward, barrel and rear [25] regions were used in this analysis to veto background events induced by cosmic-ray or beam-halo muons.

The luminosity was measured using the Bethe-Heitler reaction $ep \to e\gamma p$ with the luminosity detector which consisted of two independent systems, a photon calorimeter and a magnetic spectrometer.

The lepton beam in HERA became naturally transversely polarised through the Sokolov-Ternov effect [26]. The characteristic build-up time in HERA was approximately 40 minutes. Spin rotators on either side of the ZEUS detector changed the transverse polarisation of the beam into longitudinal polarisation. The electron beam polarisation was measured using two independent polarimeters, the transverse polarimeter (TPOL) [27, 28] and the longitudinal polarimeter (LPOL) [29]. Both devices exploited the spin-dependent cross section for Compton scattering of circularly polarised photons off electrons to measure the beam polarisation. The luminosity and polarisation measurements were made over times that were much shorter than the polarisation build-up time.

4 Monte Carlo simulation

Monte Carlo (MC) simulated events were used to determine the efficiency for selecting events, the accuracy of kinematic reconstruction, to estimate the background rate and to correct for detector acceptance.

NC DIS events were simulated including radiative effects, using the HERACLES [30] program with the DJANGOH 1.6 [31, 32] interface to the hadronisation programs and using CTEQ5D [33] PDFs. The hadronic final state was simulated using the colour-dipole model in ARIADNE 4.10 [34]. To investigate systematic uncertainties, the MEPS model of LEPTO6.5 [35] was also used. The Lund string model of JETSET7.4 [36–38] was used for the hadroni-

sation. Diffractive NC events were generated using the RAPGAP 2.08/06 [39] program and mixed with the non-diffractive MC events to simulate the observed hadronic final states. Background from photoproduction events was simulated using HERWIG 5.9 [40].

The simulated samples were at least five times larger than the corresponding data samples. They were normalised to the integrated luminosity of the data.

The ZEUS detector response was simulated using a program based on GEANT 3.21 [41]. The generated events were passed through the detector simulation, subjected to the same trigger requirements as the data and processed by the same reconstruction programs.

5 Event reconstruction

Neutral Current events at high Q^2 are characterised by the presence of an isolated high-energy electron in the final state. The transverse momentum of the scattered electron balances that of the hadronic final state, and therefore the measured net transverse momentum, p_T, should be small. The measured p_T and the net transverse energy, E_T, are defined as

$$p_T^2 = p_X^2 + p_Y^2 = \left(\sum_i E_i \sin\theta_i \cos\phi_i \right)^2 + \left(\sum_i E_i \sin\theta_i \sin\phi_i \right)^2, \qquad (14)$$

$$E_T = \sum_i E_i \sin\theta_i,$$

where the sum runs over all calorimeter energy deposits, E_i. The polar and azimuthal angles, θ_i and ϕ_i, of the calorimeter energy deposits are measured in a coordinate system with the event vertex as origin. The variable δ, also used in the event selection, is defined as

$$\delta \equiv \sum_i (E - p_Z)_i = \sum_i (E_i - E_i \cos\theta_i). \qquad (15)$$

Conservation of energy and longitudinal momentum requires $\delta = 2E_e = 55$ GeV if all final-state particles are detected and perfectly measured. Undetected particles that escape through the forward beam-pipe have a negligible effect on δ. However, particles lost through the rear beam-pipe can lead to a substantial reduction in δ.

Backsplash of low energy particles originating from secondary interactions and deposited at large angles were suppressed by removing low energy deposits with a polar angle greater than $\gamma_{\max}$, which was calculated on an event-by-event basis. The specific value of $\gamma_{\max}$ was tuned using both

Fig. 1 Comparison of the final $e^- p$ NC data sample with the expectations of the MC simulation described in the text. The MCs are normalised to the data luminosity. The distributions of (**a**) Q^2_{DA}, (**b**) x_{DA}, (**c**) y_{DA}, (**d**) the energy of the scattered electron, E'_e, (**e**) the angle of the scattered electron, θ_e, (**f**) the hadronic angle, γ_h, (**g**) the transverse momentum of the hadronic system, $p_{T,h}$, and (**h**) the Z coordinate of the event vertex, Z_{vtx}, are shown

ZEUS
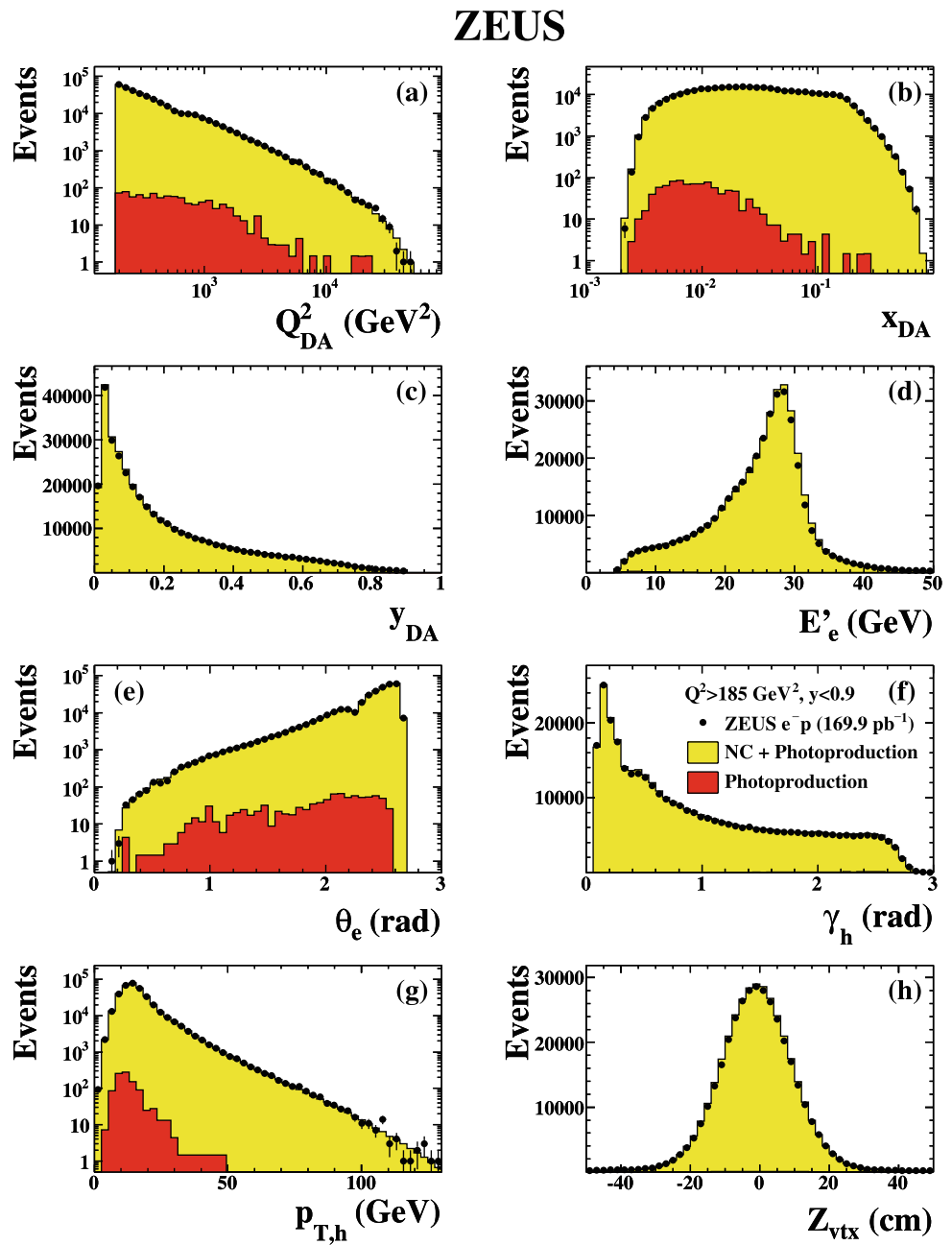
data and MC samples containing a reduced amount of backsplash. Studies [42] have shown that this procedure depends on the Q^2 threshold of the sample. This effect is accounted for in the study of systematic effects.

Furthermore, CAL energy deposits are separated into those associated with the scattered electron, and all other energy deposits. The sum of the latter is called the hadronic energy. In the naive quark-parton model, the hadronic polar angle, γ_h, defined as

$$\cos \gamma_h = \frac{p^2_{T,h} - \delta^2_h}{p^2_{T,h} + \delta^2_h} , \qquad (16)$$

is the scattering angle of the struck quark, where the quantities $p_{T,h}$ and δ_h are derived from (14)–(15) using only the hadronic energy.

The double-angle (DA) method [43, 44] is used for reconstructing the kinematic variables. It makes use of the polar angle of the scattered electron, θ_e, and γ_h to reconstruct the kinematic variables x_{DA}, y_{DA}, and Q^2_{DA}. The DA method is insensitive to uncertainties in the overall energy scale of the calorimeter. However, it is sensitive to initial-state QED radiation and an accurate simulation of the detector response is necessary. The variable y is also reconstructed using the electron method, y_e, and the Jacquet-Blondel method, y_{JB}
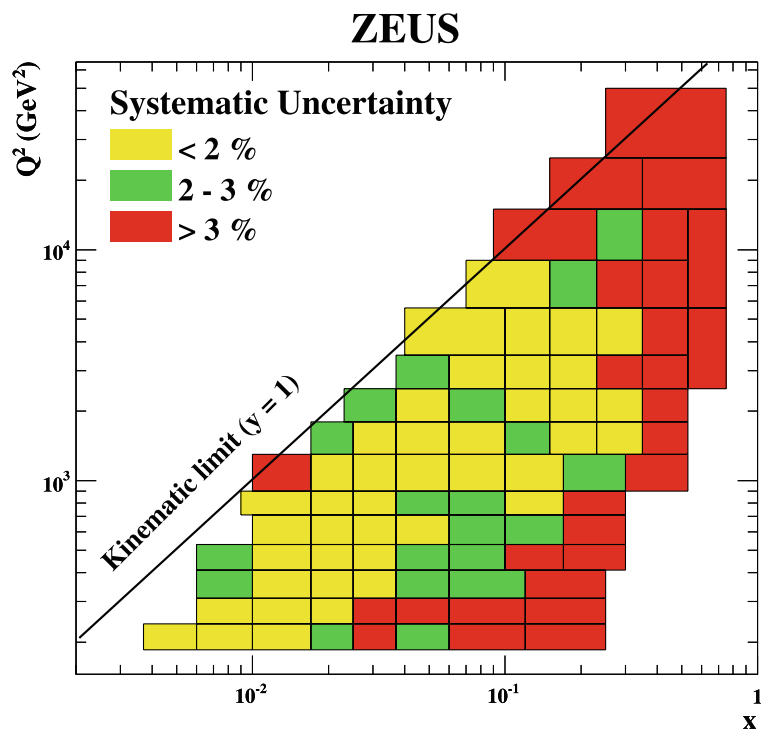
[45]. These estimators for y are used only for the event selection.

6 Neutral current event selection

ZEUS operated a three-level trigger system [15, 46, 47]. At the first level, only coarse calorimeter and tracking information were available. Events were selected using criteria based on an energy deposit in the CAL consistent with an isolated electron. In addition, events with high E_T in coincidence with a CTD track were accepted. At the second level, a requirement on δ was used to select NC DIS events. Timing information from the calorimeter was used to reject events inconsistent with the bunch-crossing time. At the third level, events were fully reconstructed. The requirements were similar to, but looser than, the offline cuts described below.

Scattered electrons were identified using an algorithm that combined information from the energy deposits in the calorimeter with tracks measured in the central tracking detectors [1]. To ensure high electron finding efficiency and to reject backgrounds, the identified electron was required to have an energy of at least 10 GeV. A track matched to the energy deposit in the calorimeter was required for events in which an electron was found within the acceptance of the tracking detectors. This was done by requiring the distance of closest approach (DCA) between the track extrapolated to the calorimeter surface and the energy cluster position to

be less than 10 cm and the electron track momentum, p_e^{trk}, to be larger than 3 GeV. A matched track was not required if the electron emerged at a polar angle outside the acceptance of the tracking detector. If the electron emerged in FCAL with a polar angle outside the acceptance of the tracking detector, it was required to have energy greater than 30 GeV. An isolation requirement was imposed such that the energy not associated with the electron in an $\eta - \phi$ cone of radius 0.8 centred on the electron was less than 5 GeV.

In photoproduction events where the electron emerges at very small scattering angles, δ is substantially smaller than 55 GeV, and in beam-gas events overlaid on NC events, δ is substantially larger than 55 GeV. A requirement $38 < \delta < 65$ GeV was imposed to remove these backgrounds. To further reduce background from photoproduction events, y_e was required to be less than 0.95. The net transverse momentum was expected to be small for balanced NC events, so to remove cosmic-ray events and beam-related background events the quantity $p_T / \sqrt{E_T}$ was required to be less than $4\sqrt{\text{GeV}}$ and the quantity p_T / E_T was required to be less than 0.7.

In order to reject events where most of the hadronic final state was lost in the forward beam-pipe, the projection of γ_h onto the face of FCAL was required to be outside a radius of 20 cm centred on the beam-pipe axis. The Z coordinate of the ep interaction vertex, reconstructed using tracks in the CTD and the MVD, was required to satisfy $|Z_{\text{vtx}}| < 50$ cm. The final event sample was defined by requiring $Q_{\text{DA}}^2 > 185$ GeV^2 and $y_{\text{DA}} < 0.9$.

Eur. Phys. J. C (2009) 62: 625–658

633

Table 1 The single differential cross section $d\sigma/dQ^2$ ($y < 0.9$) for the reaction $e^- p \to e^- X$ ($\mathcal{L} = 169.9\,\text{pb}^{-1}$, $P_e = -0.03$). The bin range, bin centre (Q_c^2) and measured cross section corrected to the electroweak Born level are shown. The first (second) error on the cross section corresponds to the statistical (systematic) uncertainties. The number of observed data events (N_{data}) and simulated background events ($N_{\text{bg}}^{\text{MC}}$) are also shown

Q^2 range (GeV^2)	Q_c^2 (GeV^2)	$d\sigma/dQ^2$ (pb/GeV^2)	N_{data}	$N_{\text{bg}}^{\text{MC}}$
185 – 210	195	$(1.96 \pm 0.01\,^{+0.02}_{-0.02}) \times 10^1$	58678	65.4
210 – 240	220	$(1.47 \pm 0.01\,^{+0.02}_{-0.02}) \times 10^1$	51660	83.5
240 – 270	255	$(1.01 \pm 0.01\,^{+0.01}_{-0.01}) \times 10^1$	37659	52.4
270 – 300	285	$7.89 \pm 0.05\,^{+0.11}_{-0.09}$	29355	51.1
300 – 340	320	$5.93 \pm 0.04\,^{+0.08}_{-0.07}$	29377	53.3
340 – 380	360	$4.51 \pm 0.03\,^{+0.06}_{-0.05}$	22298	55.0
380 – 430	400	$3.52 \pm 0.03\,^{+0.05}_{-0.04}$	21008	59.4
430 – 480	450	$2.63 \pm 0.02\,^{+0.06}_{-0.05}$	15502	54.9
480 – 540	510	$1.92 \pm 0.02\,^{+0.03}_{-0.02}$	13332	45.5
540 – 600	570	$1.45 \pm 0.02\,^{+0.02}_{-0.01}$	9290	49.4
600 – 670	630	$1.16 \pm 0.01\,^{+0.02}_{-0.01}$	8405	48.6
670 – 740	700	$(8.98 \pm 0.11\,^{+0.07}_{-0.07}) \times 10^{-1}$	7483	20.6
740 – 820	780	$(6.88 \pm 0.08\,^{+0.06}_{-0.06}) \times 10^{-1}$	7608	26.3
820 – 900	860	$(5.33 \pm 0.07\,^{+0.04}_{-0.04}) \times 10^{-1}$	6287	33.5
900 – 990	940	$(4.27 \pm 0.06\,^{+0.05}_{-0.04}) \times 10^{-1}$	5690	32.1
990 – 1080	1030	$(3.41 \pm 0.05\,^{+0.05}_{-0.05}) \times 10^{-1}$	4644	29.4
1080 – 1200	1130	$(2.75 \pm 0.04\,^{+0.03}_{-0.03}) \times 10^{-1}$	4907	30.5
1200 – 1350	1270	$(2.02 \pm 0.03\,^{+0.01}_{-0.01}) \times 10^{-1}$	4645	24.4
1350 – 1500	1420	$(1.52 \pm 0.03\,^{+0.02}_{-0.01}) \times 10^{-1}$	3499	31.8
1500 – 1700	1590	$(1.12 \pm 0.02\,^{+0.01}_{-0.01}) \times 10^{-1}$	3452	27.6
1700 – 1900	1790	$(8.40 \pm 0.17\,^{+0.09}_{-0.09}) \times 10^{-2}$	2611	18.8
1900 – 2100	1990	$(6.25 \pm 0.14\,^{+0.09}_{-0.10}) \times 10^{-2}$	1957	7.2
2100 – 2600	2300	$(4.39 \pm 0.08\,^{+0.03}_{-0.03}) \times 10^{-2}$	3315	13.3
2600 – 3200	2800	$(2.65 \pm 0.06\,^{+0.04}_{-0.02}) \times 10^{-2}$	2345	21.9
3200 – 3900	3500	$(1.48 \pm 0.04\,^{+0.01}_{-0.01}) \times 10^{-2}$	1597	4.5
3900 – 4700	4200	$(9.32 \pm 0.28\,^{+0.18}_{-0.08}) \times 10^{-3}$	1111	2.9
4700 – 5600	5100	$(5.08 \pm 0.19\,^{+0.11}_{-0.06}) \times 10^{-3}$	708	2.8
5600 – 6600	6050	$(3.81 \pm 0.16\,^{+0.10}_{-0.09}) \times 10^{-3}$	586	4.4
6600 – 7800	7100	$(2.23 \pm 0.11\,^{+0.07}_{-0.04}) \times 10^{-3}$	401	1.5
7800 – 9200	8400	$(1.59 \pm 0.09\,^{+0.06}_{-0.02}) \times 10^{-3}$	331	0.0
9200 – 12800	10800	$(6.90 \pm 0.36\,^{+0.19}_{-0.05}) \times 10^{-4}$	369	1.4
12800 – 18100	15200	$(2.45 \pm 0.18\,^{+0.07}_{-0.09}) \times 10^{-4}$	193	1.4
18100 – 25600	21500	$(7.99\,^{+0.93}_{-0.85}\,^{+0.65}_{-0.24}) \times 10^{-5}$	97	3.0
25600 – 51200	36200	$(6.62\,^{+1.28}_{-1.08}\,^{+0.45}_{-0.33}) \times 10^{-6}$	37	0.0

A total of 360 437 candidate events passed the selection criteria. The background is dominated by photoproduction which was estimated to contribute, on average, about 0.3% to the event sample but tend to populate mainly in smaller Q^2 and larger y regions. Other backgrounds were negligible.

A comparison between data and MC distributions is shown in Fig. 1 for the variables Q_{DA}^2, x_{DA}, y_{DA}, energy E_e' and θ_e of the scattered electron, γ_h and $p_{T,h}$ of the final hadronic system, and Z_{vtx} for the event. The distributions from the data and MC (NC + photoproduction) agree well.

7 Cross section determination

The single-differential cross-sections $d\sigma/dQ^2$, $d\sigma/dx$ and $d\sigma/dy$ for $Q^2 > 185\,\text{GeV}^2$ and $y < 0.9$, and $d\sigma/dx$ and $d\sigma/dy$ for $Q^2 > 3\,000\,\text{GeV}^2$ and $y < 0.9$, and the double-differential cross-section $d^2\sigma/dx\,dQ^2$ were measured. The

Table 2 Systematic uncertainties with bin-to-bin correlations for $d\sigma/dQ^2$ ($y < 0.9$) for the reaction $e^-p \to e^-X$ ($\mathcal{L} = 169.9\,\text{pb}^{-1}$, $P_e = -0.03$). The left four columns of the table contain the bin centre (Q_c^2), the measured cross section, the statistical uncertainty and the total systematic uncertainty. The right eight columns of the table list the bin-to-bin correlated systematic uncertainties for δ_1–δ_7, and the systematic uncertainties summed in quadrature for δ_8–δ_{13}, as defined in Sect. 8. The upper and lower correlated uncertainties correspond to a positive or negative variation of a cut value for example. However, if this is not possible for a particular systematic, the uncertainty is symmetrised

Q_c^2 (GeV²)	$d\sigma/dQ^2$ (pb/ GeV²)	stat. (%)	sys. (%)	δ_1 (%)	δ_2 (%)	δ_3 (%)	δ_4 (%)	δ_5 (%)	δ_6 (%)	δ_7 (%)	δ_8–δ_{13} (%)
195	1.96×10^1	±0.4	+1.2 / −1.1	+0.0 / −0.1	−0.5 / +0.6	+0.4 / −0.4	+0.1 / −0.1	−0.1 / +0.1	+0.1 / +0.2	+0.0 / −0.0	+0.9 / −0.9
220	1.47×10^1	±0.5	+1.3 / −1.2	+0.4 / −0.0	−0.5 / +0.6	+0.4 / −0.4	+0.6 / −0.6	−0.0 / +0.1	−0.0 / +0.2	+0.1 / −0.1	+0.6 / −0.8
255	1.01×10^1	±0.6	+1.5 / −1.3	+0.6 / −0.0	−0.5 / +0.6	+0.8 / −0.8	+0.6 / −0.6	−0.1 / +0.2	−0.1 / +0.2	+0.1 / −0.1	+0.7 / −0.7
285	7.89	±0.6	+1.4 / −1.1	+0.7 / −0.0	−0.5 / +0.7	+0.2 / −0.2	+0.7 / −0.7	−0.1 / +0.2	−0.1 / +0.1	+0.1 / −0.1	+0.6 / −0.6
320	5.93	±0.6	+1.4 / −1.2	+0.5 / +0.0	−0.5 / +0.7	+0.6 / −0.6	+0.5 / −0.5	−0.1 / +0.3	−0.2 / +0.2	+0.1 / −0.1	+0.7 / −0.7
360	4.51	±0.7	+1.4 / −1.2	+0.8 / −0.1	−0.5 / +0.6	+0.4 / −0.4	+0.7 / −0.7	+0.1 / +0.1	−0.2 / +0.1	+0.1 / −0.1	+0.6 / −0.7
400	3.52	±0.7	+1.5 / −1.2	+0.5 / −0.0	−0.5 / +0.6	−0.1 / +0.1	+0.9 / −0.9	−0.0 / +0.0	−0.4 / +0.5	+0.1 / −0.1	+0.6 / −0.5
450	2.63	±0.8	+2.1 / −1.9	+0.5 / −0.0	−0.5 / +0.6	+0.9 / −0.9	+1.4 / −1.4	−0.2 / +0.5	−0.3 / +0.7	+0.1 / −0.1	+0.6 / −0.7
510	1.92	±0.9	+1.5 / −1.0	+1.0 / −0.0	−0.6 / +0.7	+0.3 / −0.3	+0.2 / −0.2	−0.1 / +0.1	−0.3 / +0.4	+0.1 / −0.1	+0.7 / −0.6
570	1.45	±1.1	+1.4 / −0.9	+0.8 / −0.1	−0.5 / +0.7	+0.3 / −0.3	+0.1 / −0.1	−0.2 / +0.4	+0.1 / +0.2	+0.2 / −0.2	+0.7 / −0.6
630	1.16	±1.1	+1.5 / −1.1	+1.0 / −0.2	−0.7 / +0.7	+0.0 / −0.0	−0.7 / +0.7	+0.1 / −0.1	+0.1 / +0.2	+0.2 / −0.2	+0.2 / −0.3
700	8.98×10^{-1}	±1.2	+0.8 / −0.7	+0.1 / −0.2	−0.6 / +0.7	+0.1 / −0.1	+0.1 / −0.1	+0.1 / +0.2	+0.3 / −0.1	+0.1 / −0.1	+0.3 / −0.4
780	6.88×10^{-1}	±1.2	+0.9 / −0.9	+0.0 / −0.4	−0.5 / +0.6	+0.5 / −0.5	+0.5 / −0.5	+0.1 / +0.0	+0.1 / +0.0	+0.1 / −0.1	+0.2 / −0.3
860	5.33×10^{-1}	±1.3	+0.8 / −0.8	+0.4 / +0.0	−0.4 / +0.5	−0.4 / +0.4	−0.1 / +0.1	−0.3 / −0.3	−0.1 / −0.1	+0.2 / −0.2	+0.3 / −0.4
940	4.27×10^{-1}	±1.4	+1.1 / −0.9	+0.0 / −0.2	−0.4 / +0.5	−0.4 / +0.4	+0.6 / −0.6	+0.4 / −0.1	−0.0 / −0.1	+0.2 / −0.2	+0.4 / −0.2
1030	3.41×10^{-1}	±1.5	+1.5 / −1.4	+0.4 / −0.1	−0.3 / +0.5	+0.7 / −0.7	+1.1 / −1.1	+0.1 / +0.2	−0.1 / −0.4	+0.3 / −0.3	+0.4 / −0.4
1130	2.75×10^{-1}	±1.5	+1.2 / −1.2	+0.2 / −0.3	−0.4 / +0.4	+0.9 / −0.9	−0.1 / +0.1	−0.1 / +0.4	+0.1 / −0.4	+0.2 / −0.3	+0.3 / −0.4
1270	2.02×10^{-1}	±1.5	+0.7 / −0.7	+0.0 / −0.1	−0.3 / +0.4	−0.4 / +0.4	−0.1 / +0.1	+0.1 / −0.1	−0.1 / −0.2	+0.3 / −0.2	+0.3 / −0.4
1420	1.52×10^{-1}	±1.7	+1.0 / −0.9	+0.5 / +0.0	−0.3 / +0.4	+0.1 / −0.1	−0.6 / +0.6	+0.1 / −0.2	−0.1 / −0.0	+0.4 / −0.4	+0.4 / −0.4
1590	1.12×10^{-1}	±1.7	+1.0 / −0.6	+0.6 / −0.1	−0.3 / +0.3	+0.1 / −0.1	−0.2 / +0.2	+0.3 / +0.0	+0.0 / +0.3	+0.4 / −0.3	+0.3 / −0.3
1790	8.40×10^{-2}	±2.0	+1.0 / −1.1	+0.5 / −0.1	−0.3 / +0.3	+0.6 / −0.6	−0.5 / +0.5	+0.2 / −0.1	−0.5 / −0.4	+0.3 / −0.3	+0.3 / −0.4
1990	6.25×10^{-2}	±2.3	+1.5 / −1.6	+0.1 / −0.7	−0.3 / +0.4	−0.5 / +0.5	+1.3 / −1.3	+0.1 / +0.0	+0.1 / −0.2	+0.1 / −0.2	+0.3 / −0.3
2300	4.39×10^{-2}	±1.8	+0.7 / −0.6	+0.2 / +0.0	−0.2 / +0.3	+0.2 / −0.2	+0.1 / −0.1	−0.2 / −0.0	+0.3 / +0.1	+0.3 / −0.2	+0.3 / −0.4
2800	2.65×10^{-2}	±2.1	+1.6 / −0.7	+1.4 / −0.3	−0.2 / +0.3	−0.2 / +0.2	+0.4 / −0.4	+0.1 / +0.0	+0.3 / +0.1	+0.4 / −0.4	+0.4 / −0.2
3500	1.48×10^{-2}	±2.5	+0.8 / −0.8	+0.2 / +0.0	−0.2 / +0.3	−0.5 / +0.5	−0.2 / +0.2	−0.1 / −0.0	+0.0 / −0.4	+0.3 / −0.1	+0.4 / −0.4
4200	9.32×10^{-3}	±3.0	+1.9 / −0.8	+1.8 / −0.3	−0.2 / +0.3	+0.4 / −0.4	−0.0 / +0.0	+0.1 / −0.0	−0.4 / +0.0	+0.1 / −0.2	+0.2 / −0.4
5100	5.08×10^{-3}	±3.8	+2.2 / −1.1	+1.9 / −0.3	−0.2 / +0.2	+0.9 / −0.9	−0.0 / +0.0	+0.0 / +0.0	+0.1 / +0.2	+0.2 / −0.2	+0.5 / −0.5
6050	3.81×10^{-3}	±4.2	+2.5 / −2.4	+1.0 / +0.0	−0.2 / +0.3	−2.1 / +2.1	−0.4 / +0.4	+0.0 / +0.0	−0.8 / −0.1	+0.8 / −0.3	+0.4 / −0.4
7100	2.23×10^{-3}	±5.0	+3.0 / −1.9	+2.4 / −0.1	−0.3 / +0.3	+1.4 / −1.4	+0.9 / −0.9	+0.0 / +0.0	−0.8 / +0.5	+0.2 / −0.1	+0.4 / −0.5
8400	1.59×10^{-3}	±5.5	+3.7 / −1.2	+3.7 / −0.9	−0.3 / +0.4	−0.2 / +0.2	+0.1 / −0.1	+0.0 / +0.0	−0.0 / −0.0	+0.2 / +0.0	+0.3 / −0.8
10800	6.90×10^{-4}	±5.2	+2.8 / −0.7	+2.7 / +0.0	−0.3 / +0.4	−0.2 / +0.2	+0.1 / −0.1	+0.0 / +0.0	−0.2 / −0.1	+0.3 / −0.2	+0.4 / −0.5
15200	2.45×10^{-4}	±7.2	+2.8 / −3.7	+1.4 / −0.7	−1.1 / +0.3	−2.1 / +2.1	+0.7 / −0.7	+0.0 / +0.0	−0.9 / −2.6	+0.6 / −0.3	+0.5 / −0.6
21500	7.99×10^{-5}	+11.7 / −10.6	+8.1 / −2.9	+7.8 / −1.4	−0.2 / +0.2	+0.1 / −0.1	+1.1 / −1.1	+0.0 / +0.0	−1.7 / +0.4	+1.5 / −1.3	+1.0 / −1.0
36200	6.62×10^{-6}	+19.3 / −16.4	+6.7 / −4.9	+6.5 / +0.0	−0.3 / +0.3	−0.9 / +0.9	+0.8 / −0.8	+0.0 / +0.0	+0.1 / −3.0	+0.0 / −3.5	+1.4 / −1.4

cross sections in a particular bin ($d^2\sigma/dxdQ^2$ is shown as an example) was determined according to

$$\frac{d^2\sigma}{dxdQ^2} = \frac{N_{\text{data}} - N_{\text{bg}}}{N_{\text{MC}}} \cdot \frac{d^2\sigma^{\text{SM}}_{\text{Born}}}{dxdQ^2},$$

where N_{data} is the number of data events in the bin, N_{bg} is the number of background events predicted from the photoproduction MC, and N_{MC} is the number of signal MC events normalised to the luminosity of the data. The SM prediction for the Born-level cross section, $d^2\sigma^{\text{SM}}_{\text{Born}}/dxdQ^2$, was evaluated using CTEQ5D PDFs [33] as in the MC simulation and using the PDG [48] values for the fine-structure constant, the mass of the Z boson, and the weak mixing angle. This procedure implicitly takes into account the acceptance, bin-centering, and radiative corrections from the MC simulation. The bin sizes used for the determination of the

Table 3 The single differential cross section $d\sigma/dx$ ($y < 0.9$) for $Q^2 > 185\,\text{GeV}^2$ and $Q^2 > 3000\,\text{GeV}^2$ for the reaction $e^- p \to e^- X$ ($\mathcal{L} = 169.9\,\text{pb}^{-1}$, $P_e = -0.03$). The Q^2 and bin range, bin centre (x_c) and measured cross section corrected to the electroweak Born level are shown. The first (second) error on the cross section corresponds to the statistical (systematic) uncertainties. The number of observed data events (N_{data}) and simulated background events ($N_{\text{bg}}^{\text{MC}}$) are also shown

$Q^2 >$ (GeV²)	x range	x_c	$d\sigma/dx$ (pb)	N_{data}	$N_{\text{bg}}^{\text{MC}}$
185	$(0.63 - 1.00) \times 10^{-2}$	0.794×10^{-2}	$(8.66 \pm 0.05\,^{+0.15}_{-0.13}) \times 10^4$	39875	243.8
	$(0.10 - 0.16) \times 10^{-1}$	0.126×10^{-1}	$(5.80 \pm 0.03\,^{+0.08}_{-0.07}) \times 10^4$	48561	202.6
	$(0.16 - 0.25) \times 10^{-1}$	0.200×10^{-1}	$(3.60 \pm 0.02\,^{+0.04}_{-0.03}) \times 10^4$	49042	122.0
	$(0.25 - 0.40) \times 10^{-1}$	0.316×10^{-1}	$(2.11 \pm 0.01\,^{+0.05}_{-0.04}) \times 10^4$	49989	58.2
	$(0.40 - 0.63) \times 10^{-1}$	0.501×10^{-1}	$(1.24 \pm 0.01\,^{+0.03}_{-0.03}) \times 10^4$	41427	14.5
	$(0.63 - 1.00) \times 10^{-1}$	0.794×10^{-1}	$(7.05 \pm 0.04\,^{+0.18}_{-0.18}) \times 10^3$	37564	8.6
	$0.10 - 0.16$	0.126	$(3.96 \pm 0.02\,^{+0.14}_{-0.14}) \times 10^3$	34201	4.3
	$0.16 - 0.25$	0.200	$(2.03 \pm 0.02\,^{+0.09}_{-0.09}) \times 10^3$	19029	2.9
3000	$(0.40 - 0.63) \times 10^{-1}$	0.501×10^{-1}	$(1.89 \pm 0.08\,^{+0.08}_{-0.04}) \times 10^2$	640	7.4
	$(0.63 - 1.00) \times 10^{-1}$	0.794×10^{-1}	$(2.11 \pm 0.06\,^{+0.03}_{-0.02}) \times 10^2$	1211	5.8
	$0.10 - 0.16$	0.126	$(1.62 \pm 0.04\,^{+0.02}_{-0.01}) \times 10^2$	1522	4.3
	$0.16 - 0.25$	0.200	$(9.37 \pm 0.26\,^{+0.17}_{-0.15}) \times 10^1$	1306	2.9
	$0.25 - 0.40$	0.316	$(4.21 \pm 0.14\,^{+0.04}_{-0.04}) \times 10^1$	941	1.5
	$0.40 - 0.75$	0.687	$1.42 \pm 0.07\,^{+0.06}_{-0.05}$	381	0.0

Table 4 Systematic uncertainties with bin-to-bin correlations for $d\sigma/dx$ ($y < 0.9$) for $Q^2 > 185\,\text{GeV}^2$ and $Q^2 > 3000\,\text{GeV}^2$ for the reaction $e^- p \to e^- X$ ($\mathcal{L} = 169.9\,\text{pb}^{-1}$, $P_e = -0.03$). The left five columns of the table contain the Q^2 range, bin centre (x_c), the measured cross section, the statistical uncertainty and the total systematic uncertainty. The right eight columns of the table list the bin-to-bin correlated systematic uncertainties for δ_1–δ_7, and the systematic uncertainties summed in quadrature for δ_8–δ_{13}, as defined in Sect. 8. The upper and lower correlated uncertainties correspond to a positive or negative variation of a cut value for example. However, if this is not possible for a particular systematic, the uncertainty is symmetrised

$Q^2 >$ (GeV²)	x_c	$d\sigma/dx$(pb)	stat. (%)	sys. (%)	δ_1 (%)	δ_2 (%)	δ_3 (%)	δ_4 (%)	δ_5 (%)	δ_6 (%)	δ_7 (%)	δ_8–δ_{13} (%)
185	0.794×10^{-2}	8.66×10^4	± 0.5	$^{+1.7}_{-1.5}$	$^{+0.6}_{-0.1}$	$^{-0.7}_{+0.8}$	$^{+0.4}_{-0.4}$	$^{-1.0}_{+1.0}$	$^{+0.0}_{+0.0}$	$^{-0.1}_{+0.4}$	$^{+0.2}_{-0.2}$	$^{+0.7}_{-0.7}$
	0.126×10^{-1}	5.80×10^4	± 0.5	$^{+1.4}_{-1.3}$	$^{+0.4}_{-0.0}$	$^{-0.5}_{+0.6}$	$^{-0.0}_{+0.0}$	$^{-1.0}_{+1.0}$	$^{+0.0}_{+0.0}$	$^{-0.2}_{+0.3}$	$^{+0.2}_{-0.2}$	$^{+0.6}_{-0.6}$
	0.200×10^{-1}	3.60×10^4	± 0.5	$^{+1.1}_{-0.9}$	$^{+0.5}_{-0.0}$	$^{-0.4}_{+0.5}$	$^{-0.4}_{+0.4}$	$^{+0.4}_{-0.4}$	$^{+0.0}_{+0.0}$	$^{-0.2}_{+0.2}$	$^{+0.1}_{-0.1}$	$^{+0.6}_{-0.6}$
	0.316×10^{-1}	2.11×10^4	± 0.5	$^{+2.2}_{-2.1}$	$^{+0.4}_{-0.0}$	$^{-0.3}_{+0.4}$	$^{-1.0}_{+1.0}$	$^{+1.7}_{-1.7}$	$^{+0.0}_{+0.0}$	$^{-0.1}_{+0.2}$	$^{+0.1}_{-0.0}$	$^{+0.6}_{-0.7}$
	0.501×10^{-1}	1.24×10^4	± 0.5	$^{+2.3}_{-2.2}$	$^{+0.3}_{-0.0}$	$^{-0.2}_{+0.3}$	$^{-1.3}_{+1.3}$	$^{+1.7}_{-1.7}$	$^{+0.0}_{+0.0}$	$^{-0.0}_{+0.2}$	$^{+0.0}_{-0.0}$	$^{+0.6}_{-0.6}$
	0.794×10^{-1}	7.05×10^3	± 0.5	$^{+2.5}_{-2.5}$	$^{+0.3}_{-0.0}$	$^{-0.1}_{+0.3}$	$^{+1.8}_{-1.8}$	$^{+1.5}_{-1.5}$	$^{+0.0}_{+0.0}$	$^{+0.0}_{+0.0}$	$^{+0.0}_{-0.0}$	$^{+0.6}_{-0.7}$
	0.126	3.96×10^3	± 0.6	$^{+3.6}_{-3.6}$	$^{+0.3}_{+0.0}$	$^{-0.1}_{+0.2}$	$^{+3.1}_{-3.1}$	$^{+1.6}_{-1.6}$	$^{-0.1}_{+0.0}$	$^{-0.1}_{+0.1}$	$^{+0.0}_{-0.0}$	$^{+0.6}_{-0.6}$
	0.200	2.03×10^3	± 0.8	$^{+4.7}_{-4.5}$	$^{+0.3}_{-0.0}$	$^{-0.1}_{+0.2}$	$^{+4.4}_{-4.4}$	$^{+0.5}_{-0.5}$	$^{-0.3}_{+1.3}$	$^{-0.0}_{+0.1}$	$^{+0.0}_{-0.0}$	$^{+0.6}_{-0.6}$
3000	0.501×10^{-1}	1.89×10^2	± 4.0	$^{+4.2}_{-2.1}$	$^{+3.8}_{+0.0}$	$^{-0.2}_{+0.1}$	$^{-1.7}_{+1.7}$	$^{-0.1}_{+0.1}$	$^{+0.0}_{+0.0}$	$^{-0.4}_{-0.9}$	$^{+0.6}_{-0.5}$	$^{+0.7}_{-0.5}$
	0.794×10^{-1}	2.11×10^2	± 2.9	$^{+1.4}_{-1.1}$	$^{+1.0}_{-0.3}$	$^{-0.2}_{+0.3}$	$^{+0.5}_{-0.5}$	$^{+0.6}_{-0.6}$	$^{+0.0}_{+0.0}$	$^{-0.5}_{-0.3}$	$^{+0.5}_{-0.2}$	$^{+0.3}_{-0.4}$
	0.126	1.62×10^2	± 2.6	$^{+1.1}_{-0.5}$	$^{+1.0}_{-0.0}$	$^{-0.2}_{+0.3}$	$^{+0.0}_{-0.0}$	$^{-0.1}_{+0.1}$	$^{+0.0}_{+0.0}$	$^{-0.4}_{-0.1}$	$^{+0.1}_{-0.1}$	$^{+0.2}_{-0.2}$
	0.200	9.37×10^1	± 2.8	$^{+1.8}_{-1.6}$	$^{+1.0}_{-0.1}$	$^{-0.3}_{+0.2}$	$^{-1.5}_{+1.5}$	$^{+0.1}_{-0.1}$	$^{+0.0}_{+0.0}$	$^{+0.1}_{-0.3}$	$^{+0.2}_{-0.1}$	$^{+0.3}_{-0.3}$
	0.316	4.21×10^1	± 3.3	$^{+0.9}_{-1.0}$	$^{+0.6}_{-0.5}$	$^{-0.2}_{+0.2}$	$^{-0.2}_{+0.2}$	$^{-0.3}_{+0.3}$	$^{+0.0}_{+0.0}$	$^{+0.1}_{-0.5}$	$^{+0.1}_{-0.1}$	$^{+0.4}_{-0.5}$
	0.687	1.42	± 5.1	$^{+4.3}_{-3.9}$	$^{+1.9}_{+0.0}$	$^{-0.4}_{+0.6}$	$^{+3.6}_{-3.6}$	$^{-0.3}_{+0.3}$	$^{+0.3}_{+0.1}$	$^{-1.1}_{+1.1}$	$^{+0.0}_{-0.2}$	$^{+0.8}_{-0.9}$

single- and double-differential cross sections were chosen to be commensurate with the detector resolutions. The statistical uncertainties on the cross sections were calculated from the numbers of events observed in the bins, taking into account the statistical uncertainty of the MC simulation (signal and background). Poisson statistics were used for all bins.

636

Eur. Phys. J. C (2009) 62: 625–658

Table 5 The single differential cross section $d\sigma/dy$ for $Q^2 > 185\,\mathrm{GeV}^2$ and $Q^2 > 3000\,\mathrm{GeV}^2$ for the reaction $e^-p \to e^-X$ ($\mathcal{L} = 169.9\,\mathrm{pb}^{-1}$, $P_e = -0.03$). The Q^2 and bin range, bin centre (y_c) and measured cross section corrected to the electroweak Born level are shown. The first (second) error on the cross section corresponds to the statistical (systematic) uncertainties. The number of observed data events (N_{data}) and simulated background events ($N_{\mathrm{bg}}^{\mathrm{MC}}$) are also shown

$Q^2 >$ (GeV^2)	y range	y_c	$d\sigma/dy$ (pb)	N_{data}	$N_{\mathrm{bg}}^{\mathrm{MC}}$
185	0.00 – 0.05	0.025	$(1.62 \pm 0.01\,^{+0.07}_{-0.07}) \times 10^4$	77160	0.0
	0.05 – 0.10	0.075	$(8.04 \pm 0.03\,^{+0.20}_{-0.20}) \times 10^3$	63212	0.0
	0.10 – 0.15	0.125	$(5.65 \pm 0.03\,^{+0.07}_{-0.06}) \times 10^3$	44182	0.0
	0.15 – 0.20	0.175	$(4.33 \pm 0.03\,^{+0.05}_{-0.04}) \times 10^3$	32450	2.9
	0.20 – 0.25	0.225	$(3.54 \pm 0.02\,^{+0.03}_{-0.03}) \times 10^3$	25546	18.8
	0.25 – 0.30	0.275	$(2.97 \pm 0.02\,^{+0.04}_{-0.04}) \times 10^3$	20660	11.4
	0.30 – 0.35	0.325	$(2.59 \pm 0.02\,^{+0.04}_{-0.03}) \times 10^3$	17536	34.0
	0.35 – 0.40	0.375	$(2.23 \pm 0.02\,^{+0.03}_{-0.02}) \times 10^3$	14668	53.5
	0.40 – 0.45	0.425	$(1.98 \pm 0.02\,^{+0.03}_{-0.02}) \times 10^3$	12363	69.7
	0.45 – 0.50	0.475	$(1.76 \pm 0.02\,^{+0.03}_{-0.02}) \times 10^3$	10889	101.1
	0.50 – 0.55	0.525	$(1.60 \pm 0.02\,^{+0.03}_{-0.02}) \times 10^3$	9651	108.2
	0.55 – 0.60	0.575	$(1.47 \pm 0.02\,^{+0.03}_{-0.03}) \times 10^3$	8568	81.8
	0.60 – 0.65	0.625	$(1.33 \pm 0.02\,^{+0.04}_{-0.04}) \times 10^3$	7248	99.8
	0.65 – 0.70	0.675	$(1.21 \pm 0.02\,^{+0.04}_{-0.04}) \times 10^3$	5936	95.1
	0.70 – 0.75	0.725	$(1.12 \pm 0.02\,^{+0.06}_{-0.05}) \times 10^3$	4376	83.4
3000	0.05 – 0.10	0.075	$(3.46 \pm 0.22\,^{+0.07}_{-0.06}) \times 10^1$	242	0.0
	0.10 – 0.15	0.125	$(6.09 \pm 0.29\,^{+0.21}_{-0.18}) \times 10^1$	452	0.0
	0.15 – 0.20	0.175	$(6.49 \pm 0.29\,^{+0.10}_{-0.10}) \times 10^1$	493	0.0
	0.20 – 0.25	0.225	$(6.25 \pm 0.28\,^{+0.05}_{-0.07}) \times 10^1$	505	0.0
	0.25 – 0.30	0.275	$(6.39 \pm 0.28\,^{+0.11}_{-0.07}) \times 10^1$	525	0.0
	0.30 – 0.35	0.325	$(6.15 \pm 0.28\,^{+0.12}_{-0.07}) \times 10^1$	501	1.4
	0.35 – 0.40	0.375	$(5.22 \pm 0.25\,^{+0.13}_{-0.07}) \times 10^1$	425	0.0
	0.40 – 0.45	0.425	$(5.34 \pm 0.26\,^{+0.18}_{-0.17}) \times 10^1$	439	0.0
	0.45 – 0.50	0.475	$(5.19 \pm 0.25\,^{+0.14}_{-0.11}) \times 10^1$	421	0.0
	0.50 – 0.55	0.525	$(4.14 \pm 0.23\,^{+0.12}_{-0.13}) \times 10^1$	332	2.9
	0.55 – 0.60	0.575	$(4.28 \pm 0.23\,^{+0.05}_{-0.07}) \times 10^1$	335	0.0
	0.60 – 0.65	0.625	$(3.72 \pm 0.22\,^{+0.08}_{-0.18}) \times 10^1$	286	0.0
	0.65 – 0.70	0.675	$(3.93 \pm 0.23\,^{+0.09}_{-0.20}) \times 10^1$	301	3.0
	0.70 – 0.75	0.725	$(2.92 \pm 0.20\,^{+0.08}_{-0.08}) \times 10^1$	218	1.5
	0.75 – 0.80	0.775	$(2.98 \pm 0.20\,^{+0.10}_{-0.10}) \times 10^1$	219	1.5
	0.80 – 0.85	0.825	$(2.85 \pm 0.20\,^{+0.39}_{-0.12}) \times 10^1$	201	4.4
	0.85 – 0.90	0.875	$(2.57 \pm 0.21\,^{+0.14}_{-0.43}) \times 10^1$	173	8.7

8 Systematic uncertainties

Systematic uncertainties were estimated by re-calculating the cross sections after modifying the analysis to account for known uncertainties. The positive and negative deviations from the nominal cross-section values were added in quadrature separately to obtain the total positive and negative systematic uncertainty. The total systematic uncertainties for the bins used in the reduced cross section measurements are shown in Fig. 2. The description of each systematic uncertainty follows.

The following systematic uncertainties were treated as correlated between bins:

- $\{\delta_1\}$ to estimate the systematic uncertainty associated with the electron finder, an alternative electron-finding algorithm [49] was used and the results were compared to those using the nominal algorithm. In addition, to evaluate the systematic uncertainty of electron finding in an environment of densely packed energy deposits, the electron isolation requirement was varied by $\pm2\,\mathrm{GeV}$. These two checks were combined to give the systematic uncertainty from electron finding which was less than 1% for the bulk

Table 6 Systematic uncertainties with bin-to-bin correlations for $d\sigma/dy$ for $Q^2 > 185\,\mathrm{GeV}^2$ and $Q^2 > 3000\,\mathrm{GeV}^2$ for the reaction $e^-p \to e^-X$ ($\mathcal{L} = 169.9\,\mathrm{pb}^{-1}$, $P_e = -0.03$). The left five columns of the table contain the Q^2 range, bin centre (y_c), the measured cross section, the statistical uncertainty and the total systematic uncertainty. The right eight columns of the table list the bin-to-bin correlated system- atic uncertainties for δ_1–δ_7, and the systematic uncertainties summed in quadrature for δ_8–δ_{13}, as defined in Sect. 8. The upper and lower correlated uncertainties correspond to a positive or negative variation of a cut value for example. However, if this is not possible for a partic- ular systematic, the uncertainty is symmetrised

$Q^2 >$ (GeV²)	y_c	$d\sigma/dy$(pb)	stat. (%)	sys. (%)	δ_1 (%)	δ_2 (%)	δ_3 (%)	δ_4 (%)	δ_5 (%)	δ_6 (%)	δ_7 (%)	δ_8–δ_{13} (%)
185	0.025	1.62×10^4	± 0.4	$^{+4.1}_{-4.1}$	$^{+0.1}_{-0.0}$	$^{-0.1}_{+0.2}$	$^{+3.6}_{-3.6}$	$^{+1.7}_{-1.7}$	$^{-0.1}_{+0.5}$	$^{-0.0}_{+0.2}$	$^{+0.0}_{+0.0}$	$^{+0.7}_{-0.8}$
	0.075	8.04×10^3	± 0.4	$^{+2.5}_{-2.5}$	$^{+0.4}_{-0.0}$	$^{-0.2}_{+0.3}$	$^{-1.5}_{+1.5}$	$^{+1.9}_{-1.9}$	$^{+0.0}_{-0.0}$	$^{+0.0}_{+0.2}$	$^{+0.0}_{+0.0}$	$^{+0.7}_{-0.7}$
	0.125	5.65×10^3	± 0.5	$^{+1.2}_{-1.1}$	$^{+0.5}_{-0.0}$	$^{-0.3}_{+0.4}$	$^{-0.5}_{+0.5}$	$^{+0.7}_{-0.7}$	$^{+0.0}_{+0.0}$	$^{-0.1}_{+0.2}$	$^{+0.0}_{+0.0}$	$^{+0.6}_{-0.6}$
	0.175	4.33×10^3	± 0.6	$^{+1.1}_{-1.0}$	$^{+0.4}_{-0.0}$	$^{-0.4}_{+0.5}$	$^{-0.2}_{+0.2}$	$^{-0.6}_{+0.6}$	$^{+0.0}_{+0.0}$	$^{+0.0}_{+0.2}$	$^{+0.0}_{-0.0}$	$^{+0.5}_{-0.7}$
	0.225	3.54×10^3	± 0.7	$^{+1.0}_{-0.8}$	$^{+0.4}_{+0.0}$	$^{-0.4}_{+0.5}$	$^{+0.1}_{-0.1}$	$^{-0.4}_{+0.4}$	$^{+0.0}_{+0.0}$	$^{-0.1}_{+0.2}$	$^{+0.0}_{-0.0}$	$^{+0.6}_{-0.5}$
	0.275	2.97×10^3	± 0.7	$^{+1.2}_{-1.2}$	$^{+0.4}_{-0.0}$	$^{-0.4}_{+0.5}$	$^{-0.2}_{+0.2}$	$^{-0.8}_{+0.8}$	$^{+0.0}_{+0.0}$	$^{-0.2}_{+0.2}$	$^{+0.0}_{+0.0}$	$^{+0.6}_{-0.7}$
	0.325	2.59×10^3	± 0.8	$^{+1.4}_{-1.2}$	$^{+0.7}_{-0.1}$	$^{-0.4}_{+0.4}$	$^{+0.2}_{-0.2}$	$^{-1.0}_{+1.0}$	$^{+0.0}_{+0.0}$	$^{-0.1}_{+0.4}$	$^{+0.1}_{-0.1}$	$^{+0.5}_{-0.6}$
	0.375	2.23×10^3	± 0.9	$^{+1.1}_{-0.8}$	$^{+0.7}_{-0.0}$	$^{-0.3}_{+0.5}$	$^{-0.0}_{+0.0}$	$^{+0.1}_{-0.1}$	$^{+0.0}_{+0.0}$	$^{-0.2}_{+0.3}$	$^{+0.1}_{-0.1}$	$^{+0.6}_{-0.7}$
	0.425	1.98×10^3	± 1.0	$^{+1.4}_{-1.0}$	$^{+0.9}_{-0.0}$	$^{-0.3}_{+0.5}$	$^{+0.8}_{-0.8}$	$^{-0.1}_{+0.1}$	$^{+0.0}_{+0.0}$	$^{-0.1}_{-0.0}$	$^{+0.2}_{-0.2}$	$^{+0.5}_{-0.5}$
	0.475	1.76×10^3	± 1.0	$^{+1.9}_{-1.0}$	$^{+1.7}_{-0.2}$	$^{-0.3}_{+0.5}$	$^{-0.3}_{+0.3}$	$^{+0.1}_{-0.1}$	$^{+0.0}_{+0.0}$	$^{+0.1}_{+0.2}$	$^{+0.4}_{-0.4}$	$^{+0.6}_{-0.7}$
	0.525	1.60×10^3	± 1.1	$^{+1.6}_{-1.3}$	$^{+0.9}_{-0.0}$	$^{-0.5}_{+0.6}$	$^{+0.6}_{-0.6}$	$^{-0.8}_{+0.8}$	$^{+0.0}_{+0.0}$	$^{-0.3}_{+0.2}$	$^{+0.5}_{-0.5}$	$^{+0.5}_{-0.4}$
	0.575	1.47×10^3	± 1.2	$^{+2.3}_{-2.3}$	$^{+0.1}_{-0.3}$	$^{-0.7}_{+0.9}$	$^{+0.8}_{-0.8}$	$^{-1.8}_{+1.8}$	$^{+0.0}_{+0.0}$	$^{-0.1}_{+0.1}$	$^{+0.4}_{-0.4}$	$^{+0.4}_{-0.5}$
	0.625	1.33×10^3	± 1.3	$^{+3.3}_{-3.2}$	$^{+0.5}_{-0.1}$	$^{-1.5}_{+1.6}$	$^{-1.8}_{+1.8}$	$^{-2.1}_{+2.1}$	$^{+0.0}_{+0.0}$	$^{-0.3}_{+0.1}$	$^{+0.6}_{-0.6}$	$^{+0.4}_{-0.4}$
	0.675	1.21×10^3	± 1.4	$^{+3.5}_{-3.2}$	$^{+0.4}_{-0.9}$	$^{-2.7}_{+3.2}$	$^{+0.6}_{-0.6}$	$^{-0.8}_{+0.8}$	$^{+0.0}_{+0.0}$	$^{-0.1}_{+0.4}$	$^{+0.7}_{-0.7}$	$^{+0.4}_{-0.5}$
	0.725	1.12×10^3	± 1.6	$^{+5.7}_{-4.7}$	$^{+0.2}_{-0.1}$	$^{-4.3}_{+5.3}$	$^{+0.1}_{-0.1}$	$^{-1.6}_{+1.6}$	$^{+0.0}_{+0.0}$	$^{-0.1}_{+0.2}$	$^{+0.8}_{-0.8}$	$^{+0.8}_{-0.8}$
3000	0.075	3.46×10^1	± 6.5	$^{+1.9}_{-1.7}$	$^{+0.1}_{-0.0}$	$^{-0.4}_{+0.5}$	$^{-0.2}_{+0.2}$	$^{-0.3}_{+0.3}$	$^{+1.3}_{-0.1}$	$^{-1.0}_{+0.5}$	$^{+0.0}_{+0.0}$	$^{+1.2}_{-1.3}$
	0.125	6.09×10^1	± 4.7	$^{+3.4}_{-2.9}$	$^{+1.4}_{-0.0}$	$^{-0.2}_{+0.3}$	$^{+2.5}_{-2.5}$	$^{-1.3}_{+1.3}$	$^{+0.0}_{+0.0}$	$^{+1.0}_{-0.1}$	$^{+0.0}_{+0.0}$	$^{+0.4}_{-0.6}$
	0.175	6.49×10^1	± 4.5	$^{+1.5}_{-1.5}$	$^{+0.1}_{-0.4}$	$^{-0.3}_{+0.3}$	$^{-1.3}_{+1.3}$	$^{-0.5}_{+0.5}$	$^{+0.0}_{+0.0}$	$^{+0.1}_{-0.2}$	$^{+0.0}_{+0.0}$	$^{+0.5}_{-0.3}$
	0.225	6.25×10^1	± 4.5	$^{+0.8}_{-1.2}$	$^{+0.2}_{-0.5}$	$^{-0.2}_{+0.3}$	$^{+0.5}_{-0.5}$	$^{+0.2}_{-0.2}$	$^{+0.0}_{+0.0}$	$^{-0.9}_{-0.1}$	$^{+0.0}_{+0.0}$	$^{+0.5}_{-0.3}$
	0.275	6.39×10^1	± 4.4	$^{+1.8}_{-1.1}$	$^{+1.5}_{-0.1}$	$^{-0.2}_{+0.2}$	$^{-0.9}_{+0.9}$	$^{-0.1}_{+0.1}$	$^{+0.0}_{+0.0}$	$^{-0.6}_{-0.4}$	$^{+0.0}_{+0.0}$	$^{+0.4}_{-0.3}$
	0.325	6.15×10^1	± 4.5	$^{+2.0}_{-1.2}$	$^{+1.6}_{-0.1}$	$^{-0.2}_{+0.3}$	$^{+0.5}_{-0.5}$	$^{+0.8}_{-0.8}$	$^{+0.0}_{+0.0}$	$^{+0.5}_{+0.2}$	$^{+0.1}_{-0.1}$	$^{+0.4}_{-0.6}$
	0.375	5.22×10^1	± 4.9	$^{+2.5}_{-1.3}$	$^{+2.3}_{-0.2}$	$^{-0.2}_{+0.3}$	$^{+0.6}_{-0.6}$	$^{+0.8}_{-0.8}$	$^{+0.0}_{+0.0}$	$^{+0.1}_{+0.0}$	$^{+0.0}_{+0.0}$	$^{+0.4}_{-0.7}$
	0.425	5.34×10^1	± 4.8	$^{+3.3}_{-3.1}$	$^{+1.0}_{-0.3}$	$^{-0.2}_{+0.3}$	$^{-3.0}_{+3.0}$	$^{+0.9}_{-0.9}$	$^{+0.0}_{+0.0}$	$^{-0.3}_{-0.3}$	$^{+0.0}_{+0.0}$	$^{+0.4}_{-0.4}$
	0.475	5.19×10^1	± 4.9	$^{+2.7}_{-2.1}$	$^{+2.1}_{+0.0}$	$^{-0.2}_{+0.3}$	$^{+1.5}_{-1.5}$	$^{+0.9}_{-0.9}$	$^{+0.0}_{+0.0}$	$^{-0.0}_{-0.9}$	$^{+0.0}_{+0.0}$	$^{+0.3}_{-0.7}$
	0.525	4.14×10^1	± 5.5	$^{+3.0}_{-3.2}$	$^{+0.2}_{-0.8}$	$^{-0.3}_{+0.3}$	$^{-2.8}_{+2.8}$	$^{+0.0}_{-0.0}$	$^{+0.0}_{+0.0}$	$^{-0.5}_{+0.4}$	$^{+0.4}_{-0.4}$	$^{+0.9}_{-1.0}$
	0.575	4.28×10^1	± 5.5	$^{+1.2}_{-1.5}$	$^{+0.4}_{-0.6}$	$^{-0.2}_{+0.2}$	$^{+1.1}_{-1.1}$	$^{+0.0}_{-0.0}$	$^{+0.0}_{+0.0}$	$^{-0.8}_{-0.2}$	$^{+0.0}_{+0.0}$	$^{+0.3}_{-0.4}$
	0.625	3.72×10^1	± 5.9	$^{+2.1}_{-4.9}$	$^{+0.9}_{-4.5}$	$^{-0.2}_{+0.3}$	$^{-1.8}_{+1.8}$	$^{-0.6}_{+0.6}$	$^{+0.0}_{+0.0}$	$^{-0.6}_{+0.0}$	$^{+0.0}_{+0.0}$	$^{+0.5}_{-0.3}$
	0.675	3.93×10^1	± 5.9	$^{+2.2}_{-5.0}$	$^{+1.8}_{-4.9}$	$^{-0.2}_{+0.2}$	$^{+0.9}_{-0.9}$	$^{+0.5}_{-0.5}$	$^{+0.0}_{+0.0}$	$^{-0.6}_{+0.2}$	$^{+0.4}_{-0.4}$	$^{+0.7}_{-0.6}$
	0.725	2.92×10^1	± 6.8	$^{+2.8}_{-2.8}$	$^{+0.1}_{-2.0}$	$^{-0.2}_{+0.2}$	$^{-1.5}_{+1.5}$	$^{-1.0}_{+1.0}$	$^{+0.0}_{+0.0}$	$^{-0.7}_{+1.8}$	$^{+0.3}_{-0.3}$	$^{+1.2}_{-0.7}$
	0.775	2.98×10^1	± 6.8	$^{+3.4}_{-3.4}$	$^{+3.1}_{+0.0}$	$^{-0.2}_{+0.2}$	$^{+0.9}_{-0.9}$	$^{+0.5}_{-0.5}$	$^{+0.0}_{+0.0}$	$^{-0.6}_{-3.1}$	$^{+0.3}_{-0.3}$	$^{+0.7}_{-0.7}$
	0.825	2.85×10^1	± 7.2	$^{+13.8}_{-4.1}$	$^{+13.7}_{-0.5}$	$^{-0.1}_{+0.2}$	$^{+0.2}_{-0.2}$	$^{-0.0}_{+0.0}$	$^{+0.0}_{+0.0}$	$^{+1.6}_{-3.9}$	$^{+1.1}_{-0.9}$	$^{+0.6}_{-0.5}$
	0.875	2.57×10^1	± 8.2	$^{+5.3}_{-16.8}$	$^{+2.1}_{-16.1}$	$^{-1.5}_{+0.5}$	$^{+0.6}_{-0.6}$	$^{+0.2}_{-0.2}$	$^{+0.0}_{+0.0}$	$^{-3.9}_{-0.1}$	$^{+4.6}_{-2.1}$	$^{+1.4}_{-2.0}$

of the phase space. In the double-differential cross-section bins at high Q^2 and high y, the uncertainty was about 4%, and increased to 18% in the high-y bins of $d\sigma/dy$ for $Q^2 > 3000\,\mathrm{GeV}^2$;

- {δ_2} the variation of the electron energy scale by $\pm 2\%$ in the MC resulted in changes less than 1% in the cross sections over most of the kinematic region due to the use of the DA reconstruction method. The effect was at most 5% at high y in $d\sigma/dy$;

- {δ_3} the nominal procedure to calculate $\gamma_{\max}$ used MC sample with a similar Q^2 cut as in the NC event selec- tion. To account for the Q^2 dependence of $\gamma_{\max}$ in the backsplash removal procedure, it was also derived with higher Q^2 thresholds and the results were compared. The effect on the cross sections was generally less than 1%, but increased to typically 5% in the high-x bins;

- {δ_4} the systematic uncertainty in the parton-shower scheme was evaluated by using the MEPS model of LEPTO

Fig. 3 The e^-p NC DIS cross sections: (**a**) $d\sigma/dQ^2$ for $y < 0.9$ and the ratio to the SM prediction, (**b**) $d\sigma/dx$ for $Q^2 > 185\,\text{GeV}^2$ and $Q^2 > 3000\,\text{GeV}^2$ for $y < 0.9$ and (**c**) $d\sigma/dy$ for $Q^2 > 185\,\text{GeV}^2$ and $Q^2 > 3000\,\text{GeV}^2$. The *closed circles* represent data points in which the *inner error bars* show the statistical uncertainty while the *outer bars* show the statistical and systematic uncertainties added in quadrature. The *curves* show the predictions of the SM evaluated using the ZEUS-JETS PDFs at a polarisation corresponding to the residual polarisation in the data and the *shaded band* shows the uncertainties from the ZEUS-JETS PDFs
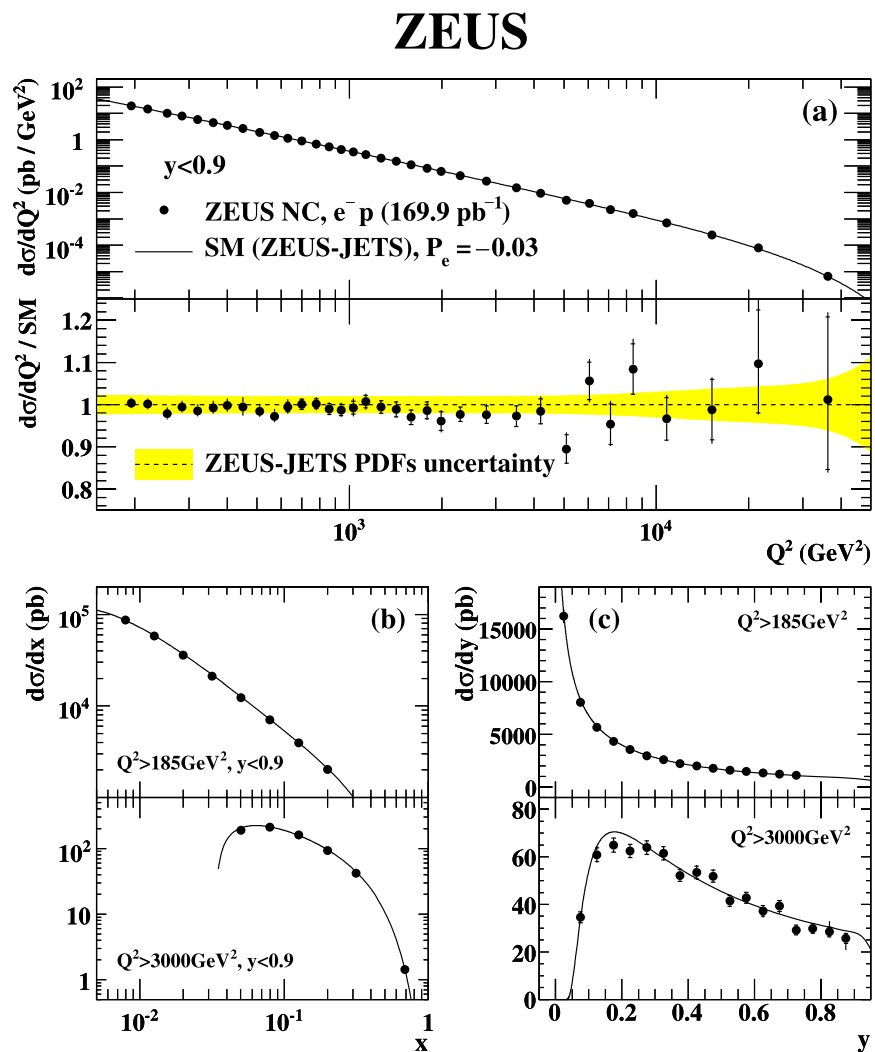
to calculate the acceptance instead of ARIADNE.[3] The uncertainty was typically within $\pm2\%$ but reached 5% in some bins of the double-differential cross sections;

- $\{\delta_5\}$ the cut of 20 cm on the projected radius of the hadronic angle onto the FCAL was varied by ±3 cm. The cross sections typically changed less than $\pm1\%$. The effect increased up to $\pm6\%$ for the highest x bins of both $d\sigma/dx$ and the double-differential cross section;

- $\{\delta_6\}$ the uncertainty due to "overlay" events, in which a normal DIS event coincided with additional energy deposits in the RCAL from some other interaction, and photoproduction contamination was estimated by narrowing or widening the $38 < \delta < 65$ GeV interval symmetrically by ±4 GeV. The effect on the cross sections was typically

below 2%. In a few high-Q^2 bins the uncertainty was as large as 4%;

- $\{\delta_7\}$ systematic uncertainties arising from the normalisation of the photoproduction background were estimated by changing the background normalisation by $\pm40\%$. In addition, systematic uncertainties arising from the estimation of the photoproduction background were also estimated by reducing the cut on y_e to $y_e < 0.9$. The resulting changes in the cross sections were typically below $\pm1\%$, and at most 2% in the high-Q^2 bins of the double-differential cross-section.

The following systematic uncertainties are either small or not correlated between bins:

- $\{\delta_8\}$ the energy resolution used in the MC for the scattered electron was varied by $\pm1\%$, and the effect was less than 0.5% over the full kinematic range;

- $\{\delta_9\}$ to reflect uncertainties in the alignment of the CAL with respect to the CTD, the electron scattering angle was

---

[3]Since the simulation of parton-shower scheme also changes the description of the electron isolation, the comparison was made without the electron isolation requirement to prevent double counting of systematic errors.

Eur. Phys. J. C (2009) 62: 625–658

639

Table 7 The reduced cross section $\tilde{\sigma}$ for the reaction $e^- p \rightarrow e^- X$ ($\mathcal{L} = 169.9\,\mathrm{pb}^{-1}$, $P_e = 0$). The bin range, bin centre (Q_c^2 and x_c) and measured cross section corrected to the electroweak Born level are shown. The first (second) error on the cross section corresponds to the statistical (systematic) uncertainties. The number of observed data events (N_{data}) and simulated background events ($N_{\mathrm{bg}}^{\mathrm{MC}}$) are also shown

Q^2 range (GeV^2)	Q_c^2 (GeV^2)	x range	x_c	$\tilde{\sigma}$	N_{data}	$N_{\mathrm{bg}}^{\mathrm{MC}}$
185 – 240	200	0.0037 – 0.006	0.005	$1.092 \pm 0.010\,^{+0.014}_{-0.011}$	14079	88.0
		0.006 – 0.01	0.008	$0.922 \pm 0.008\,^{+0.018}_{-0.018}$	16389	23.3
		0.01 – 0.017	0.013	$0.783 \pm 0.006\,^{+0.013}_{-0.013}$	17628	2.9
		0.017 – 0.025	0.021	$0.662 \pm 0.006\,^{+0.014}_{-0.014}$	12598	0.0
		0.025 – 0.037	0.032	$0.561 \pm 0.006\,^{+0.023}_{-0.022}$	11904	0.0
		0.037 – 0.06	0.05	$0.500 \pm 0.005\,^{+0.012}_{-0.012}$	11002	0.0
		0.06 – 0.12	0.08	$0.441 \pm 0.004\,^{+0.024}_{-0.024}$	14235	0.0
		0.12 – 0.25	0.18	$0.334 \pm 0.004\,^{+0.018}_{-0.018}$	7372	0.0
240 – 310	250	0.006 – 0.01	0.008	$0.936 \pm 0.010\,^{+0.014}_{-0.012}$	11341	26.1
		0.01 – 0.017	0.013	$0.793 \pm 0.008\,^{+0.013}_{-0.012}$	12602	6.0
		0.017 – 0.025	0.021	$0.656 \pm 0.008\,^{+0.011}_{-0.009}$	8935	1.5
		0.025 – 0.037	0.032	$0.565 \pm 0.007\,^{+0.019}_{-0.019}$	8745	0.0
		0.037 – 0.06	0.05	$0.494 \pm 0.006\,^{+0.017}_{-0.016}$	8494	0.0
		0.06 – 0.12	0.08	$0.429 \pm 0.005\,^{+0.022}_{-0.022}$	10350	0.0
		0.12 – 0.25	0.18	$0.331 \pm 0.004\,^{+0.016}_{-0.015}$	6985	0.0
310 – 410	350	0.006 – 0.01	0.008	$0.969 \pm 0.013\,^{+0.021}_{-0.015}$	6903	71.5
		0.01 – 0.017	0.013	$0.821 \pm 0.009\,^{+0.016}_{-0.010}$	9505	8.8
		0.017 – 0.025	0.021	$0.693 \pm 0.009\,^{+0.006}_{-0.004}$	7274	0.0
		0.025 – 0.037	0.032	$0.605 \pm 0.008\,^{+0.012}_{-0.011}$	7071	0.0
		0.037 – 0.06	0.05	$0.509 \pm 0.006\,^{+0.014}_{-0.013}$	7509	0.0
		0.06 – 0.12	0.08	$0.435 \pm 0.005\,^{+0.009}_{-0.009}$	8417	0.0
		0.12 – 0.25	0.18	$0.314 \pm 0.004\,^{+0.020}_{-0.020}$	6571	0.0
410 – 530	450	0.006 – 0.01	0.008	$0.993 \pm 0.014\,^{+0.023}_{-0.021}$	5334	84.2
		0.01 – 0.017	0.013	$0.857 \pm 0.013\,^{+0.010}_{-0.009}$	4719	16.1
		0.017 – 0.025	0.021	$0.685 \pm 0.012\,^{+0.013}_{-0.012}$	3668	1.3
		0.025 – 0.037	0.032	$0.591 \pm 0.009\,^{+0.011}_{-0.010}$	4173	0.0
		0.037 – 0.06	0.05	$0.519 \pm 0.007\,^{+0.013}_{-0.012}$	5225	0.0
		0.06 – 0.1	0.08	$0.432 \pm 0.007\,^{+0.009}_{-0.008}$	4249	0.0
		0.1 – 0.17	0.13	$0.359 \pm 0.006\,^{+0.018}_{-0.018}$	3727	0.0
		0.17 – 0.3	0.25	$0.262 \pm 0.005\,^{+0.015}_{-0.014}$	2819	0.0
530 – 710	650	0.01 – 0.017	0.013	$0.878 \pm 0.013\,^{+0.013}_{-0.007}$	5347	59.5
		0.017 – 0.025	0.021	$0.755 \pm 0.013\,^{+0.009}_{-0.008}$	3568	5.7
		0.025 – 0.037	0.032	$0.597 \pm 0.012\,^{+0.007}_{-0.006}$	2740	1.3
		0.037 – 0.06	0.05	$0.512 \pm 0.010\,^{+0.005}_{-0.005}$	2908	0.0
		0.06 – 0.1	0.08	$0.424 \pm 0.009\,^{+0.010}_{-0.010}$	2418	0.0
		0.1 – 0.17	0.13	$0.361 \pm 0.008\,^{+0.010}_{-0.009}$	2201	0.0
		0.17 – 0.3	0.25	$0.253 \pm 0.006\,^{+0.017}_{-0.017}$	1887	0.0
710 – 900	800	0.009 – 0.017	0.013	$0.860 \pm 0.016\,^{+0.015}_{-0.016}$	3339	49.4
		0.017 – 0.025	0.021	$0.733 \pm 0.016\,^{+0.008}_{-0.006}$	2360	3.1
		0.025 – 0.037	0.032	$0.634 \pm 0.013\,^{+0.009}_{-0.009}$	2453	7.4
		0.037 – 0.06	0.05	$0.522 \pm 0.010\,^{+0.011}_{-0.011}$	2719	0.0
		0.06 – 0.1	0.08	$0.448 \pm 0.010\,^{+0.012}_{-0.012}$	2332	0.0
		0.1 – 0.17	0.13	$0.377 \pm 0.009\,^{+0.004}_{-0.004}$	1903	0.0
		0.17 – 0.3	0.25	$0.257 \pm 0.007\,^{+0.009}_{-0.009}$	1405	0.0

640

Eur. Phys. J. C (2009) 62: 625–658

Table 7 (*Continued*)

Q^2 range (GeV^2)	Q^2_c (GeV^2)	x range	x_c	$\tilde{\sigma}$	N_{data}	$N^{\text{MC}}_{\text{bg}}$
900 – 1300	1200	0.01 – 0.017	0.014	$0.892 \pm 0.020\ ^{+0.022}_{-0.029}$	2217	75.7
		0.017 – 0.025	0.021	$0.791 \pm 0.016\ ^{+0.015}_{-0.013}$	2553	23.2
		0.025 – 0.037	0.032	$0.608 \pm 0.013\ ^{+0.007}_{-0.007}$	2478	11.7
		0.037 – 0.06	0.05	$0.551 \pm 0.010\ ^{+0.007}_{-0.008}$	3197	1.3
		0.06 – 0.1	0.08	$0.456 \pm 0.009\ ^{+0.006}_{-0.006}$	3039	0.0
		0.1 – 0.17	0.13	$0.375 \pm 0.008\ ^{+0.004}_{-0.004}$	2451	0.0
		0.17 – 0.3	0.25	$0.247 \pm 0.006\ ^{+0.006}_{-0.006}$	1872	0.0
		0.3 – 0.53	0.4	$0.125 \pm 0.005\ ^{+0.010}_{-0.007}$	641	0.0
1300 – 1800	1500	0.017 – 0.025	0.021	$0.765 \pm 0.023\ ^{+0.020}_{-0.018}$	1273	58.3
		0.025 – 0.037	0.032	$0.629 \pm 0.017\ ^{+0.005}_{-0.004}$	1402	7.1
		0.037 – 0.06	0.05	$0.522 \pm 0.013\ ^{+0.005}_{-0.004}$	1756	1.4
		0.06 – 0.1	0.08	$0.477 \pm 0.011\ ^{+0.005}_{-0.005}$	1887	0.0
		0.1 – 0.15	0.13	$0.376 \pm 0.011\ ^{+0.008}_{-0.007}$	1201	0.0
		0.15 – 0.23	0.18	$0.312 \pm 0.010\ ^{+0.006}_{-0.005}$	1028	0.0
		0.23 – 0.35	0.25	$0.264 \pm 0.010\ ^{+0.005}_{-0.005}$	729	0.0
		0.35 – 0.53	0.4	$0.128 \pm 0.007\ ^{+0.011}_{-0.006}$	318	0.0
1800 – 2500	2000	0.023 – 0.037	0.032	$0.636 \pm 0.021\ ^{+0.016}_{-0.009}$	977	19.1
		0.037 – 0.06	0.05	$0.571 \pm 0.016\ ^{+0.005}_{-0.005}$	1229	0.0
		0.06 – 0.1	0.08	$0.459 \pm 0.013\ ^{+0.009}_{-0.009}$	1246	1.3
		0.1 – 0.15	0.13	$0.374 \pm 0.013\ ^{+0.003}_{-0.004}$	883	0.0
		0.15 – 0.23	0.18	$0.309 \pm 0.012\ ^{+0.002}_{-0.006}$	723	0.0
		0.23 – 0.35	0.25	$0.247 \pm 0.011\ ^{+0.004}_{-0.004}$	502	0.0
		0.35 – 0.53	0.4	$0.120 \pm 0.008\ ^{+0.004}_{-0.005}$	239	0.0
2500 – 3500	3000	0.037 – 0.06	0.05	$0.581 \pm 0.021\ ^{+0.012}_{-0.006}$	777	9.0
		0.06 – 0.1	0.08	$0.507 \pm 0.017\ ^{+0.006}_{-0.006}$	902	1.5
		0.1 – 0.15	0.13	$0.378 \pm 0.015\ ^{+0.004}_{-0.003}$	623	0.0
		0.15 – 0.23	0.18	$0.320 \pm 0.014\ ^{+0.004}_{-0.004}$	528	0.0
		0.23 – 0.35	0.25	$0.286 \pm 0.014\ ^{+0.021}_{-0.021}$	427	0.0
		0.35 – 0.53	0.4	$0.135 \pm 0.010\ ^{+0.005}_{-0.005}$	185	0.0
		0.53 – 0.75	0.65	$0.017\ ^{+0.002}_{-0.002}\ ^{+0.002}_{-0.002}$	62	0.0
3500 – 5600	5000	0.04 – 0.1	0.08	$0.527 \pm 0.017\ ^{+0.009}_{-0.005}$	1001	7.3
		0.1 – 0.15	0.13	$0.463 \pm 0.019\ ^{+0.005}_{-0.004}$	610	1.4
		0.15 – 0.23	0.18	$0.340 \pm 0.015\ ^{+0.003}_{-0.002}$	499	0.0
		0.23 – 0.35	0.25	$0.243 \pm 0.014\ ^{+0.004}_{-0.003}$	318	0.0
		0.35 – 0.53	0.4	$0.140 \pm 0.011\ ^{+0.009}_{-0.009}$	176	0.0
5600 – 9000	8000	0.07 – 0.15	0.13	$0.560 \pm 0.024\ ^{+0.006}_{-0.010}$	582	4.4
		0.15 – 0.23	0.18	$0.433 \pm 0.023\ ^{+0.011}_{-0.012}$	346	0.0
		0.23 – 0.35	0.25	$0.309 \pm 0.020\ ^{+0.012}_{-0.012}$	232	0.0
		0.35 – 0.53	0.4	$0.114\ ^{+0.014}_{-0.012}\ ^{+0.008}_{-0.008}$	87	0.0
		0.53 – 0.75	0.65	$0.019\ ^{+0.004}_{-0.003}\ ^{+0.001}_{-0.001}$	35	0.0
9000 – 15000	12000	0.09 – 0.23	0.18	$0.464 \pm 0.028\ ^{+0.006}_{-0.018}$	275	1.4
		0.23 – 0.35	0.25	$0.353 \pm 0.029\ ^{+0.010}_{-0.008}$	149	0.0
		0.35 – 0.53	0.4	$0.156\ ^{+0.021}_{-0.018}\ ^{+0.007}_{-0.006}$	72	0.0
15000 – 25000	20000	0.15 – 0.35	0.25	$0.461 \pm 0.043\ ^{+0.028}_{-0.017}$	129	4.4
		0.35 – 0.75	0.4	$0.183\ ^{+0.030}_{-0.026}\ ^{+0.009}_{-0.007}$	48	0.0
25000 – 50000	30000	0.25 – 0.75	0.4	$0.237\ ^{+0.042}_{-0.036}\ ^{+0.016}_{-0.014}$	42	0.0

Table 8 Systematic uncertainties with bin-to-bin correlations for the reduced cross section $\tilde{\sigma}$ for the reaction $e^- p \rightarrow e^- X$ ($\mathcal{L} = 169.9\,\text{pb}^{-1}$, $P_e = 0$). The left five columns of the table contain the bin centres, Q_c^2 and x_c, the measured cross section, the statistical uncertainty and the total systematic uncertainty. The right eight columns of the table list the bin-to-bin correlated systematic uncertainties for δ_1–δ_7, and the systematic uncertainties summed in quadrature for δ_8–δ_{13}, as defined in Sect. 8. The upper and lower correlated uncertainties correspond to a positive or negative variation of a cut value for example. However, if this is not possible for a particular systematic, the uncertainty is symmetrised

Q_c^2 (GeV²)	x_c	$\tilde{\sigma}$	stat. (%)	sys. (%)	δ_1 (%)	δ_2 (%)	δ_3 (%)	δ_4 (%)	δ_5 (%)	δ_6 (%)	δ_7 (%)	δ_8–δ_{13} (%)
200	0.005	1.092	±0.9	$^{+1.3}_{-1.0}$	$^{+0.7}_{-0.0}$	$^{-0.4}_{+0.6}$	$^{+0.4}_{-0.4}$	$^{-0.4}_{+0.4}$	$^{+0.0}_{+0.0}$	$^{+0.1}_{-0.1}$	$^{+0.3}_{-0.3}$	$^{+0.7}_{-0.7}$
	0.008	0.922	±0.8	$^{+1.9}_{-1.9}$	$^{+0.3}_{-0.0}$	$^{-0.4}_{+0.5}$	$^{+0.2}_{-0.2}$	$^{-1.6}_{+1.6}$	$^{+0.0}_{+0.0}$	$^{+0.1}_{+0.4}$	$^{+0.1}_{-0.1}$	$^{+0.8}_{-1.0}$
	0.013	0.783	±0.8	$^{+1.7}_{-1.6}$	$^{+0.2}_{+0.0}$	$^{-0.5}_{+0.5}$	$^{-0.2}_{+0.2}$	$^{-1.3}_{+1.3}$	$^{+0.0}_{+0.0}$	$^{+0.0}_{+0.4}$	$^{+0.0}_{-0.0}$	$^{+0.8}_{-0.9}$
	0.021	0.662	±1.0	$^{+2.1}_{-2.1}$	$^{+0.4}_{+0.0}$	$^{-0.3}_{+0.5}$	$^{-1.6}_{+1.6}$	$^{+0.9}_{-0.9}$	$^{+0.0}_{+0.0}$	$^{-0.1}_{+0.1}$	$^{+0.0}_{+0.0}$	$^{+0.8}_{-0.9}$
	0.032	0.561	±1.0	$^{+4.0}_{-4.0}$	$^{+0.1}_{-0.0}$	$^{-0.3}_{+0.4}$	$^{-1.5}_{+1.5}$	$^{+3.6}_{-3.6}$	$^{+0.0}_{+0.0}$	$^{+0.2}_{+0.4}$	$^{+0.0}_{+0.0}$	$^{+0.8}_{-0.8}$
	0.05	0.500	±1.0	$^{+2.5}_{-2.4}$	$^{+0.0}_{-0.3}$	$^{-0.2}_{+0.3}$	$^{-0.5}_{+0.5}$	$^{+2.2}_{-2.2}$	$^{+0.0}_{+0.0}$	$^{+0.0}_{+0.3}$	$^{+0.0}_{+0.0}$	$^{+1.0}_{-0.9}$
	0.08	0.441	±0.9	$^{+5.5}_{-5.5}$	$^{+0.0}_{-0.1}$	$^{-0.2}_{+0.2}$	$^{+5.0}_{-5.0}$	$^{+2.0}_{-2.0}$	$^{-0.0}_{+0.0}$	$^{-0.0}_{+0.1}$	$^{+0.0}_{+0.0}$	$^{+0.8}_{-1.0}$
	0.18	0.334	±1.3	$^{+5.4}_{-5.4}$	$^{+0.1}_{+0.0}$	$^{-0.1}_{+0.2}$	$^{+5.3}_{-5.3}$	$^{+0.5}_{-0.5}$	$^{+0.7}_{+0.2}$	$^{-0.1}_{+0.1}$	$^{+0.0}_{+0.0}$	$^{+0.7}_{-0.9}$
250	0.008	0.936	±1.0	$^{+1.5}_{-1.3}$	$^{+0.6}_{-0.0}$	$^{-0.3}_{+0.4}$	$^{+0.5}_{-0.5}$	$^{-0.9}_{+0.9}$	$^{+0.0}_{+0.0}$	$^{-0.2}_{+0.3}$	$^{+0.1}_{-0.1}$	$^{+0.7}_{-0.7}$
	0.013	0.793	±1.0	$^{+1.7}_{-1.5}$	$^{+0.7}_{+0.0}$	$^{-0.5}_{+0.6}$	$^{+0.0}_{-0.0}$	$^{-1.3}_{+1.3}$	$^{+0.0}_{+0.0}$	$^{-0.1}_{+0.2}$	$^{+0.0}_{-0.0}$	$^{+0.5}_{-0.7}$
	0.021	0.656	±1.1	$^{+1.6}_{-1.4}$	$^{+0.7}_{-0.0}$	$^{-0.3}_{+0.5}$	$^{-0.1}_{+0.1}$	$^{+1.1}_{-1.1}$	$^{+0.0}_{+0.0}$	$^{-0.2}_{+0.2}$	$^{+0.0}_{-0.0}$	$^{+0.8}_{-0.7}$
	0.032	0.565	±1.2	$^{+3.3}_{-3.3}$	$^{+0.6}_{-0.0}$	$^{-0.3}_{+0.4}$	$^{-0.8}_{+0.8}$	$^{+3.0}_{-3.0}$	$^{+0.0}_{+0.0}$	$^{+0.0}_{+0.1}$	$^{+0.0}_{+0.0}$	$^{+0.7}_{-0.9}$
	0.05	0.494	±1.2	$^{+3.4}_{-3.3}$	$^{+0.4}_{+0.0}$	$^{-0.1}_{+0.3}$	$^{-2.4}_{+2.4}$	$^{+2.2}_{-2.2}$	$^{+0.0}_{+0.0}$	$^{-0.0}_{-0.1}$	$^{+0.0}_{+0.0}$	$^{+0.7}_{-0.6}$
	0.08	0.429	±1.1	$^{+5.2}_{-5.1}$	$^{+0.7}_{-0.0}$	$^{-0.1}_{+0.3}$	$^{+4.6}_{-4.6}$	$^{+2.2}_{-2.2}$	$^{+0.0}_{+0.0}$	$^{-0.0}_{+0.1}$	$^{+0.0}_{+0.0}$	$^{+0.7}_{-0.7}$
	0.18	0.331	±1.3	$^{+4.8}_{-4.7}$	$^{+0.2}_{+0.0}$	$^{+0.0}_{+0.2}$	$^{+4.1}_{-4.1}$	$^{+2.0}_{-2.0}$	$^{+0.3}_{+1.0}$	$^{+0.0}_{+0.2}$	$^{+0.0}_{+0.0}$	$^{+0.8}_{-0.8}$
350	0.008	0.969	±1.3	$^{+2.1}_{-1.5}$	$^{+1.6}_{-0.1}$	$^{-0.5}_{+0.6}$	$^{+0.9}_{-0.9}$	$^{-0.4}_{+0.4}$	$^{+0.0}_{+0.0}$	$^{-0.6}_{+0.4}$	$^{+0.4}_{-0.4}$	$^{+0.6}_{-0.8}$
	0.013	0.821	±1.1	$^{+1.9}_{-1.2}$	$^{+1.4}_{-0.0}$	$^{-0.2}_{+0.5}$	$^{-0.2}_{+0.2}$	$^{-1.0}_{+1.0}$	$^{+0.0}_{+0.0}$	$^{-0.2}_{+0.5}$	$^{+0.0}_{-0.0}$	$^{+0.7}_{-0.6}$
	0.021	0.693	±1.3	$^{+0.9}_{-0.6}$	$^{+0.4}_{-0.1}$	$^{-0.3}_{+0.4}$	$^{+0.3}_{-0.3}$	$^{+0.0}_{-0.0}$	$^{+0.0}_{+0.0}$	$^{-0.2}_{-0.0}$	$^{+0.0}_{+0.0}$	$^{+0.6}_{-0.5}$
	0.032	0.605	±1.3	$^{+1.9}_{-1.8}$	$^{+0.8}_{-0.0}$	$^{-0.2}_{+0.4}$	$^{-1.6}_{+1.6}$	$^{+0.2}_{-0.2}$	$^{+0.0}_{+0.0}$	$^{-0.3}_{+0.1}$	$^{+0.0}_{+0.0}$	$^{+0.6}_{-0.7}$
	0.05	0.509	±1.2	$^{+2.7}_{-2.6}$	$^{+0.6}_{-0.0}$	$^{-0.1}_{+0.2}$	$^{-1.9}_{+1.9}$	$^{+1.6}_{-1.6}$	$^{+0.0}_{+0.0}$	$^{-0.1}_{+0.2}$	$^{+0.0}_{+0.0}$	$^{+0.5}_{-0.7}$
	0.08	0.435	±1.2	$^{+2.0}_{-2.0}$	$^{+0.3}_{+0.0}$	$^{-0.1}_{+0.2}$	$^{+1.1}_{-1.1}$	$^{+1.6}_{-1.6}$	$^{+0.0}_{+0.0}$	$^{+0.0}_{+0.1}$	$^{+0.0}_{+0.0}$	$^{+0.7}_{-0.7}$
	0.18	0.314	±1.3	$^{+6.4}_{-6.3}$	$^{+0.4}_{+0.0}$	$^{-0.0}_{+0.2}$	$^{+5.7}_{-5.7}$	$^{+2.6}_{-2.6}$	$^{-0.1}_{+1.2}$	$^{+0.1}_{+0.2}$	$^{+0.0}_{+0.0}$	$^{+0.7}_{-0.6}$
450	0.008	0.993	±1.5	$^{+2.4}_{-2.1}$	$^{+0.7}_{-0.3}$	$^{-1.4}_{+1.6}$	$^{+1.3}_{-1.3}$	$^{-0.5}_{+0.5}$	$^{+0.0}_{+0.0}$	$^{-0.2}_{+0.3}$	$^{+0.6}_{-0.6}$	$^{+0.5}_{-0.4}$
	0.013	0.857	±1.5	$^{+1.1}_{-1.1}$	$^{+0.1}_{-0.1}$	$^{-0.5}_{+0.6}$	$^{-0.4}_{+0.4}$	$^{+0.2}_{-0.2}$	$^{+0.0}_{+0.0}$	$^{-0.6}_{+0.6}$	$^{+0.1}_{-0.1}$	$^{+0.5}_{-0.6}$
	0.021	0.685	±1.7	$^{+1.8}_{-1.7}$	$^{+0.2}_{-0.1}$	$^{-0.4}_{+0.5}$	$^{-0.1}_{+0.1}$	$^{+1.3}_{-1.3}$	$^{+0.0}_{+0.0}$	$^{-0.7}_{+0.9}$	$^{+0.0}_{-0.0}$	$^{+0.8}_{-0.8}$
	0.032	0.591	±1.6	$^{+1.9}_{-1.7}$	$^{+0.8}_{-0.1}$	$^{-0.2}_{+0.4}$	$^{+0.0}_{-0.0}$	$^{+1.4}_{-1.4}$	$^{+0.0}_{+0.0}$	$^{-0.5}_{+0.4}$	$^{+0.0}_{+0.0}$	$^{+1.0}_{-0.9}$
	0.05	0.519	±1.4	$^{+2.5}_{-2.4}$	$^{+0.7}_{-0.0}$	$^{+0.0}_{+0.2}$	$^{-1.6}_{+1.6}$	$^{+1.6}_{-1.6}$	$^{+0.0}_{+0.0}$	$^{-0.4}_{+0.6}$	$^{+0.0}_{+0.0}$	$^{+0.7}_{-0.7}$
	0.08	0.432	±1.6	$^{+2.1}_{-1.9}$	$^{+0.3}_{+0.0}$	$^{+0.1}_{+0.2}$	$^{-0.7}_{+0.7}$	$^{+1.7}_{-1.7}$	$^{+0.0}_{+0.0}$	$^{+0.1}_{+0.6}$	$^{+0.0}_{+0.0}$	$^{+0.7}_{-0.5}$
	0.13	0.359	±1.7	$^{+4.9}_{-4.9}$	$^{+0.6}_{+0.0}$	$^{+0.1}_{+0.1}$	$^{+4.4}_{-4.4}$	$^{+1.9}_{-1.9}$	$^{+0.0}_{+0.0}$	$^{-0.4}_{+0.4}$	$^{+0.0}_{+0.0}$	$^{+0.5}_{-0.6}$
	0.25	0.262	±2.0	$^{+5.6}_{-5.5}$	$^{+1.1}_{+0.0}$	$^{+0.2}_{+0.1}$	$^{+5.2}_{-5.2}$	$^{+1.1}_{-1.1}$	$^{-0.9}_{+0.8}$	$^{-0.1}_{+0.6}$	$^{+0.0}_{+0.0}$	$^{+0.8}_{-0.8}$
650	0.013	0.878	±1.4	$^{+1.5}_{-0.8}$	$^{+1.2}_{-0.2}$	$^{-0.5}_{+0.6}$	$^{-0.0}_{+0.0}$	$^{-0.1}_{+0.1}$	$^{+0.0}_{+0.0}$	$^{-0.2}_{+0.3}$	$^{+0.5}_{-0.5}$	$^{+0.4}_{-0.3}$
	0.021	0.755	±1.7	$^{+1.1}_{-1.1}$	$^{+0.0}_{-0.1}$	$^{-0.4}_{+0.5}$	$^{-0.3}_{+0.3}$	$^{-0.9}_{+0.9}$	$^{+0.0}_{+0.0}$	$^{-0.2}_{+0.0}$	$^{+0.1}_{-0.1}$	$^{+0.2}_{-0.2}$
	0.032	0.597	±2.0	$^{+1.2}_{-1.0}$	$^{+0.5}_{-0.2}$	$^{-0.4}_{+0.5}$	$^{-0.5}_{+0.5}$	$^{+0.7}_{-0.7}$	$^{+0.0}_{+0.0}$	$^{+0.5}_{+0.5}$	$^{+0.0}_{-0.0}$	$^{+0.2}_{-0.2}$
	0.05	0.512	±1.9	$^{+1.0}_{-0.9}$	$^{+0.1}_{-0.0}$	$^{-0.3}_{+0.4}$	$^{-0.4}_{+0.4}$	$^{+0.7}_{-0.7}$	$^{+0.0}_{+0.0}$	$^{+0.1}_{+0.0}$	$^{+0.0}_{+0.0}$	$^{+0.5}_{-0.4}$
	0.08	0.424	±2.1	$^{+2.4}_{-2.3}$	$^{+0.7}_{-0.0}$	$^{-0.1}_{+0.3}$	$^{-1.8}_{+1.8}$	$^{+1.0}_{-1.0}$	$^{+0.0}_{+0.0}$	$^{+0.1}_{-0.0}$	$^{+0.0}_{+0.0}$	$^{+0.9}_{-1.1}$
	0.13	0.361	±2.2	$^{+2.7}_{-2.4}$	$^{+0.9}_{-0.0}$	$^{-0.1}_{+0.2}$	$^{+2.1}_{-2.1}$	$^{-0.8}_{+0.8}$	$^{+0.0}_{+0.0}$	$^{+0.1}_{+0.4}$	$^{+0.0}_{+0.0}$	$^{+1.0}_{-0.9}$
	0.25	0.253	±2.4	$^{+6.6}_{-6.5}$	$^{+1.0}_{-0.0}$	$^{-0.1}_{+0.3}$	$^{+6.3}_{-6.3}$	$^{+1.0}_{-1.0}$	$^{-0.8}_{+0.2}$	$^{-0.1}_{+0.5}$	$^{+0.0}_{+0.0}$	$^{+1.0}_{-1.1}$
800	0.013	0.860	±1.8	$^{+1.7}_{-1.9}$	$^{+0.4}_{-1.0}$	$^{-0.8}_{+1.0}$	$^{+0.4}_{-0.4}$	$^{-1.0}_{+1.0}$	$^{+0.0}_{+0.0}$	$^{-0.1}_{+0.0}$	$^{+0.6}_{-0.6}$	$^{+0.3}_{-0.4}$
	0.021	0.733	±2.1	$^{+1.1}_{-0.9}$	$^{+0.5}_{-0.1}$	$^{-0.4}_{+0.5}$	$^{+0.6}_{-0.6}$	$^{-0.2}_{+0.2}$	$^{+0.0}_{+0.0}$	$^{+0.0}_{+0.5}$	$^{+0.1}_{-0.1}$	$^{+0.4}_{-0.4}$
	0.032	0.634	±2.1	$^{+1.4}_{-1.4}$	$^{+0.0}_{-0.4}$	$^{-0.4}_{+0.5}$	$^{-0.8}_{+0.8}$	$^{-0.9}_{+0.9}$	$^{+0.0}_{+0.0}$	$^{+0.3}_{+0.0}$	$^{+0.1}_{-0.1}$	$^{+0.2}_{-0.4}$
	0.05	0.522	±2.0	$^{+2.2}_{-2.2}$	$^{+0.3}_{+0.0}$	$^{-0.3}_{+0.4}$	$^{+0.7}_{-0.7}$	$^{+2.0}_{-2.0}$	$^{+0.0}_{+0.0}$	$^{-0.4}_{+0.1}$	$^{+0.0}_{+0.0}$	$^{+0.3}_{-0.4}$
	0.08	0.448	±2.1	$^{+2.6}_{-2.6}$	$^{+0.5}_{-0.0}$	$^{-0.2}_{+0.3}$	$^{-2.5}_{+2.5}$	$^{+0.1}_{-0.1}$	$^{+0.0}_{+0.0}$	$^{+0.5}_{-0.7}$	$^{+0.0}_{+0.0}$	$^{+0.3}_{-0.4}$
	0.13	0.377	±2.4	$^{+1.1}_{-1.0}$	$^{+0.5}_{-0.0}$	$^{-0.2}_{+0.3}$	$^{+0.7}_{-0.7}$	$^{+0.6}_{-0.6}$	$^{+0.0}_{+0.0}$	$^{+0.1}_{-0.4}$	$^{+0.0}_{+0.0}$	$^{+0.2}_{-0.2}$
	0.25	0.257	±2.8	$^{+3.7}_{-3.4}$	$^{+0.3}_{+0.0}$	$^{-0.2}_{+0.2}$	$^{+3.3}_{-3.3}$	$^{+0.8}_{-0.8}$	$^{+1.2}_{-0.1}$	$^{+0.7}_{-0.5}$	$^{+0.0}_{+0.0}$	$^{+0.2}_{-0.3}$

Table 8 (*Continued*)

Q_c^2 (GeV²)	x_c	$\tilde\sigma$	stat. (%)	sys. (%)	δ_1 (%)	δ_2 (%)	δ_3 (%)	δ_4 (%)	δ_5 (%)	δ_6 (%)	δ_7 (%)	δ_8–δ_{13} (%)
1200	0.014	0.892	±2.3	+2.4 / −3.2	+0.6 / −2.2	−0.8 / +1.0	−0.7 / +0.7	−1.4 / +1.4	+0.0 / +0.0	−0.3 / −0.8	+1.4 / −1.4	+0.5 / −0.2
	0.021	0.791	±2.1	+1.9 / −1.6	+0.9 / −0.1	−0.5 / +0.5	+1.5 / −1.5	+0.0 / −0.0	+0.0 / +0.0	+0.1 / +0.4	+0.4 / −0.4	+0.3 / −0.4
	0.032	0.608	±2.1	+1.2 / −1.1	+0.0 / −0.1	−0.4 / +0.5	−0.5 / +0.5	−0.7 / +0.7	+0.0 / +0.0	+0.1 / +0.1	+0.2 / −0.2	+0.6 / −0.6
	0.05	0.551	±1.8	+1.3 / −1.4	+0.1 / −0.0	−0.3 / +0.3	−0.1 / +0.1	+1.2 / −1.2	+0.0 / +0.0	−0.3 / −0.4	+0.0 / −0.0	+0.4 / −0.4
	0.08	0.456	±1.9	+1.4 / −1.3	+0.3 / −0.0	−0.2 / +0.4	−0.3 / +0.3	+1.2 / −1.2	+0.0 / +0.0	+0.3 / −0.3	+0.0 / +0.0	+0.4 / −0.3
	0.13	0.375	±2.1	+1.1 / −1.2	+0.1 / −0.0	−0.1 / +0.2	−0.9 / +0.9	+0.4 / −0.4	+0.0 / +0.0	+0.1 / −0.5	+0.0 / +0.0	+0.3 / −0.4
	0.25	0.247	±2.4	+2.4 / −2.3	+0.3 / +0.0	−0.2 / +0.3	+2.0 / −2.0	+1.0 / −1.0	+0.0 / +0.0	−0.3 / −0.1	+0.0 / +0.0	+0.5 / −0.4
	0.4	0.125	±4.1	+8.1 / −5.7	+0.0 / −0.1	−0.4 / +0.4	+5.6 / −5.6	+0.6 / −0.6	+5.8 / +3.4	+0.5 / −1.0	+0.0 / +0.0	+0.5 / −0.5
1500	0.021	0.765	±3.0	+2.6 / −2.3	+0.9 / −0.2	−0.6 / +0.4	−0.4 / +0.4	−0.1 / +0.1	+0.0 / +0.0	−1.0 / +0.1	+2.3 / −1.9	+0.4 / −0.4
	0.032	0.629	±2.7	+0.7 / −0.6	+0.3 / −0.1	−0.3 / +0.3	−0.1 / +0.1	−0.3 / +0.3	+0.0 / +0.0	−0.1 / −0.1	+0.2 / −0.2	+0.4 / −0.3
	0.05	0.522	±2.4	+0.9 / −0.8	+0.2 / −0.0	−0.3 / +0.4	+0.2 / −0.2	+0.4 / −0.4	+0.0 / +0.0	−0.4 / +0.5	+0.0 / −0.0	+0.3 / −0.4
	0.08	0.477	±2.3	+1.0 / −1.1	+0.2 / −0.0	−0.3 / +0.4	−0.9 / +0.9	−0.2 / +0.2	+0.0 / +0.0	−0.4 / +0.1	+0.0 / +0.0	+0.3 / −0.5
	0.13	0.376	±2.9	+2.1 / −1.8	+0.8 / −0.0	−0.1 / +0.3	−1.3 / +1.3	−1.1 / +1.1	+0.0 / +0.0	+0.8 / −0.2	+0.0 / +0.0	+0.3 / −0.4
	0.18	0.312	±3.2	+1.8 / −1.7	+0.6 / −0.1	−0.3 / +0.2	+0.0 / −0.0	−1.6 / +1.6	+0.0 / +0.0	−0.3 / −0.2	+0.0 / +0.0	+0.4 / −0.4
	0.25	0.264	±3.8	+1.9 / −1.9	+0.0 / −0.3	−0.3 / +0.3	+1.7 / −1.7	+0.6 / −0.6	+0.1 / +0.0	−0.1 / −0.3	+0.0 / +0.0	+0.3 / −0.3
	0.4	0.128	±5.7	+8.8 / −4.3	+0.6 / +0.0	−0.5 / +0.3	+2.0 / −2.0	−0.9 / +0.9	+8.4 / −3.6	+0.3 / −0.4	+0.0 / +0.0	+0.6 / −0.5
2000	0.032	0.636	±3.3	+2.5 / −1.4	+1.8 / +0.0	−0.2 / +0.2	+0.3 / −0.3	+1.0 / −1.0	+0.0 / +0.0	+0.4 / +0.7	+1.1 / −0.8	+0.3 / −0.4
	0.05	0.571	±2.9	+1.0 / −0.8	+0.5 / −0.0	−0.3 / +0.4	−0.3 / +0.3	−0.6 / +0.6	+0.0 / +0.0	+0.1 / +0.1	+0.0 / +0.0	+0.3 / −0.3
	0.08	0.459	±2.9	+2.0 / −2.0	+0.1 / −0.1	−0.3 / +0.4	−0.1 / +0.1	+1.9 / −1.9	+0.0 / +0.0	+0.2 / +0.0	+0.0 / −0.0	+0.3 / −0.3
	0.13	0.374	±3.4	+0.8 / −1.2	+0.1 / −0.6	−0.2 / +0.3	−0.5 / +0.5	+0.5 / −0.5	+0.0 / +0.0	+0.1 / −0.6	+0.0 / +0.0	+0.3 / −0.4
	0.18	0.309	±3.8	+0.6 / −1.9	+0.0 / −0.7	−0.2 / +0.2	−0.3 / +0.3	+0.1 / −0.1	+0.0 / +0.0	−0.4 / −1.6	+0.0 / +0.0	+0.4 / −0.6
	0.25	0.247	±4.5	+1.7 / −1.6	+0.3 / −0.0	−0.2 / +0.3	+1.5 / −1.5	+0.5 / −0.5	+0.0 / +0.0	+0.4 / +0.5	+0.0 / +0.0	+0.5 / −0.5
	0.4	0.120	±6.5	+3.7 / −3.9	+0.0 / −0.2	−0.3 / +0.4	+3.1 / −3.1	+1.1 / −1.1	−0.5 / +1.0	+0.1 / −1.3	+0.0 / +0.0	+1.2 / −1.4
3000	0.05	0.581	±3.7	+2.0 / −1.1	+1.6 / −0.1	−0.3 / +0.4	+0.9 / −0.9	−0.0 / +0.0	+0.0 / +0.0	+0.4 / +0.2	+0.5 / −0.5	+0.4 / −0.3
	0.08	0.507	±3.4	+1.1 / −1.1	+0.2 / −0.4	−0.2 / +0.3	−0.4 / +0.4	+0.8 / −0.8	+0.0 / +0.0	+0.5 / −0.1	+0.1 / −0.1	+0.3 / −0.5
	0.13	0.378	±4.0	+0.9 / −0.7	+0.1 / −0.1	−0.2 / +0.3	+0.6 / −0.6	−0.1 / +0.1	+0.0 / +0.0	−0.3 / −0.3	+0.0 / +0.0	+0.7 / −0.1
	0.18	0.320	±4.4	+1.2 / −1.3	+0.0 / −0.3	−0.2 / +0.2	−0.9 / +0.9	−0.6 / +0.6	+0.0 / +0.0	−0.5 / +0.2	+0.0 / +0.0	+0.4 / −0.3
	0.25	0.286	±4.9	+7.4 / −7.3	+0.6 / −0.0	−0.2 / +0.2	+7.3 / −7.3	+0.2 / −0.2	+0.0 / +0.0	+1.1 / +0.3	+0.0 / +0.0	+0.8 / −0.6
	0.4	0.135	±7.4	+3.8 / −3.5	+1.3 / −0.0	−0.2 / +0.4	−3.4 / +3.4	+0.5 / −0.5	+0.4 / −0.3	+0.8 / −0.3	+0.0 / +0.0	+0.6 / −0.6
	0.65	0.017	+14.4 / −12.7	+10.2 / −10.4	+0.0 / −0.6	−0.8 / +1.0	−8.7 / +8.7	+4.6 / −4.6	+1.8 / +0.7	−2.7 / +0.9	+0.0 / +0.0	+1.7 / −2.0
5000	0.08	0.527	±3.2	+1.8 / −0.9	+1.6 / −0.3	−0.2 / +0.2	−0.3 / +0.3	+0.2 / −0.2	+0.0 / +0.0	−0.6 / −0.4	+0.3 / −0.3	+0.5 / −0.3
	0.13	0.463	±4.1	+1.0 / −0.8	+0.8 / +0.0	−0.2 / +0.2	−0.4 / +0.4	+0.3 / −0.3	+0.0 / +0.0	+0.1 / −0.3	+0.1 / −0.1	+0.2 / −0.5
	0.18	0.340	±4.5	+1.0 / −0.5	+0.2 / −0.1	−0.3 / +0.2	+0.2 / −0.2	+0.3 / −0.3	+0.0 / +0.0	−0.1 / +0.7	+0.0 / +0.0	+0.5 / −0.3
	0.25	0.243	±5.6	+1.8 / −1.2	+0.7 / −0.0	−0.2 / +0.3	+0.7 / −0.7	−0.7 / +0.7	+0.0 / +0.0	+1.2 / −0.6	+0.0 / +0.0	+0.4 / −0.3
	0.4	0.140	±7.6	+6.5 / −6.4	+0.0 / −0.3	−0.2 / +0.3	+6.0 / −6.0	−2.1 / +2.1	+0.0 / +0.0	+0.4 / +1.3	+0.0 / +0.0	+1.1 / −1.1
8000	0.13	0.560	±4.2	+1.0 / −1.9	+0.0 / −1.0	−0.3 / +0.3	−0.5 / +0.5	−0.1 / +0.1	+0.0 / +0.0	−1.3 / +0.3	+0.5 / −0.3	+0.5 / −0.5
	0.18	0.433	±5.4	+2.6 / −2.9	+0.1 / −0.3	−0.2 / +0.2	−2.4 / +2.4	+0.6 / −0.6	+0.0 / +0.0	+0.5 / −0.3	+0.0 / +0.0	+0.6 / −1.3
	0.25	0.309	±6.6	+3.8 / −3.9	+0.7 / −0.1	−0.3 / +0.2	−3.6 / +3.6	+0.4 / −0.4	+0.0 / +0.0	−1.1 / −0.6	+0.0 / +0.0	+0.4 / −0.4
	0.4	0.114	+11.9 / −10.7	+7.1 / −7.3	+0.1 / −0.0	−0.3 / +0.4	+7.0 / −7.0	−0.6 / +0.6	+0.0 / +0.0	−0.3 / +0.5	+0.0 / +0.0	+0.6 / −2.0
	0.65	0.019	+19.9 / −16.9	+4.1 / −4.2	+0.2 / −1.4	−0.9 / +0.9	+1.5 / −1.5	+2.3 / −2.3	+0.0 / +0.0	−2.6 / +2.8	+0.0 / +0.0	+0.8 / −0.6
12000	0.18	0.464	±6.1	+1.3 / −3.8	+1.0 / −3.6	−0.3 / +0.4	−0.4 / +0.4	−0.2 / +0.2	+0.0 / +0.0	−0.3 / −0.8	+0.2 / −0.3	+0.5 / −0.6
	0.25	0.353	±8.2	+2.8 / −2.3	+2.4 / −0.6	−0.2 / +0.2	+0.3 / −0.3	+0.8 / −0.8	+0.0 / +0.0	+0.3 / −1.6	+0.0 / +0.0	+1.0 / −1.2
	0.4	0.156	+13.4 / −11.8	+4.6 / −3.8	+2.7 / −0.2	−0.3 / +0.4	+3.2 / −3.2	−0.8 / +0.8	+0.0 / +0.0	−1.2 / +1.5	+0.0 / +0.0	+0.6 / −1.3
20000	0.25	0.461	±9.2	+6.1 / −3.6	+4.9 / −1.8	−1.5 / +0.2	−2.2 / +2.2	+0.1 / −0.1	+0.0 / +0.0	−0.7 / −0.2	+2.7 / −1.4	+0.6 / −0.5
	0.4	0.183	+16.6 / −14.4	+4.9 / −3.8	+3.6 / +0.0	−0.4 / +0.4	+0.9 / −0.9	+3.0 / −3.0	+0.0 / +0.0	−1.8 / −0.3	+0.0 / +0.0	+1.1 / −1.2
30000	0.4	0.237	+17.9 / −15.4	+6.9 / −5.9	+6.7 / +0.0	−0.2 / +0.3	−0.8 / +0.8	+0.7 / −0.7	+0.0 / +0.0	+0.1 / −4.9	+0.0 / −2.9	+1.3 / −1.3

Eur. Phys. J. C (2009) 62: 625–658

643

Fig. 4 The $e^{\pm}p$ unpolarised NC DIS reduced cross section $\tilde{\sigma}$ plotted as a function of x at fixed Q^2. The *closed (open) circles* represent data points for e^-p (e^+p) collisions in which the *inner error bars* show the statistical uncertainty while the *outer bars* show the statistical and systematic uncertainties added in quadrature, although errors are too small to be seen in most cases. The *curves* show the predictions of the SM evaluated using the ZEUS-JETS PDFs
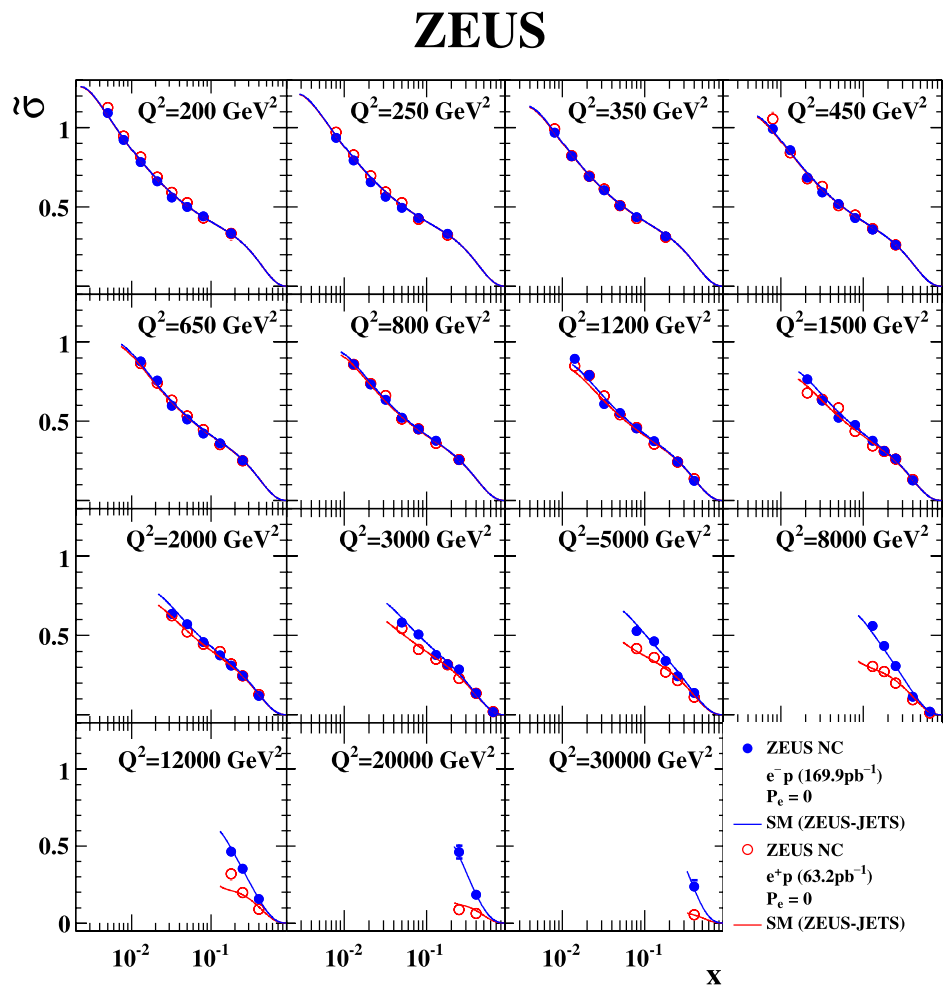
ZEUS

Fig. 5 The structure function $x\tilde{F}_3$ plotted as a function of x at fixed-Q^2. The *closed circles* represent the ZEUS data. The *inner error bars* show the statistical uncertainty while the *outer* ones show the statistical and systematic uncertainties added in quadrature. The *curves* show the predictions of the SM evaluated using the ZEUS-JETS PDFs with the *shaded band* indicating the uncertainties

ZEUS
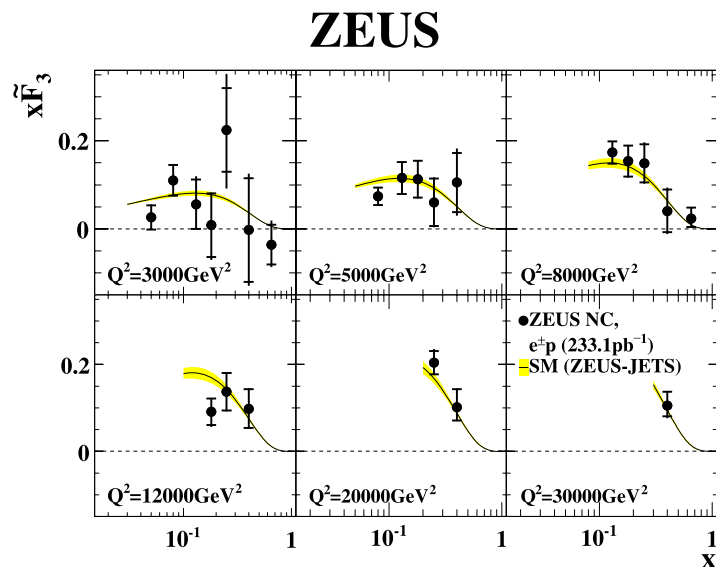
varied by ± 1 mrad. Typically, the deviations were within $\pm 1\%$ over the full kinematic range;

- $\{\delta_{10}\}$ to account for differences in the description of the p_e^{trk} distribution between data and MC, the p_e^{trk} require-

ment was varied by ± 1 GeV, resulting in a variation of the cross section by $\pm 1\%$ over most of the kinematic range, and up to 2% in a few double-differential cross-section bins;

644

Eur. Phys. J. C (2009) 62: 625–658

Table 9 The structure function $x\tilde{F}_3$ extracted using the e^-p data set ($\mathcal{L} = 169.9\,\mathrm{pb}^{-1}$, $P_e = 0$) and previously published NC e^+p DIS results ($\mathcal{L} = 63.2\,\mathrm{pb}^{-1}$, $P_e = 0$). The bin range and bin centre for Q^2 and x, and measured $x\tilde{F}_3$ are shown. The first (second) error on the measurement refers to the statistical (systematic) uncertainties

Q^2 range (GeV^2)	Q_c^2 (GeV^2)	x range	x_c	$x\tilde{F}_3 \times 10$
2500 – 3500	3000	0.037 – 0.06	0.05	$0.26 \pm 0.28\,^{+0.10}_{-0.08}$
		0.06 – 0.1	0.08	$1.10 \pm 0.35\,^{+0.10}_{-0.11}$
		0.1 – 0.15	0.13	$0.56 \pm 0.56\,^{+0.30}_{-0.10}$
		0.15 – 0.23	0.18	$0.08 \pm 0.72\,^{+0.17}_{-0.32}$
		0.23 – 0.35	0.25	$2.25 \pm 0.95\,^{+0.85}_{-0.93}$
		0.35 – 0.53	0.4	$-0.03 \pm 1.18\,^{+0.51}_{-0.47}$
		0.53 – 0.75	0.65	$-0.36\,^{+0.46}_{-0.44}\,^{+0.31}_{-0.23}$
3500 – 5600	5000	0.04 – 0.1	0.08	$0.74 \pm 0.20\,^{+0.09}_{-0.06}$
		0.1 – 0.15	0.13	$1.16 \pm 0.36\,^{+0.07}_{-0.07}$
		0.15 – 0.23	0.18	$1.13 \pm 0.42\,^{+0.09}_{-0.13}$
		0.23 – 0.35	0.25	$0.60 \pm 0.54\,^{+0.17}_{-0.16}$
		0.35 – 0.53	0.4	$1.05 \pm 0.67\,^{+0.38}_{-0.35}$
5600 – 9000	8000	0.07 – 0.15	0.13	$1.74 \pm 0.25\,^{+0.07}_{-0.09}$
		0.15 – 0.23	0.18	$1.54 \pm 0.35\,^{+0.11}_{-0.14}$
		0.23 – 0.35	0.25	$1.49 \pm 0.43\,^{+0.19}_{-0.18}$
		0.35 – 0.53	0.4	$0.40\,^{+0.50}_{-0.48}\,^{+0.22}_{-0.21}$
		0.53 – 0.75	0.65	$0.23\,^{+0.25}_{-0.19}\,^{+0.04}_{-0.05}$
9000 – 15000	12000	0.09 – 0.23	0.18	$0.91 \pm 0.31\,^{+0.07}_{-0.17}$
		0.23 – 0.35	0.25	$1.37 \pm 0.43\,^{+0.09}_{-0.14}$
		0.35 – 0.53	0.4	$0.97\,^{+0.46}_{-0.43}\,^{+0.14}_{-0.15}$
15000 – 25000	20000	0.15 – 0.35	0.25	$2.04 \pm 0.27\,^{+0.16}_{-0.09}$
		0.35 – 0.75	0.4	$1.02\,^{+0.41}_{-0.31}\,^{+0.12}_{-0.11}$
25000 – 50000	30000	0.25 – 0.75	0.4	$1.05\,^{+0.32}_{-0.25}\,^{+0.10}_{-0.15}$

Table 10 The interference structure function $xF_3^{\gamma Z}$ evaluated at $Q^2 = 5\,000\,\mathrm{GeV}^2$ for x bins centred on x_c. The first (second) error on the measurement refers to the statistical (systematic) uncertainties.

Q^2 (GeV^2)	x_c	$xF_3^{\gamma Z} \times 10$
5000	0.032	$1.53 \pm 1.41 \pm 0.80$
	0.05	$1.01 \pm 1.19 \pm 0.38$
	0.08	$3.26 \pm 0.66 \pm 0.24$
	0.13	$4.62 \pm 0.62 \pm 0.16$
	0.18	$3.01 \pm 0.54 \pm 0.19$
	0.25	$3.93 \pm 0.44 \pm 0.17$
	0.4	$2.08 \pm 0.39 \pm 0.15$
	0.65	$0.55 \pm 0.63 \pm 0.13$

- $\{\delta_{11}\}$ the uncertainty resulting from the hadronic energy scale was evaluated by varying the hadronic energy in the MC by $\pm 1\%$. This caused changes of less than $\pm 1\%$ over the full kinematic range in the MC;

- $\{\delta_{12}\}$ the DCA requirement was changed to $8\,\mathrm{cm}$ to estimate the uncertainty in the background contamination due to falsely identified electrons. The uncertainties in the cross sections associated with this variation were below $\pm 1\%$ over the full kinematic range;

- $\{\delta_{13}\}$ the systematic uncertainty associated with cosmic-ray rejection was evaluated by varying the $p_T/\sqrt{E_T}$ cut by $\pm 1\sqrt{\mathrm{GeV}}$. The cross-section uncertainties were below $\pm 1\%$ over the full kinematic range.

The relative uncertainty in the measured polarisation was 3.6% using the LPOL and 4.2% using the TPOL. The choice of polarimeter was made run-by-run to maximise the available luminosity and minimise the uncertainty in the measured polarisation. The measured luminosity was assigned a relative uncertainty of 2.6%. The uncertainties in the luminosity and polarisation measurements were not included in the total systematic uncertainty shown in the final results.

Eur. Phys. J. C (2009) 62: 625–658

645

Fig. 6 The structure function $xF_3^{\gamma Z}$ extrapolated to a single Q^2 value of $5\,000\,\mathrm{GeV}^2$ and plotted as a function of x. The *closed circles* represent data points in which the *inner error bars* show the statistical uncertainty while the *outer bars* show the statistical and systematic uncertainties added in quadrature. The *curves* show the predictions of the SM evaluated using several PDFs : ZEUS-JETS (*shaded band* shows the uncertainties), CTEQ6.6 and MRST2004. The measurements by the BCDMS collaboration are shown as open squares
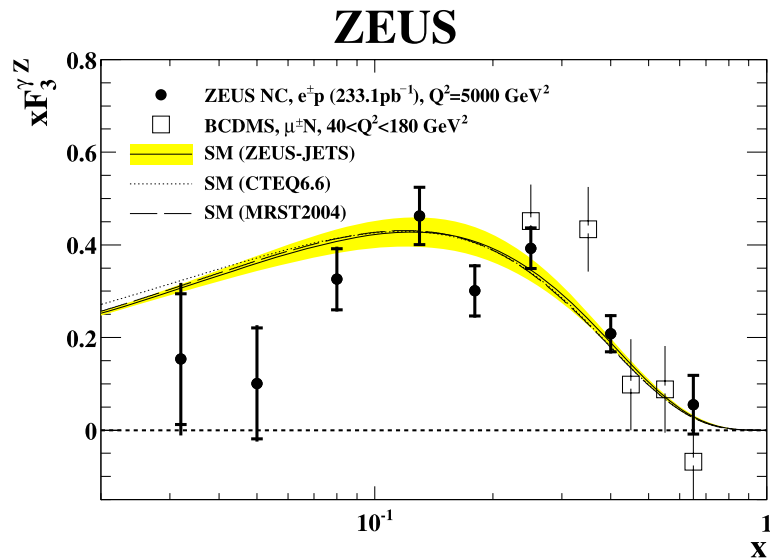
9 Results

9.1 Unpolarised cross sections

The single-differential cross-sections with respect to Q^2, x and y, tabulated in Tables 1, 2, 3, 4, 5 and 6, are shown in Fig. 3 for $Q^2 > 185\,\mathrm{GeV}^2$ and $y < 0.9$ for the combined positive and negative polarisation samples having a residual polarisation of -0.03. The cross-sections $d\sigma/dx$ and $d\sigma/dy$ for $Q^2 > 3\,000\,\mathrm{GeV}^2$ and $y < 0.9$ are also presented in Fig. 3. The measured cross sections demonstrate the precision of this measurement. The measured cross sections are well described by the SM prediction evaluated using the ZEUS-JETS PDFs [50]. The measurement of $d\sigma/dQ^2$ spans two orders of magnitude in Q^2, and at $Q^2 \sim 40\,000\,\mathrm{GeV}^2$, the spatial resolution reaches $\sim 10^{-18}$ m.

The reduced cross sections of unpolarised $e^- p$ NC DIS, tabulated in Tables 7 and 8, are presented in Fig. 4 with the residual polarisation of -0.03 corrected using theoretical predictions. The correction factors were at most 2% in the highest-Q^2 bins. The SM predictions are in good agreement with the measurements over the full kinematic range. Also shown are unpolarised $e^+ p$ NC DIS measurements with an integrated luminosity of $63.2\,\mathrm{pb}^{-1}$ collected in 1999 and 2000 [4]. As discussed earlier, a significant difference between the $e^- p$ and $e^+ p$ unpolarised reduced cross sections is seen at high-Q^2 values due to the contribution of $x\tilde{F}_3$.

Figure 5 shows the structure function $x\tilde{F}_3$ obtained from the unpolarised $e^- p$ and $e^+ p$ reduced cross sections in the high-Q^2 region, according to (3). The systematic uncertainties between the measurements were treated as uncorrelated. The results are also given in Table 9. The reduced cross sections visibly differ and are well described by the SM predictions.

The structure function $xF_3^{\gamma Z}$ has little dependence on Q^2 and so the measurements from $1\,500 < Q^2 < 30\,000\,\mathrm{GeV}^2$ have been extrapolated to $5\,000\,\mathrm{GeV}^2$, and then averaged, to obtain a higher statistical significance. The structure function $xF_3^{\gamma Z}$ measured at $Q^2 = 5\,000\,\mathrm{GeV}^2$, tabulated in Table 10, is shown in Fig. 6. It is well described by the SM predictions. The integral of $xF_3^{\gamma Z}$ in the region of $0.032 < x < 0.65$ is

$$\int_{0.032}^{0.65} \frac{dx}{x} xF_3^{\gamma Z} = 0.80 \pm 0.08(\text{stat.}) \pm 0.03(\text{syst.}). \qquad (18)$$

This value is consistent with the SM prediction of 0.94 ± 0.02 as evaluated with the ZEUS-JETS PDFs, where the error is from the PDF uncertainty. Figure 6 also shows the measurement of $xF_3^{\gamma Z}$ obtained by the BCDMS collaboration from NC muon-carbon scattering at lower energies, which was extracted over the kinematic range $40 < Q^2 < 180\,\mathrm{GeV}^2$ and $0.2 < x < 0.7$ [51]. The BCDMS measurements were corrected for the difference of the u-valence and d-valence quark PDFs so as to be directly comparable to the $xF_3^{\gamma Z}$ obtained from NC $e^- p$ scattering.[4] The measurements presented in this paper extend the x range for $xF_3^{\gamma Z}$ data down to $x \sim 0.03$, well below the range of the BCDMS measurements. Furthermore, they are extracted at higher Q^2 values where perturbative QCD calculations are more reliable. Moreover, this measurement is also free from heavy-target corrections and isospin-symmetry assumptions which are inherent in previous fixed-target measurements. Therefore, at Bjorken x values from $\sim 10^{-2}$ to 0.65, this measure-

---

[4]In ep scattering, $xF_3^{\gamma Z} = (2u_v + d_v)/3$, while in eN scattering, $xF_3^{\gamma Z} = (u_v + d_v)/2$. The correction was evaluated by using the ZEUS-JETS PDFs and was typically about 15%.

646

Eur. Phys. J. C (2009) 62: 625–658

Table 11 The reduced cross section $\tilde{\sigma}$ for the reaction $e^- p \rightarrow e^- X$ ($\mathcal{L} = 71.2\,\mathrm{pb}^{-1}$, $P_e = +0.29$). The bin range, bin centre (Q_c^2 and x_c) and measured cross section corrected to the electroweak Born level are shown. The first (second) error on the cross section corresponds to the statistical (systematic) uncertainties. The number of observed data events (N_{data}) and simulated background events ($N_{\mathrm{bg}}^{\mathrm{MC}}$) are also shown

Q^2 range (GeV^2)	Q_c^2 (GeV^2)	x range	x_c	$\tilde{\sigma}$	N_{data}	$N_{\mathrm{bg}}^{\mathrm{MC}}$
185 – 240	200	0.0037 – 0.006	0.005	$1.094 \pm 0.015\,^{+0.014}_{-0.011}$	5913	36.8
		0.006 – 0.01	0.008	$0.928 \pm 0.012\,^{+0.018}_{-0.018}$	6914	9.8
		0.01 – 0.017	0.013	$0.785 \pm 0.009\,^{+0.013}_{-0.013}$	7406	1.2
		0.017 – 0.025	0.021	$0.669 \pm 0.009\,^{+0.014}_{-0.014}$	5337	0.0
		0.025 – 0.037	0.032	$0.558 \pm 0.008\,^{+0.023}_{-0.022}$	4970	0.0
		0.037 – 0.06	0.05	$0.500 \pm 0.008\,^{+0.012}_{-0.012}$	4615	0.0
		0.06 – 0.12	0.08	$0.435 \pm 0.006\,^{+0.024}_{-0.024}$	5891	0.0
		0.12 – 0.25	0.18	$0.325 \pm 0.006\,^{+0.017}_{-0.017}$	3003	0.0
240 – 310	250	0.006 – 0.01	0.008	$0.920 \pm 0.014\,^{+0.014}_{-0.012}$	4675	10.9
		0.01 – 0.017	0.013	$0.787 \pm 0.011\,^{+0.013}_{-0.012}$	5247	2.5
		0.017 – 0.025	0.021	$0.649 \pm 0.011\,^{+0.010}_{-0.009}$	3703	0.6
		0.025 – 0.037	0.032	$0.564 \pm 0.010\,^{+0.019}_{-0.018}$	3657	0.0
		0.037 – 0.06	0.05	$0.481 \pm 0.008\,^{+0.016}_{-0.016}$	3465	0.0
		0.06 – 0.12	0.08	$0.431 \pm 0.007\,^{+0.022}_{-0.022}$	4353	0.0
		0.12 – 0.25	0.18	$0.324 \pm 0.006\,^{+0.016}_{-0.015}$	2864	0.0
310 – 410	350	0.006 – 0.01	0.008	$0.973 \pm 0.019\,^{+0.021}_{-0.015}$	2902	30.0
		0.01 – 0.017	0.013	$0.826 \pm 0.014\,^{+0.016}_{-0.010}$	4010	3.7
		0.017 – 0.025	0.021	$0.692 \pm 0.013\,^{+0.006}_{-0.004}$	3044	0.0
		0.025 – 0.037	0.032	$0.603 \pm 0.011\,^{+0.012}_{-0.011}$	2953	0.0
		0.037 – 0.06	0.05	$0.503 \pm 0.009\,^{+0.013}_{-0.013}$	3112	0.0
		0.06 – 0.12	0.08	$0.432 \pm 0.008\,^{+0.009}_{-0.009}$	3501	0.0
		0.12 – 0.25	0.18	$0.306 \pm 0.006\,^{+0.020}_{-0.019}$	2689	0.0
410 – 530	450	0.006 – 0.01	0.008	$1.004 \pm 0.022\,^{+0.024}_{-0.021}$	2262	35.3
		0.01 – 0.017	0.013	$0.843 \pm 0.019\,^{+0.010}_{-0.009}$	1948	6.8
		0.017 – 0.025	0.021	$0.681 \pm 0.018\,^{+0.012}_{-0.012}$	1523	0.5
		0.025 – 0.037	0.032	$0.567 \pm 0.014\,^{+0.011}_{-0.010}$	1676	0.0
		0.037 – 0.06	0.05	$0.504 \pm 0.011\,^{+0.013}_{-0.012}$	2125	0.0
		0.06 – 0.1	0.08	$0.409 \pm 0.010\,^{+0.008}_{-0.008}$	1687	0.0
		0.1 – 0.17	0.13	$0.355 \pm 0.009\,^{+0.017}_{-0.017}$	1545	0.0
		0.17 – 0.3	0.25	$0.252 \pm 0.008\,^{+0.014}_{-0.014}$	1135	0.0
530 – 710	650	0.01 – 0.017	0.013	$0.874 \pm 0.019\,^{+0.013}_{-0.007}$	2231	25.1
		0.017 – 0.025	0.021	$0.761 \pm 0.020\,^{+0.009}_{-0.008}$	1511	2.4
		0.025 – 0.037	0.032	$0.597 \pm 0.018\,^{+0.007}_{-0.006}$	1151	0.6
		0.037 – 0.06	0.05	$0.499 \pm 0.015\,^{+0.005}_{-0.005}$	1186	0.0
		0.06 – 0.1	0.08	$0.415 \pm 0.013\,^{+0.010}_{-0.010}$	988	0.0
		0.1 – 0.17	0.13	$0.349 \pm 0.012\,^{+0.009}_{-0.008}$	891	0.0
		0.17 – 0.3	0.25	$0.250 \pm 0.009\,^{+0.016}_{-0.016}$	780	0.0
710 – 900	800	0.009 – 0.017	0.013	$0.828 \pm 0.023\,^{+0.014}_{-0.016}$	1347	20.7
		0.017 – 0.025	0.021	$0.685 \pm 0.023\,^{+0.008}_{-0.006}$	924	1.3
		0.025 – 0.037	0.032	$0.617 \pm 0.020\,^{+0.008}_{-0.009}$	1000	3.1
		0.037 – 0.06	0.05	$0.495 \pm 0.015\,^{+0.011}_{-0.011}$	1082	0.0
		0.06 – 0.1	0.08	$0.446 \pm 0.014\,^{+0.012}_{-0.012}$	974	0.0
		0.1 – 0.17	0.13	$0.375 \pm 0.013\,^{+0.004}_{-0.004}$	797	0.0
		0.17 – 0.3	0.25	$0.239 \pm 0.010\,^{+0.009}_{-0.008}$	552	0.0

Table 11 (*Continued*)

Q^2 range (GeV²)	Q_c^2 (GeV²)	x range	x_c	$\tilde{\sigma}$	N_{data}	$N_{\text{bg}}^{\text{MC}}$
900 – 1300	1200	0.01 –0.017	0.014	$0.875 \pm 0.030^{+0.021}_{-0.028}$	911	31.9
		0.017–0.025	0.021	$0.744 \pm 0.024^{+0.014}_{-0.012}$	1005	9.8
		0.025–0.037	0.032	$0.594 \pm 0.019^{+0.007}_{-0.007}$	1013	4.9
		0.037–0.06	0.05	$0.557 \pm 0.015^{+0.007}_{-0.008}$	1352	0.5
		0.06 –0.1	0.08	$0.436 \pm 0.013^{+0.006}_{-0.006}$	1215	0.0
		0.1 –0.17	0.13	$0.364 \pm 0.012^{+0.004}_{-0.004}$	995	0.0
		0.17 –0.3	0.25	$0.225 \pm 0.009^{+0.005}_{-0.005}$	716	0.0
		0.3 –0.53	0.4	$0.120 \pm 0.008^{+0.010}_{-0.007}$	257	0.0
1300 – 1800	1500	0.017–0.025	0.021	$0.761 \pm 0.034^{+0.019}_{-0.018}$	530	24.5
		0.025–0.037	0.032	$0.617 \pm 0.026^{+0.004}_{-0.004}$	575	3.0
		0.037–0.06	0.05	$0.538 \pm 0.020^{+0.005}_{-0.004}$	756	0.6
		0.06 –0.1	0.08	$0.454 \pm 0.017^{+0.005}_{-0.005}$	751	0.0
		0.1 –0.15	0.13	$0.365 \pm 0.017^{+0.008}_{-0.006}$	487	0.0
		0.15 –0.23	0.18	$0.293 \pm 0.015^{+0.005}_{-0.005}$	403	0.0
		0.23 –0.35	0.25	$0.263 \pm 0.015^{+0.005}_{-0.005}$	304	0.0
		0.35 –0.53	0.4	$0.122 \pm 0.011^{+0.011}_{-0.005}$	126	0.0
1800 – 2500	2000	0.023–0.037	0.032	$0.631 \pm 0.032^{+0.016}_{-0.009}$	405	8.0
		0.037–0.06	0.05	$0.529 \pm 0.024^{+0.005}_{-0.004}$	476	0.0
		0.06 –0.1	0.08	$0.438 \pm 0.020^{+0.009}_{-0.009}$	497	0.5
		0.1 –0.15	0.13	$0.417 \pm 0.021^{+0.003}_{-0.005}$	412	0.0
		0.15 –0.23	0.18	$0.295 \pm 0.017^{+0.002}_{-0.006}$	288	0.0
		0.23 –0.35	0.25	$0.232 \pm 0.017^{+0.004}_{-0.004}$	197	0.0
		0.35 –0.53	0.4	$0.118^{+0.013}_{-0.012}\ ^{+0.004}_{-0.005}$	98	0.0
2500 – 3500	3000	0.037–0.06	0.05	$0.557 \pm 0.032^{+0.011}_{-0.006}$	311	3.8
		0.06 –0.1	0.08	$0.508 \pm 0.026^{+0.006}_{-0.006}$	377	0.6
		0.1 –0.15	0.13	$0.378 \pm 0.024^{+0.004}_{-0.003}$	260	0.0
		0.15 –0.23	0.18	$0.292 \pm 0.021^{+0.003}_{-0.004}$	201	0.0
		0.23 –0.35	0.25	$0.304 \pm 0.022^{+0.023}_{-0.022}$	190	0.0
		0.35 –0.53	0.4	$0.106^{+0.015}_{-0.014}\ ^{+0.004}_{-0.004}$	61	0.0
		0.53 –0.75	0.65	$0.015^{+0.004}_{-0.003}\ ^{+0.002}_{-0.002}$	23	0.0
3500 – 5600	5000	0.04 –0.1	0.08	$0.480 \pm 0.025^{+0.009}_{-0.004}$	380	3.1
		0.1 –0.15	0.13	$0.430 \pm 0.028^{+0.004}_{-0.003}$	236	0.6
		0.15 –0.23	0.18	$0.325 \pm 0.023^{+0.003}_{-0.002}$	199	0.0
		0.23 –0.35	0.25	$0.260 \pm 0.022^{+0.005}_{-0.003}$	142	0.0
		0.35 –0.53	0.4	$0.152^{+0.019}_{-0.017}\ ^{+0.010}_{-0.010}$	80	0.0
5600 – 9000	8000	0.07 –0.15	0.13	$0.534 \pm 0.035^{+0.005}_{-0.010}$	231	1.9
		0.15 –0.23	0.18	$0.430 \pm 0.036^{+0.011}_{-0.012}$	143	0.0
		0.23 –0.35	0.25	$0.294^{+0.034}_{-0.031}\ ^{+0.011}_{-0.011}$	92	0.0
		0.35 –0.53	0.4	$0.113^{+0.022}_{-0.019}\ ^{+0.008}_{-0.008}$	36	0.0
		0.53 –0.75	0.65	$0.018^{+0.006}_{-0.005}\ ^{+0.001}_{-0.001}$	14	0.0
9000 –15000	12000	0.09 –0.23	0.18	$0.401^{+0.045}_{-0.040}\ ^{+0.005}_{-0.015}$	99	0.6
		0.23 –0.35	0.25	$0.359^{+0.051}_{-0.045}\ ^{+0.010}_{-0.008}$	63	0.0
		0.35 –0.53	0.4	$0.172^{+0.035}_{-0.030}\ ^{+0.008}_{-0.007}$	33	0.0
15000 –25000	20000	0.15 –0.35	0.25	$0.456^{+0.073}_{-0.064}\ ^{+0.028}_{-0.016}$	53	1.8
		0.35 –0.75	0.4	$0.175^{+0.050}_{-0.040}\ ^{+0.009}_{-0.007}$	19	0.0
25000 –50000	30000	0.25 –0.75	0.4	$0.190^{+0.066}_{-0.050}\ ^{+0.013}_{-0.011}$	14	0.0

Table 12 Systematic uncertainties with bin-to-bin correlations for the reduced cross section $\tilde{\sigma}$ for the reaction $e^- p \rightarrow e^- X$ ($\mathcal{L} = 71.2\,\text{pb}^{-1}$, $P_e = +0.29$). The left five columns of the table contain the bin centres, Q_c^2 and x_c, the measured cross section, the statistical uncertainty and the total systematic uncertainty. The right eight columns of the table list the bin-to-bin correlated systematic uncertainties for δ_1–δ_7, and the systematic uncertainties summed in quadrature for δ_8–δ_{13}, as defined in Sect. 8. The upper and lower correlated uncertainties correspond to a positive or negative variation of a cut value for example. However, if this is not possible for a particular systematic, the uncertainty is symmetrised

Q_c^2 (GeV²)	x_c	$\tilde{\sigma}$	stat. (%)	sys. (%)	δ_1 (%)	δ_2 (%)	δ_3 (%)	δ_4 (%)	δ_5 (%)	δ_6 (%)	δ_7 (%)	δ_8–δ_{13} (%)
200	0.005	1.094	±1.4	+1.3 / −1.0	+0.7 / −0.0	−0.4 / +0.6	+0.4 / −0.4	−0.4 / +0.4	+0.0 / +0.0	+0.1 / −0.1	+0.3 / −0.3	+0.7 / −0.7
	0.008	0.928	±1.2	+1.9 / −1.9	+0.3 / −0.0	−0.4 / +0.5	+0.2 / −0.2	−1.6 / +1.6	+0.0 / +0.0	+0.1 / +0.4	+0.1 / −0.1	+0.8 / −1.0
	0.013	0.785	±1.2	+1.7 / −1.6	+0.2 / +0.0	−0.5 / +0.5	−0.2 / +0.2	−1.3 / +1.3	+0.0 / +0.0	+0.0 / +0.4	+0.0 / −0.0	+0.8 / −0.9
	0.021	0.669	±1.4	+2.1 / −2.1	+0.4 / +0.0	−0.3 / +0.5	−1.6 / +1.6	+0.9 / −0.9	+0.0 / +0.0	−0.1 / +0.1	+0.0 / +0.0	+0.8 / −0.9
	0.032	0.558	±1.5	+4.0 / −4.0	+0.1 / −0.0	−0.3 / +0.4	−1.5 / +1.5	+3.6 / −3.6	+0.0 / +0.0	+0.2 / +0.4	+0.0 / +0.0	+0.8 / −0.8
	0.05	0.500	±1.5	+2.5 / −2.4	+0.0 / −0.3	−0.2 / +0.3	−0.5 / +0.5	+2.2 / −2.2	+0.0 / +0.0	+0.0 / +0.3	+0.0 / +0.0	+1.0 / −0.9
	0.08	0.435	±1.3	+5.5 / −5.5	+0.0 / −0.1	−0.2 / +0.2	+5.0 / −5.0	+2.0 / −2.0	+0.0 / +0.0	−0.0 / +0.1	+0.0 / +0.0	+0.8 / −1.0
	0.18	0.325	±1.9	+5.4 / −5.4	+0.1 / +0.0	−0.1 / +0.2	+5.3 / −5.3	+0.5 / −0.5	+0.7 / +0.2	−0.1 / +0.1	+0.0 / +0.0	+0.7 / −0.9
250	0.008	0.920	±1.5	+1.5 / −1.3	+0.6 / −0.0	−0.3 / +0.4	+0.5 / −0.5	−0.9 / +0.9	+0.0 / +0.0	−0.2 / +0.3	+0.1 / −0.1	+0.7 / −0.7
	0.013	0.787	±1.4	+1.7 / −1.5	+0.7 / +0.0	−0.5 / +0.6	+0.0 / −0.0	−1.3 / +1.3	+0.0 / +0.0	−0.1 / +0.2	+0.0 / −0.0	+0.5 / −0.7
	0.021	0.649	±1.7	+1.6 / −1.4	+0.7 / −0.0	−0.3 / +0.5	−0.1 / +0.1	+1.1 / −1.1	+0.0 / +0.0	−0.2 / +0.2	+0.0 / −0.0	+0.8 / −0.7
	0.032	0.564	±1.7	+3.3 / −3.3	+0.6 / −0.0	−0.3 / +0.4	−0.8 / +0.8	+3.0 / −3.0	+0.0 / +0.0	+0.0 / +0.1	+0.0 / +0.0	+0.7 / −0.9
	0.05	0.481	±1.8	+3.4 / −3.3	+0.4 / +0.0	−0.1 / +0.3	−2.4 / +2.4	+2.2 / −2.2	+0.0 / +0.0	−0.0 / −0.1	+0.0 / +0.0	+0.7 / −0.6
	0.08	0.431	±1.6	+5.2 / −5.1	+0.7 / −0.0	−0.1 / +0.3	+4.6 / −4.6	+2.2 / −2.2	+0.0 / +0.0	−0.0 / +0.1	+0.0 / +0.0	+0.7 / −0.7
	0.18	0.324	±1.9	+4.8 / −4.7	+0.2 / +0.0	+0.0 / +0.2	+4.1 / −4.1	+2.0 / −2.0	+0.3 / +1.0	+0.0 / +0.2	+0.0 / +0.0	+0.8 / −0.8
350	0.008	0.973	±1.9	+2.1 / −1.5	+1.6 / −0.1	−0.5 / +0.6	+0.9 / −0.9	−0.4 / +0.4	+0.0 / +0.0	−0.6 / +0.4	+0.4 / −0.4	+0.6 / −0.8
	0.013	0.826	±1.6	+1.9 / −1.2	+1.4 / −0.0	−0.2 / +0.5	−0.2 / +0.2	−1.0 / +1.0	+0.0 / +0.0	−0.2 / +0.5	+0.0 / −0.0	+0.7 / −0.6
	0.021	0.692	±1.9	+0.9 / −0.6	+0.4 / −0.1	−0.3 / +0.4	+0.3 / −0.3	+0.0 / −0.0	+0.0 / +0.0	−0.2 / −0.0	+0.0 / +0.0	+0.6 / −0.5
	0.032	0.603	±1.9	+1.9 / −1.8	+0.8 / −0.0	−0.2 / +0.4	−1.6 / +1.6	+0.2 / −0.2	+0.0 / +0.0	−0.3 / +0.1	+0.0 / +0.0	+0.6 / −0.7
	0.05	0.503	±1.9	+2.7 / −2.6	+0.6 / −0.0	−0.1 / +0.2	−1.9 / +1.9	+1.6 / −1.6	+0.0 / +0.0	−0.1 / +0.2	+0.0 / +0.0	+0.5 / −0.7
	0.08	0.432	±1.7	+2.0 / −2.0	+0.3 / +0.0	−0.1 / +0.2	+1.1 / −1.1	+1.6 / −1.6	+0.0 / +0.0	+0.0 / +0.1	+0.0 / +0.0	+0.7 / −0.7
	0.18	0.306	±2.0	+6.4 / −6.3	+0.4 / +0.0	−0.0 / +0.2	+5.7 / −5.7	+2.6 / −2.6	−0.1 / +1.2	+0.1 / +0.2	+0.0 / +0.0	+0.7 / −0.6
450	0.008	1.004	±2.2	+2.4 / −2.1	+0.7 / −0.3	−1.4 / +1.6	+1.3 / −1.3	−0.5 / +0.5	+0.0 / +0.0	−0.2 / +0.3	+0.6 / −0.6	+0.5 / −0.4
	0.013	0.843	±2.3	+1.1 / −1.1	+0.1 / −0.1	−0.5 / +0.6	−0.4 / +0.4	+0.2 / −0.2	+0.0 / +0.0	−0.6 / +0.6	+0.1 / −0.1	+0.5 / −0.6
	0.021	0.681	±2.6	+1.8 / −1.7	+0.2 / −0.1	−0.4 / +0.5	−0.1 / +0.1	+1.3 / −1.3	+0.0 / +0.0	−0.7 / +0.9	+0.0 / −0.0	+0.8 / −0.8
	0.032	0.567	±2.5	+1.9 / −1.7	+0.8 / −0.1	−0.2 / +0.4	+0.0 / −0.0	+1.4 / −1.4	+0.0 / +0.0	−0.5 / +0.4	+0.0 / +0.0	+1.0 / −0.9
	0.05	0.504	±2.2	+2.5 / −2.4	+0.7 / −0.0	+0.0 / +0.2	−1.6 / +1.6	+1.6 / −1.6	+0.0 / +0.0	−0.4 / +0.6	+0.0 / +0.0	+0.7 / −0.7
	0.08	0.409	±2.5	+2.1 / −1.9	+0.3 / +0.0	+0.1 / +0.2	−0.7 / +0.7	+1.7 / −1.7	+0.0 / +0.0	+0.1 / +0.6	+0.0 / +0.0	+0.7 / −0.5
	0.13	0.355	±2.6	+4.9 / −4.9	+0.6 / +0.0	+0.1 / +0.1	+4.4 / −4.4	+1.9 / −1.9	+0.0 / +0.0	−0.4 / +0.4	+0.0 / +0.0	+0.5 / −0.6
	0.25	0.252	±3.0	+5.6 / −5.5	+1.1 / +0.0	+0.2 / +0.1	+5.2 / −5.2	+1.1 / −1.1	−0.9 / +0.8	−0.1 / +0.6	+0.0 / +0.0	+0.8 / −0.8
650	0.013	0.874	±2.2	+1.5 / −0.8	+1.2 / −0.2	−0.5 / +0.6	−0.0 / +0.0	−0.1 / +0.1	+0.0 / +0.0	−0.2 / +0.3	+0.5 / −0.5	+0.4 / −0.3
	0.021	0.761	±2.6	+1.1 / −1.1	+0.0 / −0.1	−0.4 / +0.5	−0.3 / +0.3	−0.9 / +0.9	+0.0 / +0.0	−0.2 / +0.0	+0.1 / −0.1	+0.2 / −0.2
	0.032	0.597	±3.0	+1.2 / −1.0	+0.5 / −0.2	−0.4 / +0.5	−0.5 / +0.5	+0.7 / −0.7	+0.0 / +0.0	+0.5 / +0.5	+0.0 / −0.0	+0.2 / −0.2
	0.05	0.499	±2.9	+1.0 / −0.9	+0.1 / −0.0	−0.3 / +0.4	−0.4 / +0.4	+0.7 / −0.7	+0.0 / +0.0	+0.1 / +0.0	+0.0 / +0.0	+0.5 / −0.4
	0.08	0.415	±3.2	+2.4 / −2.3	+0.7 / −0.0	−0.1 / +0.3	−1.8 / +1.8	+1.0 / −1.0	+0.0 / +0.0	+0.1 / −0.0	+0.0 / +0.0	+0.9 / −1.1
	0.13	0.349	±3.4	+2.7 / −2.4	+0.9 / −0.0	−0.1 / +0.2	+2.1 / −2.1	−0.8 / +0.8	+0.0 / +0.0	+0.1 / +0.4	+0.0 / +0.0	+1.0 / −0.9
	0.25	0.250	±3.6	+6.6 / −6.5	+1.0 / −0.0	−0.1 / +0.3	+6.3 / −6.3	+1.0 / −1.0	−0.8 / +0.2	−0.1 / +0.5	+0.0 / +0.0	+1.0 / −1.1
800	0.013	0.828	±2.8	+1.7 / −1.9	+0.4 / −1.0	−0.8 / +1.0	+0.4 / −0.4	−1.0 / +1.0	+0.0 / +0.0	−0.1 / +0.0	+0.6 / −0.6	+0.3 / −0.4
	0.021	0.685	±3.3	+1.1 / −0.9	+0.5 / −0.1	−0.4 / +0.5	+0.6 / −0.6	−0.2 / +0.2	+0.0 / +0.0	+0.0 / +0.5	+0.1 / −0.1	+0.4 / −0.4
	0.032	0.617	±3.2	+1.4 / −1.4	+0.0 / −0.4	−0.4 / +0.5	−0.8 / +0.8	−0.9 / +0.9	+0.0 / +0.0	+0.3 / +0.0	+0.1 / −0.1	+0.2 / −0.4
	0.05	0.495	±3.1	+2.2 / −2.2	+0.3 / +0.0	−0.3 / +0.4	+0.7 / −0.7	+2.0 / −2.0	+0.0 / +0.0	−0.4 / +0.1	+0.0 / +0.0	+0.3 / −0.4
	0.08	0.446	±3.2	+2.6 / −2.6	+0.5 / −0.0	−0.2 / +0.3	−2.5 / +2.5	+0.1 / −0.1	+0.0 / +0.0	+0.5 / −0.7	+0.0 / +0.0	+0.3 / −0.4
	0.13	0.375	±3.6	+1.1 / −1.0	+0.5 / −0.0	−0.2 / +0.3	+0.7 / −0.7	+0.6 / −0.6	+0.0 / +0.0	+0.1 / −0.4	+0.0 / +0.0	+0.2 / −0.2
	0.25	0.239	±4.3	+3.7 / −3.4	+0.3 / +0.0	−0.2 / +0.2	+3.3 / −3.3	+0.8 / −0.8	+1.2 / −0.1	+0.7 / −0.5	+0.0 / +0.0	+0.2 / −0.3

Table 12 (*Continued*)

Q_c^2 (GeV²)	x_c	$\tilde\sigma$	stat. (%)	sys. (%)	δ_1 (%)	δ_2 (%)	δ_3 (%)	δ_4 (%)	δ_5 (%)	δ_6 (%)	δ_7 (%)	δ_8–δ_{13} (%)
1200	0.014	0.875	± 3.4	$^{+2.4}_{-3.2}$	$^{+0.6}_{-2.2}$	$^{-0.8}_{+1.0}$	$^{-0.7}_{+0.7}$	$^{-1.4}_{+1.4}$	$^{+0.0}_{+0.0}$	$^{-0.3}_{-0.8}$	$^{+1.4}_{-1.4}$	$^{+0.5}_{-0.2}$
	0.021	0.744	± 3.2	$^{+1.9}_{-1.6}$	$^{+0.9}_{-0.1}$	$^{-0.5}_{+0.5}$	$^{+1.5}_{-1.5}$	$^{+0.0}_{-0.0}$	$^{+0.0}_{+0.0}$	$^{+0.1}_{+0.4}$	$^{+0.4}_{-0.4}$	$^{+0.3}_{-0.4}$
	0.032	0.594	± 3.2	$^{+1.2}_{-1.1}$	$^{+0.0}_{-0.1}$	$^{-0.4}_{+0.5}$	$^{-0.5}_{+0.5}$	$^{-0.7}_{+0.7}$	$^{+0.0}_{+0.0}$	$^{+0.1}_{+0.1}$	$^{+0.2}_{-0.2}$	$^{+0.6}_{-0.6}$
	0.05	0.557	± 2.8	$^{+1.3}_{-1.4}$	$^{+0.1}_{-0.0}$	$^{-0.3}_{+0.3}$	$^{-0.1}_{+0.1}$	$^{+1.2}_{-1.2}$	$^{+0.0}_{+0.0}$	$^{-0.3}_{-0.4}$	$^{+0.0}_{-0.0}$	$^{+0.4}_{-0.4}$
	0.08	0.436	± 2.9	$^{+1.4}_{-1.3}$	$^{+0.3}_{-0.0}$	$^{-0.2}_{+0.4}$	$^{-0.3}_{+0.3}$	$^{+1.2}_{-1.2}$	$^{+0.0}_{+0.0}$	$^{+0.3}_{-0.3}$	$^{+0.0}_{+0.0}$	$^{+0.4}_{-0.3}$
	0.13	0.364	± 3.2	$^{+1.1}_{-1.2}$	$^{+0.1}_{-0.0}$	$^{-0.1}_{+0.2}$	$^{-0.9}_{+0.9}$	$^{+0.4}_{-0.4}$	$^{+0.0}_{+0.0}$	$^{+0.1}_{-0.5}$	$^{+0.0}_{+0.0}$	$^{+0.3}_{-0.4}$
	0.25	0.225	± 3.8	$^{+2.4}_{-2.3}$	$^{+0.3}_{+0.0}$	$^{-0.2}_{+0.3}$	$^{+2.0}_{-2.0}$	$^{+1.0}_{-1.0}$	$^{+0.0}_{+0.0}$	$^{-0.3}_{-0.1}$	$^{+0.0}_{+0.0}$	$^{+0.5}_{-0.4}$
	0.4	0.120	± 6.3	$^{+8.1}_{-5.7}$	$^{+0.0}_{-0.1}$	$^{-0.4}_{+0.4}$	$^{+5.6}_{-5.6}$	$^{+0.6}_{-0.6}$	$^{+5.8}_{+3.4}$	$^{+0.5}_{-1.0}$	$^{+0.0}_{+0.0}$	$^{+0.5}_{-0.5}$
1500	0.021	0.761	± 4.5	$^{+2.6}_{-2.3}$	$^{+0.9}_{-0.2}$	$^{-0.6}_{+0.4}$	$^{-0.4}_{+0.4}$	$^{-0.1}_{+0.1}$	$^{+0.0}_{+0.0}$	$^{-1.0}_{+0.1}$	$^{+2.3}_{-1.9}$	$^{+0.4}_{-0.4}$
	0.032	0.617	± 4.2	$^{+0.7}_{-0.6}$	$^{+0.3}_{-0.1}$	$^{-0.3}_{+0.3}$	$^{-0.1}_{+0.1}$	$^{-0.3}_{+0.3}$	$^{+0.0}_{+0.0}$	$^{-0.1}_{-0.1}$	$^{+0.2}_{-0.2}$	$^{+0.4}_{-0.3}$
	0.05	0.538	± 3.7	$^{+0.9}_{-0.8}$	$^{+0.2}_{-0.0}$	$^{-0.3}_{+0.4}$	$^{+0.2}_{-0.2}$	$^{+0.4}_{-0.4}$	$^{+0.0}_{+0.0}$	$^{-0.4}_{+0.5}$	$^{+0.0}_{-0.0}$	$^{+0.3}_{-0.4}$
	0.08	0.454	± 3.7	$^{+1.0}_{-1.1}$	$^{+0.2}_{-0.0}$	$^{-0.3}_{+0.4}$	$^{-0.9}_{+0.9}$	$^{-0.2}_{+0.2}$	$^{+0.0}_{+0.0}$	$^{-0.4}_{+0.1}$	$^{+0.0}_{+0.0}$	$^{+0.3}_{-0.5}$
	0.13	0.365	± 4.6	$^{+2.1}_{-1.8}$	$^{+0.8}_{-0.0}$	$^{-0.1}_{+0.3}$	$^{-1.3}_{+1.3}$	$^{-1.1}_{+1.1}$	$^{+0.0}_{+0.0}$	$^{+0.8}_{-0.2}$	$^{+0.0}_{+0.0}$	$^{+0.3}_{-0.4}$
	0.18	0.293	± 5.0	$^{+1.8}_{-1.7}$	$^{+0.6}_{-0.1}$	$^{-0.3}_{+0.2}$	$^{+0.0}_{-0.0}$	$^{-1.6}_{+1.6}$	$^{+0.0}_{+0.0}$	$^{-0.3}_{-0.2}$	$^{+0.0}_{+0.0}$	$^{+0.4}_{-0.4}$
	0.25	0.263	± 5.8	$^{+1.9}_{-1.9}$	$^{+0.0}_{-0.3}$	$^{-0.3}_{+0.3}$	$^{+1.7}_{-1.7}$	$^{+0.6}_{-0.6}$	$^{+0.1}_{-0.3}$	$^{-0.1}_{-0.3}$	$^{+0.0}_{+0.0}$	$^{+0.3}_{-0.3}$
	0.4	0.122	± 9.0	$^{+8.8}_{-4.3}$	$^{+0.6}_{+0.0}$	$^{-0.5}_{+0.3}$	$^{+2.0}_{-2.0}$	$^{-0.9}_{+0.9}$	$^{+8.4}_{-3.6}$	$^{+0.3}_{-0.4}$	$^{+0.0}_{+0.0}$	$^{+0.6}_{-0.5}$
2000	0.032	0.631	± 5.1	$^{+2.5}_{-1.4}$	$^{+1.8}_{+0.0}$	$^{-0.2}_{+0.2}$	$^{+0.3}_{-0.3}$	$^{+1.0}_{-1.0}$	$^{+0.0}_{+0.0}$	$^{+0.4}_{+0.7}$	$^{+1.1}_{-0.8}$	$^{+0.3}_{-0.4}$
	0.05	0.529	± 4.6	$^{+1.0}_{-0.8}$	$^{+0.5}_{-0.0}$	$^{-0.3}_{+0.4}$	$^{-0.3}_{+0.3}$	$^{-0.6}_{+0.6}$	$^{+0.0}_{+0.0}$	$^{+0.1}_{+0.1}$	$^{+0.0}_{+0.0}$	$^{+0.3}_{-0.3}$
	0.08	0.438	± 4.5	$^{+2.0}_{-2.0}$	$^{+0.1}_{-0.1}$	$^{-0.3}_{+0.4}$	$^{-0.1}_{+0.1}$	$^{+1.9}_{-1.9}$	$^{+0.0}_{+0.0}$	$^{+0.2}_{+0.0}$	$^{+0.0}_{-0.0}$	$^{+0.3}_{-0.3}$
	0.13	0.417	± 5.0	$^{+0.8}_{-1.2}$	$^{+0.1}_{-0.6}$	$^{-0.2}_{+0.3}$	$^{-0.5}_{+0.5}$	$^{+0.5}_{-0.5}$	$^{+0.0}_{+0.0}$	$^{+0.1}_{-0.6}$	$^{+0.0}_{+0.0}$	$^{+0.3}_{-0.4}$
	0.18	0.295	± 5.9	$^{+0.6}_{-1.9}$	$^{+0.0}_{-0.7}$	$^{-0.2}_{+0.2}$	$^{-0.3}_{+0.3}$	$^{+0.1}_{-0.1}$	$^{+0.0}_{+0.0}$	$^{-0.4}_{-1.6}$	$^{+0.0}_{+0.0}$	$^{+0.4}_{-0.6}$
	0.25	0.232	± 7.2	$^{+1.7}_{-1.6}$	$^{+0.3}_{-0.0}$	$^{-0.2}_{+0.3}$	$^{+1.5}_{-1.5}$	$^{+0.5}_{-0.5}$	$^{+0.0}_{+0.0}$	$^{+0.4}_{+0.5}$	$^{+0.0}_{+0.0}$	$^{+0.5}_{-0.5}$
	0.4	0.118	$^{+11.2}_{-10.1}$	$^{+3.7}_{-3.9}$	$^{+0.0}_{-0.2}$	$^{-0.3}_{+0.4}$	$^{+3.1}_{-3.1}$	$^{+1.1}_{-1.1}$	$^{-0.5}_{+1.0}$	$^{+0.1}_{-1.3}$	$^{+0.0}_{+0.0}$	$^{+1.2}_{-1.4}$
3000	0.05	0.557	± 5.7	$^{+2.0}_{-1.1}$	$^{+1.6}_{-0.1}$	$^{-0.3}_{+0.4}$	$^{+0.9}_{-0.9}$	$^{-0.0}_{+0.0}$	$^{+0.0}_{+0.0}$	$^{+0.4}_{+0.2}$	$^{+0.5}_{-0.5}$	$^{+0.4}_{-0.3}$
	0.08	0.508	± 5.2	$^{+1.1}_{-1.1}$	$^{+0.2}_{-0.4}$	$^{-0.2}_{+0.3}$	$^{-0.4}_{+0.4}$	$^{+0.8}_{-0.8}$	$^{+0.0}_{+0.0}$	$^{+0.5}_{-0.1}$	$^{+0.1}_{-0.1}$	$^{+0.3}_{-0.5}$
	0.13	0.378	± 6.2	$^{+0.9}_{-0.7}$	$^{+0.1}_{-0.1}$	$^{-0.2}_{+0.3}$	$^{+0.6}_{-0.6}$	$^{-0.1}_{+0.1}$	$^{+0.0}_{+0.0}$	$^{-0.3}_{-0.3}$	$^{+0.0}_{+0.0}$	$^{+0.7}_{-0.1}$
	0.18	0.292	± 7.1	$^{+1.2}_{-1.3}$	$^{+0.0}_{-0.3}$	$^{-0.2}_{+0.2}$	$^{-0.9}_{+0.9}$	$^{-0.6}_{+0.6}$	$^{+0.0}_{+0.0}$	$^{-0.5}_{+0.2}$	$^{+0.0}_{+0.0}$	$^{+0.4}_{-0.3}$
	0.25	0.304	± 7.3	$^{+7.4}_{-7.3}$	$^{+0.6}_{-0.0}$	$^{-0.2}_{+0.2}$	$^{+7.3}_{-7.3}$	$^{+0.2}_{-0.2}$	$^{+0.0}_{+0.0}$	$^{+1.1}_{+0.3}$	$^{+0.0}_{+0.0}$	$^{+0.8}_{-0.6}$
	0.4	0.106	$^{+14.5}_{-12.8}$	$^{+3.8}_{-3.5}$	$^{+1.3}_{-0.0}$	$^{-0.2}_{+0.4}$	$^{-3.4}_{+3.4}$	$^{+0.5}_{-0.5}$	$^{+0.4}_{-0.0}$	$^{+0.8}_{-0.3}$	$^{+0.0}_{+0.0}$	$^{+0.6}_{-0.6}$
	0.65	0.015	$^{+25.5}_{-20.7}$	$^{+10.2}_{-10.4}$	$^{+0.0}_{-0.6}$	$^{-0.8}_{+1.0}$	$^{-8.7}_{+8.7}$	$^{+4.6}_{-4.6}$	$^{+1.8}_{+0.7}$	$^{-2.7}_{+0.9}$	$^{+0.0}_{+0.0}$	$^{+1.7}_{-2.0}$
5000	0.08	0.480	± 5.2	$^{+1.8}_{-0.9}$	$^{+1.6}_{-0.3}$	$^{-0.2}_{+0.2}$	$^{-0.3}_{+0.3}$	$^{+0.2}_{-0.2}$	$^{+0.0}_{+0.0}$	$^{-0.6}_{-0.4}$	$^{+0.3}_{-0.3}$	$^{+0.5}_{-0.3}$
	0.13	0.430	± 6.5	$^{+1.0}_{-0.8}$	$^{+0.8}_{+0.0}$	$^{-0.2}_{+0.2}$	$^{-0.4}_{+0.4}$	$^{+0.3}_{-0.3}$	$^{+0.0}_{+0.0}$	$^{+0.1}_{-0.3}$	$^{+0.1}_{-0.1}$	$^{+0.2}_{-0.5}$
	0.18	0.325	± 7.1	$^{+1.0}_{-0.5}$	$^{+0.2}_{-0.1}$	$^{-0.3}_{+0.2}$	$^{+0.2}_{-0.2}$	$^{+0.3}_{-0.3}$	$^{+0.0}_{+0.0}$	$^{-0.1}_{+0.7}$	$^{+0.0}_{+0.0}$	$^{+0.5}_{-0.3}$
	0.25	0.260	± 8.4	$^{+1.8}_{-1.2}$	$^{+0.7}_{-0.0}$	$^{-0.2}_{+0.3}$	$^{+0.7}_{-0.7}$	$^{-0.7}_{+0.7}$	$^{+0.0}_{+0.0}$	$^{+1.2}_{-0.6}$	$^{+0.0}_{+0.0}$	$^{+0.4}_{-0.3}$
	0.4	0.152	$^{+12.5}_{-11.2}$	$^{+6.5}_{-6.4}$	$^{+0.0}_{-0.3}$	$^{-0.2}_{+0.3}$	$^{+6.0}_{-6.0}$	$^{-2.1}_{+2.1}$	$^{+0.0}_{+0.0}$	$^{+0.4}_{+1.3}$	$^{+0.0}_{+0.0}$	$^{+1.1}_{-1.1}$
8000	0.13	0.534	± 6.6	$^{+1.0}_{-1.9}$	$^{+0.0}_{-1.0}$	$^{-0.3}_{+0.3}$	$^{-0.5}_{+0.5}$	$^{-0.1}_{+0.1}$	$^{+0.0}_{+0.0}$	$^{-1.3}_{+0.3}$	$^{+0.5}_{-0.3}$	$^{+0.5}_{-0.5}$
	0.18	0.430	± 8.4	$^{+2.6}_{-2.9}$	$^{+0.1}_{-0.3}$	$^{-0.2}_{+0.2}$	$^{-2.4}_{+2.4}$	$^{+0.6}_{-0.6}$	$^{+0.0}_{+0.0}$	$^{+0.5}_{-0.3}$	$^{+0.0}_{+0.0}$	$^{+0.6}_{-1.3}$
	0.25	0.294	$^{+11.6}_{-10.4}$	$^{+3.8}_{-3.9}$	$^{+0.7}_{-0.1}$	$^{-0.3}_{+0.2}$	$^{-3.6}_{+3.6}$	$^{+0.4}_{-0.4}$	$^{+0.0}_{+0.0}$	$^{-1.1}_{-0.6}$	$^{+0.0}_{+0.0}$	$^{+0.4}_{-0.4}$
	0.4	0.113	$^{+19.6}_{-16.6}$	$^{+7.1}_{-7.3}$	$^{+0.1}_{-0.0}$	$^{-0.3}_{+0.4}$	$^{+7.0}_{-7.0}$	$^{-0.6}_{+0.6}$	$^{+0.0}_{+0.0}$	$^{-0.3}_{+0.5}$	$^{+0.0}_{+0.0}$	$^{+0.6}_{-2.0}$
	0.65	0.018	$^{+34.5}_{-26.5}$	$^{+4.1}_{-4.2}$	$^{+0.2}_{-1.4}$	$^{-0.9}_{+0.9}$	$^{+1.5}_{-1.5}$	$^{+2.3}_{-2.3}$	$^{+0.0}_{+0.0}$	$^{-2.6}_{+2.8}$	$^{+0.0}_{+0.0}$	$^{+0.8}_{-0.6}$
12000	0.18	0.401	$^{+11.1}_{-10.1}$	$^{+1.3}_{-3.8}$	$^{+1.0}_{+0.4}$	$^{-0.3}_{+0.4}$	$^{-0.4}_{+0.4}$	$^{-0.2}_{+0.2}$	$^{+0.0}_{+0.0}$	$^{-0.3}_{-0.8}$	$^{+0.2}_{-0.3}$	$^{+0.5}_{-0.6}$
	0.25	0.359	$^{+14.3}_{-12.6}$	$^{+2.8}_{-2.3}$	$^{+2.4}_{-0.6}$	$^{-0.2}_{+0.2}$	$^{+0.3}_{-0.3}$	$^{+0.8}_{-0.8}$	$^{+0.0}_{+0.0}$	$^{+0.3}_{-1.6}$	$^{+0.0}_{+0.0}$	$^{+1.0}_{-1.2}$
	0.4	0.172	$^{+20.6}_{-17.3}$	$^{+4.6}_{-3.8}$	$^{+2.7}_{-0.2}$	$^{-0.3}_{+0.4}$	$^{+3.2}_{-3.2}$	$^{-0.8}_{+0.8}$	$^{+0.0}_{+0.0}$	$^{-1.2}_{+1.5}$	$^{+0.0}_{+0.0}$	$^{+0.6}_{-1.3}$
20000	0.25	0.456	$^{+16.0}_{-14.0}$	$^{+6.1}_{-3.6}$	$^{+4.9}_{-1.8}$	$^{-1.5}_{+0.2}$	$^{-2.2}_{+2.2}$	$^{+0.1}_{-0.1}$	$^{+0.0}_{+0.0}$	$^{-0.7}_{-0.2}$	$^{+2.7}_{-1.4}$	$^{+0.6}_{-0.5}$
	0.4	0.175	$^{+28.6}_{-22.7}$	$^{+4.9}_{-3.8}$	$^{+3.6}_{+0.0}$	$^{-0.4}_{+0.4}$	$^{+0.9}_{-0.9}$	$^{+3.0}_{-3.0}$	$^{+0.0}_{+0.0}$	$^{-1.8}_{-0.3}$	$^{+0.0}_{+0.0}$	$^{+1.1}_{-1.2}$
30000	0.4	0.190	$^{+34.5}_{-26.4}$	$^{+6.9}_{-5.9}$	$^{+6.7}_{+0.0}$	$^{-0.2}_{+0.3}$	$^{-0.8}_{+0.8}$	$^{+0.7}_{-0.7}$	$^{+0.0}_{+0.0}$	$^{+0.1}_{-4.9}$	$^{+0.0}_{-2.9}$	$^{+1.3}_{-1.3}$

650

Eur. Phys. J. C (2009) 62: 625–658

Table 13 The reduced cross section $\tilde{\sigma}$ for the reaction $e^- p \to e^- X$ ($\mathcal{L} = 98.7\,\text{pb}^{-1}$, $P_e = -0.27$). The bin range, bin centre (Q_c^2 and x_c) and measured cross section corrected to the electroweak Born level are shown. The first (second) error on the cross section corresponds to the statistical (systematic) uncertainties. The number of observed data events (N_{data}) and simulated background events ($N_{\text{bg}}^{\text{MC}}$) are also shown

Q^2 range (GeV^2)	Q_c^2 (GeV^2)	x range	x_c	$\tilde{\sigma}$	N_{data}	$N_{\text{bg}}^{\text{MC}}$
185–240	200	0.0037–0.006	0.005	$1.091 \pm 0.013\,^{+0.014}_{-0.011}$	8166	51.2
		0.006 –0.01	0.008	$0.919 \pm 0.010\,^{+0.018}_{-0.018}$	9475	13.6
		0.01 –0.017	0.013	$0.782 \pm 0.008\,^{+0.013}_{-0.013}$	10222	1.7
		0.017 –0.025	0.021	$0.657 \pm 0.008\,^{+0.014}_{-0.014}$	7261	0.0
		0.025 –0.037	0.032	$0.562 \pm 0.007\,^{+0.023}_{-0.022}$	6934	0.0
		0.037 –0.06	0.05	$0.500 \pm 0.007\,^{+0.012}_{-0.012}$	6387	0.0
		0.06 –0.12	0.08	$0.445 \pm 0.005\,^{+0.024}_{-0.024}$	8344	0.0
		0.12 –0.25	0.18	$0.341 \pm 0.005\,^{+0.018}_{-0.018}$	4369	0.0
240–310	250	0.006 –0.01	0.008	$0.948 \pm 0.012\,^{+0.014}_{-0.012}$	6666	15.2
		0.01 –0.017	0.013	$0.797 \pm 0.010\,^{+0.013}_{-0.012}$	7355	3.5
		0.017 –0.025	0.021	$0.662 \pm 0.010\,^{+0.011}_{-0.009}$	5232	0.8
		0.025 –0.037	0.032	$0.566 \pm 0.008\,^{+0.019}_{-0.019}$	5088	0.0
		0.037 –0.06	0.05	$0.504 \pm 0.007\,^{+0.017}_{-0.017}$	5029	0.0
		0.06 –0.12	0.08	$0.429 \pm 0.006\,^{+0.022}_{-0.022}$	5997	0.0
		0.12 –0.25	0.18	$0.336 \pm 0.006\,^{+0.016}_{-0.016}$	4121	0.0
310–410	350	0.006 –0.01	0.008	$0.968 \pm 0.016\,^{+0.021}_{-0.015}$	4001	41.5
		0.01 –0.017	0.013	$0.818 \pm 0.012\,^{+0.016}_{-0.010}$	5495	5.2
		0.017 –0.025	0.021	$0.694 \pm 0.011\,^{+0.006}_{-0.004}$	4230	0.0
		0.025 –0.037	0.032	$0.607 \pm 0.010\,^{+0.012}_{-0.011}$	4118	0.0
		0.037 –0.06	0.05	$0.513 \pm 0.008\,^{+0.014}_{-0.013}$	4397	0.0
		0.06 –0.12	0.08	$0.438 \pm 0.007\,^{+0.009}_{-0.009}$	4916	0.0
		0.12 –0.25	0.18	$0.319 \pm 0.005\,^{+0.020}_{-0.020}$	3882	0.0
410–530	450	0.006 –0.01	0.008	$0.987 \pm 0.018\,^{+0.023}_{-0.021}$	3072	48.9
		0.01 –0.017	0.013	$0.868 \pm 0.017\,^{+0.010}_{-0.010}$	2771	9.3
		0.017 –0.025	0.021	$0.690 \pm 0.015\,^{+0.013}_{-0.012}$	2145	0.8
		0.025 –0.037	0.032	$0.609 \pm 0.012\,^{+0.012}_{-0.011}$	2497	0.0
		0.037 –0.06	0.05	$0.531 \pm 0.010\,^{+0.013}_{-0.013}$	3100	0.0
		0.06 –0.1	0.08	$0.448 \pm 0.009\,^{+0.009}_{-0.008}$	2562	0.0
		0.1 –0.17	0.13	$0.362 \pm 0.008\,^{+0.018}_{-0.018}$	2182	0.0
		0.17 –0.3	0.25	$0.270 \pm 0.007\,^{+0.015}_{-0.015}$	1684	0.0
530–710	650	0.01 –0.017	0.013	$0.884 \pm 0.016\,^{+0.013}_{-0.007}$	3116	34.4
		0.017 –0.025	0.021	$0.753 \pm 0.017\,^{+0.009}_{-0.008}$	2057	3.3
		0.025 –0.037	0.032	$0.598 \pm 0.015\,^{+0.007}_{-0.006}$	1589	0.8
		0.037 –0.06	0.05	$0.523 \pm 0.013\,^{+0.005}_{-0.005}$	1722	0.0
		0.06 –0.1	0.08	$0.432 \pm 0.012\,^{+0.010}_{-0.010}$	1430	0.0
		0.1 –0.17	0.13	$0.369 \pm 0.010\,^{+0.010}_{-0.009}$	1310	0.0
		0.17 –0.3	0.25	$0.255 \pm 0.008\,^{+0.017}_{-0.017}$	1107	0.0
710–900	800	0.009 –0.017	0.013	$0.885 \pm 0.020\,^{+0.015}_{-0.017}$	1992	28.8
		0.017 –0.025	0.021	$0.769 \pm 0.021\,^{+0.009}_{-0.007}$	1436	1.8
		0.025 –0.037	0.032	$0.648 \pm 0.017\,^{+0.009}_{-0.009}$	1453	4.3
		0.037 –0.06	0.05	$0.543 \pm 0.014\,^{+0.012}_{-0.012}$	1637	0.0
		0.06 –0.1	0.08	$0.452 \pm 0.012\,^{+0.012}_{-0.012}$	1358	0.0
		0.1 –0.17	0.13	$0.379 \pm 0.012\,^{+0.004}_{-0.004}$	1106	0.0
		0.17 –0.3	0.25	$0.270 \pm 0.009\,^{+0.010}_{-0.009}$	853	0.0

Eur. Phys. J. C (2009) 62: 625–658

651

Table 13 (*Continued*)

Q^2 range (GeV²)	Q^2_c (GeV²)	x range	x_c	$\tilde{\sigma}$	N_{data}	$N_{\text{bg}}^{\text{MC}}$
900– 1300	1200	0.01 –0.017	0.014	$0.908 \pm 0.026^{+0.022}_{-0.029}$	1306	43.8
		0.017–0.025	0.021	$0.828 \pm 0.022^{+0.015}_{-0.014}$	1548	13.4
		0.025–0.037	0.032	$0.620 \pm 0.017^{+0.007}_{-0.007}$	1465	6.8
		0.037–0.06	0.05	$0.550 \pm 0.013^{+0.007}_{-0.008}$	1845	0.8
		0.06 –0.1	0.08	$0.473 \pm 0.011^{+0.007}_{-0.006}$	1824	0.0
		0.1 –0.17	0.13	$0.385 \pm 0.010^{+0.004}_{-0.005}$	1456	0.0
		0.17 –0.3	0.25	$0.263 \pm 0.008^{+0.006}_{-0.006}$	1156	0.0
		0.3 –0.53	0.4	$0.129 \pm 0.007^{+0.010}_{-0.007}$	384	0.0
1300– 1800	1500	0.017–0.025	0.021	$0.771 \pm 0.030^{+0.020}_{-0.018}$	743	33.8
		0.025–0.037	0.032	$0.641 \pm 0.023^{+0.005}_{-0.004}$	827	4.1
		0.037–0.06	0.05	$0.514 \pm 0.016^{+0.004}_{-0.004}$	1000	0.8
		0.06 –0.1	0.08	$0.496 \pm 0.015^{+0.005}_{-0.005}$	1136	0.0
		0.1 –0.15	0.13	$0.386 \pm 0.015^{+0.008}_{-0.007}$	714	0.0
		0.15 –0.23	0.18	$0.328 \pm 0.013^{+0.006}_{-0.006}$	625	0.0
		0.23 –0.35	0.25	$0.265 \pm 0.013^{+0.005}_{-0.005}$	425	0.0
		0.35 –0.53	0.4	$0.134 \pm 0.010^{+0.012}_{-0.006}$	192	0.0
1800– 2500	2000	0.023–0.037	0.032	$0.644 \pm 0.028^{+0.016}_{-0.009}$	572	11.1
		0.037–0.06	0.05	$0.605 \pm 0.022^{+0.006}_{-0.005}$	753	0.0
		0.06 –0.1	0.08	$0.477 \pm 0.018^{+0.010}_{-0.009}$	749	0.8
		0.1 –0.15	0.13	$0.345 \pm 0.016^{+0.003}_{-0.004}$	471	0.0
		0.15 –0.23	0.18	$0.322 \pm 0.016^{+0.002}_{-0.006}$	435	0.0
		0.23 –0.35	0.25	$0.259 \pm 0.015^{+0.005}_{-0.004}$	305	0.0
		0.35 –0.53	0.4	$0.122 \pm 0.010^{+0.004}_{-0.005}$	141	0.0
2500– 3500	3000	0.037–0.06	0.05	$0.603 \pm 0.028^{+0.012}_{-0.007}$	466	5.2
		0.06 –0.1	0.08	$0.511 \pm 0.022^{+0.006}_{-0.006}$	525	0.9
		0.1 –0.15	0.13	$0.381 \pm 0.020^{+0.004}_{-0.003}$	363	0.0
		0.15 –0.23	0.18	$0.343 \pm 0.019^{+0.004}_{-0.004}$	327	0.0
		0.23 –0.35	0.25	$0.274 \pm 0.018^{+0.020}_{-0.020}$	237	0.0
		0.35 –0.53	0.4	$0.156 \pm 0.014^{+0.006}_{-0.005}$	124	0.0
		0.53 –0.75	0.65	$0.018^{+0.003}_{-0.003}\,{}^{+0.002}_{-0.002}$	39	0.0
3500– 5600	5000	0.04 –0.1	0.08	$0.567 \pm 0.023^{+0.010}_{-0.005}$	621	4.2
		0.1 –0.15	0.13	$0.492 \pm 0.026^{+0.005}_{-0.004}$	374	0.8
		0.15 –0.23	0.18	$0.354 \pm 0.021^{+0.003}_{-0.002}$	300	0.0
		0.23 –0.35	0.25	$0.233 \pm 0.018^{+0.004}_{-0.003}$	176	0.0
		0.35 –0.53	0.4	$0.132^{+0.015}_{-0.013}\,{}^{+0.009}_{-0.008}$	96	0.0
5600– 9000	8000	0.07 –0.15	0.13	$0.586 \pm 0.032^{+0.006}_{-0.011}$	351	2.6
		0.15 –0.23	0.18	$0.441 \pm 0.031^{+0.012}_{-0.013}$	203	0.0
		0.23 –0.35	0.25	$0.323 \pm 0.027^{+0.012}_{-0.012}$	140	0.0
		0.35 –0.53	0.4	$0.116^{+0.019}_{-0.016}\,{}^{+0.008}_{-0.008}$	51	0.0
		0.53 –0.75	0.65	$0.020^{+0.005}_{-0.004}\,{}^{+0.001}_{-0.001}$	21	0.0
9000–15000	12000	0.09 –0.23	0.18	$0.516 \pm 0.039^{+0.007}_{-0.019}$	176	0.8
		0.23 –0.35	0.25	$0.354^{+0.042}_{-0.038}\,{}^{+0.010}_{-0.008}$	86	0.0
		0.35 –0.53	0.4	$0.146^{+0.027}_{-0.023}\,{}^{+0.007}_{-0.006}$	39	0.0
15000–25000	20000	0.15 –0.35	0.25	$0.473^{+0.062}_{-0.056}\,{}^{+0.029}_{-0.017}$	76	2.6
		0.35 –0.75	0.4	$0.193^{+0.043}_{-0.036}\,{}^{+0.009}_{-0.007}$	29	0.0
25000–50000	30000	0.25 –0.75	0.4	$0.275^{+0.062}_{-0.052}\,{}^{+0.019}_{-0.016}$	28	0.0

Table 14 Systematic uncertainties with bin-to-bin correlations for the reduced cross section $\tilde{\sigma}$ for the reaction $e^- p \rightarrow e^- X$ ($\mathcal{L} = 98.7\,\mathrm{pb}^{-1}$, $P_e = -0.27$). The left five columns of the table contain the bin centres, Q_c^2 and x_c, the measured cross section, the statistical uncertainty and the total systematic uncertainty. The right eight columns of the table list the bin-to-bin correlated systematic uncertainties for δ_1–δ_7, and the systematic uncertainties summed in quadrature for δ_8–δ_{13}, as defined in Sect. 8. The upper and lower correlated uncertainties correspond to a positive or negative variation of a cut value for example. However, if this is not possible for a particular systematic, the uncertainty is symmetrised

Q_c^2 (GeV²)	x_c	$\tilde{\sigma}$	stat. (%)	sys. (%)	δ_1 (%)	δ_2 (%)	δ_3 (%)	δ_4 (%)	δ_5 (%)	δ_6 (%)	δ_7 (%)	δ_8–δ_{13} (%)
200	0.005	1.091	± 1.2	+1.3 / −1.0	+0.7 / −0.0	−0.4 / +0.6	+0.4 / −0.4	−0.4 / +0.4	+0.0 / +0.0	+0.1 / −0.1	+0.3 / −0.3	+0.7 / −0.7
	0.008	0.919	± 1.1	+1.9 / −1.9	+0.3 / −0.0	−0.4 / +0.5	+0.2 / −0.2	−1.6 / +1.6	+0.0 / +0.0	+0.1 / +0.4	+0.1 / −0.1	+0.8 / −1.0
	0.013	0.782	± 1.0	+1.7 / −1.6	+0.2 / +0.0	−0.5 / +0.5	−0.2 / +0.2	−1.3 / +1.3	+0.0 / +0.0	+0.0 / +0.4	+0.0 / −0.0	+0.8 / −0.9
	0.021	0.657	± 1.2	+2.1 / −2.1	+0.4 / +0.0	−0.3 / +0.5	−1.6 / +1.6	+0.9 / −0.9	+0.0 / +0.0	−0.1 / +0.1	+0.0 / +0.0	+0.8 / −0.9
	0.032	0.562	± 1.3	+4.0 / −4.0	+0.1 / −0.0	−0.3 / +0.4	−1.5 / +1.5	+3.6 / −3.6	+0.0 / +0.0	+0.2 / +0.4	+0.0 / +0.0	+0.8 / −0.8
	0.05	0.500	± 1.3	+2.5 / −2.4	+0.0 / −0.3	−0.2 / +0.3	−0.5 / +0.5	+2.2 / −2.2	+0.0 / +0.0	+0.0 / +0.3	+0.0 / +0.0	+1.0 / −0.9
	0.08	0.445	± 1.1	+5.5 / −5.5	+0.0 / −0.1	−0.2 / +0.2	+5.0 / −5.0	+2.0 / −2.0	−0.0 / +0.0	−0.0 / +0.1	+0.0 / +0.0	+0.8 / −1.0
	0.18	0.341	± 1.6	+5.4 / −5.4	+0.1 / +0.0	−0.1 / +0.2	+5.3 / −5.3	+0.5 / −0.5	+0.7 / +0.2	−0.1 / +0.1	+0.0 / +0.0	+0.7 / −0.9
250	0.008	0.948	± 1.3	+1.5 / −1.3	+0.6 / −0.0	−0.3 / +0.4	+0.5 / −0.5	−0.9 / +0.9	+0.0 / +0.0	−0.2 / +0.3	+0.1 / −0.1	+0.7 / −0.7
	0.013	0.797	± 1.2	+1.7 / −1.5	+0.7 / +0.0	−0.5 / +0.6	+0.0 / −0.0	−1.3 / +1.3	+0.0 / +0.0	−0.1 / +0.2	+0.0 / −0.0	+0.5 / −0.7
	0.021	0.662	± 1.4	+1.6 / −1.4	+0.7 / −0.0	−0.3 / +0.5	−0.1 / +0.1	+1.1 / −1.1	+0.0 / +0.0	−0.2 / +0.2	+0.0 / −0.0	+0.8 / −0.7
	0.032	0.566	± 1.5	+3.3 / −3.3	+0.6 / −0.0	−0.3 / +0.4	−0.8 / +0.8	+3.0 / −3.0	+0.0 / +0.0	+0.0 / +0.1	+0.0 / +0.0	+0.7 / −0.9
	0.05	0.504	± 1.5	+3.4 / −3.3	+0.4 / +0.0	−0.1 / +0.3	−2.4 / +2.4	+2.2 / −2.2	+0.0 / +0.0	−0.0 / −0.1	+0.0 / +0.0	+0.7 / −0.6
	0.08	0.429	± 1.4	+5.2 / −5.1	+0.7 / −0.0	−0.1 / +0.3	+4.6 / −4.6	+2.2 / −2.2	+0.0 / +0.0	−0.0 / +0.1	+0.0 / +0.0	+0.7 / −0.7
	0.18	0.336	± 1.6	+4.8 / −4.7	+0.2 / +0.0	+0.0 / +0.2	+4.1 / −4.1	+2.0 / −2.0	+0.3 / +1.0	+0.0 / +0.2	+0.0 / +0.0	+0.8 / −0.8
350	0.008	0.968	± 1.7	+2.1 / −1.5	+1.6 / −0.1	−0.5 / +0.6	+0.9 / −0.9	−0.4 / +0.4	+0.0 / +0.0	−0.6 / +0.4	+0.4 / −0.4	+0.6 / −0.8
	0.013	0.818	± 1.4	+1.9 / −1.2	+1.4 / −0.0	−0.2 / +0.5	−0.2 / +0.2	−1.0 / +1.0	+0.0 / +0.0	−0.2 / +0.5	+0.0 / −0.0	+0.7 / −0.6
	0.021	0.694	± 1.6	+0.9 / −0.6	+0.4 / −0.1	−0.3 / +0.4	+0.3 / −0.3	+0.0 / −0.0	+0.0 / +0.0	−0.2 / −0.0	+0.0 / +0.0	+0.6 / −0.5
	0.032	0.607	± 1.6	+1.9 / −1.8	+0.8 / −0.0	−0.2 / +0.4	−1.6 / +1.6	+0.2 / −0.2	+0.0 / +0.0	−0.3 / +0.1	+0.0 / +0.0	+0.6 / −0.7
	0.05	0.513	± 1.6	+2.7 / −2.6	+0.6 / −0.0	−0.1 / +0.2	−1.9 / +1.9	+1.6 / −1.6	+0.0 / +0.0	−0.1 / +0.2	+0.0 / +0.0	+0.5 / −0.7
	0.08	0.438	± 1.5	+2.0 / −2.0	+0.3 / +0.0	−0.1 / +0.2	+1.1 / −1.1	+1.6 / −1.6	+0.0 / +0.0	+0.0 / +0.1	+0.0 / +0.0	+0.7 / −0.7
	0.18	0.319	± 1.7	+6.4 / −6.3	+0.4 / +0.0	−0.0 / +0.2	+5.7 / −5.7	+2.6 / −2.6	−0.1 / +1.2	+0.1 / +0.2	+0.0 / +0.0	+0.7 / −0.6
450	0.008	0.987	± 1.9	+2.4 / −2.1	+0.7 / −0.3	−1.4 / +1.6	+1.3 / −1.3	−0.5 / +0.5	+0.0 / +0.0	−0.2 / +0.3	+0.6 / −0.6	+0.5 / −0.4
	0.013	0.868	± 2.0	+1.1 / −1.1	+0.1 / −0.1	−0.5 / +0.6	−0.4 / +0.4	+0.2 / −0.2	+0.0 / +0.0	−0.6 / +0.6	+0.1 / −0.1	+0.5 / −0.6
	0.021	0.690	± 2.2	+1.8 / −1.7	+0.2 / −0.1	−0.4 / +0.5	−0.1 / +0.1	+1.3 / −1.3	+0.0 / +0.0	−0.7 / +0.9	+0.0 / −0.0	+0.8 / −0.8
	0.032	0.609	± 2.0	+1.9 / −1.7	+0.8 / −0.1	−0.2 / +0.4	+0.0 / −0.0	+1.4 / −1.4	+0.0 / +0.0	−0.5 / +0.4	+0.0 / +0.0	+1.0 / −0.9
	0.05	0.531	± 1.8	+2.5 / −2.4	+0.7 / −0.0	+0.0 / +0.2	−1.6 / +1.6	+1.6 / −1.6	+0.0 / +0.0	−0.4 / +0.6	+0.0 / +0.0	+0.7 / −0.7
	0.08	0.448	± 2.0	+2.1 / −1.9	+0.3 / +0.0	+0.1 / +0.2	−0.7 / +0.7	+1.7 / −1.7	+0.0 / +0.0	+0.1 / +0.6	+0.0 / +0.0	+0.7 / −0.5
	0.13	0.362	± 2.2	+4.9 / −4.9	+0.6 / +0.0	+0.1 / +0.1	+4.4 / −4.4	+1.9 / −1.9	+0.0 / +0.0	−0.4 / +0.4	+0.0 / +0.0	+0.5 / −0.6
	0.25	0.270	± 2.5	+5.6 / −5.5	+1.1 / +0.0	+0.2 / +0.1	+5.2 / −5.2	+1.1 / −1.1	−0.9 / +0.8	−0.1 / +0.6	+0.0 / +0.0	+0.8 / −0.8
650	0.013	0.884	± 1.8	+1.5 / −0.8	+1.2 / −0.2	−0.5 / +0.6	−0.0 / +0.0	−0.1 / +0.1	+0.0 / +0.0	−0.2 / +0.3	+0.5 / −0.5	+0.4 / −0.3
	0.021	0.753	± 2.3	+1.1 / −1.1	+0.0 / −0.1	−0.4 / +0.5	−0.3 / +0.3	−0.9 / +0.9	+0.0 / +0.0	−0.2 / +0.0	+0.1 / −0.1	+0.2 / −0.2
	0.032	0.598	± 2.6	+1.2 / −1.0	+0.5 / −0.2	−0.4 / +0.5	−0.5 / +0.5	+0.7 / −0.7	+0.0 / +0.0	+0.5 / +0.5	+0.0 / −0.0	+0.2 / −0.2
	0.05	0.523	± 2.5	+1.0 / −0.9	+0.1 / −0.0	−0.3 / +0.4	−0.4 / +0.4	+0.7 / −0.7	+0.0 / +0.0	+0.1 / +0.0	+0.0 / +0.0	+0.5 / −0.4
	0.08	0.432	± 2.7	+2.4 / −2.3	+0.7 / −0.0	−0.1 / +0.3	−1.8 / +1.8	+1.0 / −1.0	+0.0 / +0.0	+0.1 / −0.0	+0.0 / +0.0	+0.9 / −1.1
	0.13	0.369	± 2.8	+2.7 / −2.4	+0.9 / −0.0	−0.1 / +0.2	+2.1 / −2.1	−0.8 / +0.8	+0.0 / +0.0	+0.1 / +0.4	+0.0 / +0.0	+1.0 / −0.9
	0.25	0.255	± 3.1	+6.6 / −6.5	+1.0 / −0.0	−0.1 / +0.3	+6.3 / −6.3	+1.0 / −1.0	−0.8 / +0.2	−0.1 / +0.5	+0.0 / +0.0	+1.0 / −1.1
800	0.013	0.885	± 2.3	+1.7 / −1.9	+0.4 / −1.0	−0.8 / +1.0	+0.4 / −0.4	−1.0 / +1.0	+0.0 / +0.0	−0.1 / +0.0	+0.6 / −0.6	+0.3 / −0.4
	0.021	0.769	± 2.7	+1.1 / −0.9	+0.5 / −0.1	−0.4 / +0.5	+0.6 / −0.6	−0.2 / +0.2	+0.0 / +0.0	+0.0 / +0.5	+0.1 / −0.1	+0.4 / −0.4
	0.032	0.648	± 2.7	+1.4 / −1.4	+0.0 / −0.4	−0.4 / +0.5	−0.8 / +0.8	−0.9 / +0.9	+0.0 / +0.0	+0.3 / +0.0	+0.1 / −0.1	+0.2 / −0.4
	0.05	0.543	± 2.5	+2.2 / −2.2	+0.3 / +0.0	−0.3 / +0.4	+0.7 / −0.7	+2.0 / −2.0	+0.0 / +0.0	−0.4 / +0.1	+0.0 / +0.0	+0.3 / −0.4
	0.08	0.452	± 2.8	+2.6 / −2.6	+0.5 / −0.0	−0.2 / +0.3	−2.5 / +2.5	+0.1 / −0.1	+0.0 / +0.0	+0.5 / −0.7	+0.0 / +0.0	+0.3 / −0.4
	0.13	0.379	± 3.1	+1.1 / −1.0	+0.5 / −0.0	−0.2 / +0.3	+0.7 / −0.7	+0.6 / −0.6	+0.0 / +0.0	+0.1 / −0.4	+0.0 / +0.0	+0.2 / −0.2
	0.25	0.270	± 3.5	+3.7 / −3.4	+0.3 / +0.0	−0.2 / +0.2	+3.3 / −3.3	+0.8 / −0.8	+1.2 / −0.1	+0.7 / −0.5	+0.0 / +0.0	+0.2 / −0.3

Eur. Phys. J. C (2009) 62: 625–658

653

Table 14 (*Continued*)

Q_c^2 (GeV²)	x_c	$\tilde{\sigma}$	stat. (%)	sys. (%)	δ_1 (%)	δ_2 (%)	δ_3 (%)	δ_4 (%)	δ_5 (%)	δ_6 (%)	δ_7 (%)	$\delta_8-\delta_{13}$ (%)
1200	0.014	0.908	± 2.9	+2.4 / −3.2	+0.6 / −2.2	−0.8 / +1.0	−0.7 / +0.7	−1.4 / +1.4	+0.0 / +0.0	−0.3 / −0.8	+1.4 / −1.4	+0.5 / −0.2
	0.021	0.828	± 2.6	+1.9 / −1.6	+0.9 / −0.1	−0.5 / +0.5	+1.5 / −1.5	+0.0 / −0.0	+0.0 / +0.0	+0.1 / +0.4	+0.4 / −0.4	+0.3 / −0.4
	0.032	0.620	± 2.7	+1.2 / −1.1	+0.0 / −0.1	−0.4 / +0.5	−0.5 / +0.5	−0.7 / +0.7	+0.0 / +0.0	+0.1 / +0.1	+0.2 / −0.2	+0.6 / −0.6
	0.05	0.550	± 2.4	+1.3 / −1.4	+0.1 / −0.0	−0.3 / +0.3	−0.1 / +0.1	+1.2 / −1.2	+0.0 / +0.0	−0.3 / −0.4	+0.0 / −0.0	+0.4 / −0.4
	0.08	0.473	± 2.4	+1.4 / −1.3	+0.3 / −0.0	−0.2 / +0.4	−0.3 / +0.3	+1.2 / −1.2	+0.0 / +0.0	+0.3 / −0.3	+0.0 / +0.0	+0.4 / −0.3
	0.13	0.385	± 2.7	+1.1 / −1.2	+0.1 / −0.0	−0.1 / +0.2	−0.9 / +0.9	+0.4 / −0.4	+0.0 / +0.0	+0.1 / −0.5	+0.0 / +0.0	+0.3 / −0.4
	0.25	0.263	± 3.0	+2.4 / −2.3	+0.3 / +0.0	−0.2 / +0.3	+2.0 / −2.0	+1.0 / −1.0	+0.0 / +0.0	−0.3 / −0.1	+0.0 / +0.0	+0.5 / −0.4
	0.4	0.129	± 5.2	+8.1 / −5.7	+0.0 / −0.1	−0.4 / +0.4	+5.6 / −5.6	+0.6 / −0.6	+5.8 / +3.4	+0.5 / −1.0	+0.0 / −0.0	+0.5 / −0.5
1500	0.021	0.771	± 3.8	+2.6 / −2.3	+0.9 / −0.2	−0.6 / +0.4	−0.4 / +0.4	−0.1 / +0.1	+0.0 / +0.0	−1.0 / −0.1	+2.3 / −1.9	+0.4 / −0.4
	0.032	0.641	± 3.5	+0.7 / −0.6	+0.3 / −0.1	−0.3 / +0.3	−0.1 / +0.1	−0.3 / +0.3	+0.0 / +0.0	−0.1 / −0.1	+0.2 / −0.2	+0.4 / −0.3
	0.05	0.514	± 3.2	+0.9 / −0.8	+0.2 / −0.0	−0.3 / +0.4	+0.2 / −0.2	+0.4 / −0.4	+0.0 / +0.0	−0.4 / +0.5	+0.0 / −0.0	+0.3 / −0.4
	0.08	0.496	± 3.0	+1.0 / −1.1	+0.2 / −0.0	−0.3 / +0.4	−0.9 / +0.9	−0.2 / +0.2	+0.0 / +0.0	−0.4 / +0.1	+0.0 / +0.0	+0.3 / −0.5
	0.13	0.386	± 3.8	+2.1 / −1.8	+0.8 / −0.0	−0.1 / +0.3	−1.3 / +1.3	−1.1 / +1.1	+0.0 / +0.0	+0.8 / −0.2	+0.0 / +0.0	+0.3 / −0.4
	0.18	0.328	± 4.0	+1.8 / −1.7	+0.6 / −0.1	−0.3 / +0.2	+0.0 / −0.0	−1.6 / +1.6	+0.0 / +0.0	−0.3 / −0.2	+0.0 / +0.0	+0.4 / −0.4
	0.25	0.265	± 4.9	+1.9 / −1.9	+0.0 / −0.3	−0.3 / +0.3	+1.7 / −1.7	+0.6 / −0.6	+0.1 / +0.0	−0.1 / −0.3	+0.0 / +0.0	+0.3 / −0.3
	0.4	0.134	± 7.3	+8.8 / −4.3	+0.6 / +0.0	−0.5 / +0.3	+2.0 / −2.0	−0.9 / +0.9	+8.4 / −3.6	+0.3 / −0.4	+0.0 / +0.0	+0.6 / −0.5
2000	0.032	0.644	± 4.3	+2.5 / −1.4	+1.8 / +0.0	−0.2 / +0.2	+0.3 / −0.3	+1.0 / −1.0	+0.0 / +0.0	+0.4 / +0.7	+1.1 / −0.8	+0.3 / −0.4
	0.05	0.605	± 3.7	+1.0 / −0.8	+0.5 / −0.0	−0.3 / +0.4	−0.3 / +0.3	−0.6 / +0.6	+0.0 / +0.0	+0.1 / +0.1	+0.0 / +0.0	+0.3 / −0.3
	0.08	0.477	± 3.7	+2.0 / −2.0	+0.1 / −0.1	−0.3 / +0.4	−0.1 / +0.1	+1.9 / −1.9	+0.0 / +0.0	+0.2 / +0.0	+0.0 / −0.0	+0.3 / −0.3
	0.13	0.345	± 4.6	+0.8 / −1.2	+0.1 / −0.6	−0.2 / +0.3	−0.5 / +0.5	+0.5 / −0.5	+0.0 / +0.0	+0.1 / −0.6	+0.0 / +0.0	+0.3 / −0.4
	0.18	0.322	± 4.8	+0.6 / −1.9	+0.0 / −0.7	−0.2 / +0.2	−0.3 / +0.3	+0.1 / −0.1	+0.0 / +0.0	−0.4 / −1.6	+0.0 / +0.0	+0.4 / −0.6
	0.25	0.259	± 5.8	+1.7 / −1.6	+0.3 / −0.0	−0.2 / +0.3	+1.5 / −1.5	+0.5 / −0.5	+0.0 / +0.0	+0.4 / +0.5	+0.0 / +0.0	+0.5 / −0.5
	0.4	0.122	± 8.5	+3.7 / −3.9	+0.0 / −0.2	−0.3 / +0.4	+3.1 / −3.1	+1.1 / −1.1	−0.5 / +1.0	+0.1 / −1.3	+0.0 / +0.0	+1.2 / −1.4
3000	0.05	0.603	± 4.7	+2.0 / −1.1	+1.6 / −0.1	−0.3 / +0.4	+0.9 / −0.9	−0.0 / +0.0	+0.0 / +0.0	+0.4 / +0.2	+0.5 / −0.5	+0.4 / −0.3
	0.08	0.511	± 4.4	+1.1 / −1.1	+0.2 / −0.4	−0.2 / +0.3	−0.4 / +0.4	+0.8 / −0.8	+0.0 / +0.0	+0.5 / −0.1	+0.1 / −0.1	+0.3 / −0.5
	0.13	0.381	± 5.3	+0.9 / −0.7	+0.1 / −0.1	−0.2 / +0.3	+0.6 / −0.6	−0.1 / +0.1	+0.0 / +0.0	−0.3 / −0.3	+0.0 / +0.0	+0.7 / −0.1
	0.18	0.343	± 5.6	+1.2 / −1.3	+0.0 / −0.3	−0.2 / +0.2	−0.9 / +0.9	−0.6 / +0.6	+0.0 / +0.0	−0.5 / +0.2	+0.0 / +0.0	+0.4 / −0.3
	0.25	0.274	± 6.5	+7.4 / −7.3	+0.6 / −0.0	−0.2 / +0.2	+7.3 / −7.3	+0.2 / −0.2	+0.0 / +0.0	+1.1 / +0.3	+0.0 / +0.0	+0.8 / −0.6
	0.4	0.156	± 9.0	+3.8 / −3.5	+1.3 / −0.0	−0.2 / +0.4	−3.4 / +3.4	+0.5 / −0.5	+0.4 / −0.0	+0.8 / −0.3	+0.0 / +0.0	+0.6 / −0.6
	0.65	0.018	+18.8 / −16.0	+10.2 / −10.4	+0.0 / −0.6	−0.8 / +1.0	−8.7 / +8.7	+4.6 / −4.6	+1.8 / +0.7	−2.7 / +0.9	+0.0 / +0.0	+1.7 / −2.0
5000	0.08	0.567	± 4.0	+1.8 / −0.9	+1.6 / −0.3	−0.2 / +0.2	−0.3 / +0.3	+0.2 / −0.2	+0.0 / +0.0	−0.6 / −0.4	+0.3 / −0.3	+0.5 / −0.3
	0.13	0.492	± 5.2	+1.0 / −0.8	+0.8 / −0.0	−0.2 / +0.2	−0.4 / +0.4	+0.3 / −0.3	+0.0 / +0.0	+0.1 / −0.3	+0.1 / −0.1	+0.2 / −0.5
	0.18	0.354	± 5.8	+1.0 / −0.5	+0.2 / −0.1	−0.3 / +0.2	+0.2 / −0.2	+0.3 / −0.3	+0.0 / +0.0	−0.1 / +0.7	+0.0 / +0.0	+0.5 / −0.3
	0.25	0.233	± 7.6	+1.8 / −1.2	+0.7 / −0.0	−0.2 / +0.3	+0.7 / −0.7	−0.7 / +0.7	+0.0 / +0.0	+1.2 / −0.6	+0.0 / +0.0	+0.4 / −0.3
	0.4	0.132	+11.3 / −10.2	+6.5 / −6.4	+0.0 / −0.3	−0.2 / +0.3	+6.0 / −6.0	−2.1 / +2.1	+0.0 / +0.0	+0.4 / +1.3	+0.0 / +0.0	+1.1 / −1.1
8000	0.13	0.586	± 5.4	+1.0 / −1.9	+0.0 / −1.0	−0.3 / +0.3	−0.5 / +0.5	−0.1 / +0.1	+0.0 / +0.0	−1.3 / +0.3	+0.5 / −0.3	+0.5 / −0.5
	0.18	0.441	± 7.0	+2.6 / −2.9	+0.1 / −0.3	−0.2 / +0.2	−2.4 / +2.4	+0.6 / −0.6	+0.0 / +0.0	+0.5 / −0.3	+0.0 / +0.0	+0.6 / −1.3
	0.25	0.323	± 8.5	+3.8 / −3.9	+0.7 / −0.1	−0.3 / +0.2	−3.6 / +3.6	+0.4 / −0.4	+0.0 / +0.0	−1.1 / −0.6	+0.0 / +0.0	+0.4 / −0.4
	0.4	0.116	+16.1 / −14.0	+7.1 / −7.3	+0.1 / −0.0	−0.3 / +0.4	+7.0 / −7.0	−0.6 / +0.6	+0.0 / +0.0	−0.3 / +0.5	+0.0 / +0.0	+0.6 / −2.0
	0.65	0.020	+26.9 / −21.6	+4.1 / −4.2	+0.2 / −1.4	−0.9 / +0.9	+1.5 / −1.5	+2.3 / −2.3	+0.0 / +0.0	−2.6 / +2.8	+0.0 / +0.0	+0.8 / −0.6
12000	0.18	0.516	± 7.6	+1.3 / −3.8	+1.0 / −3.6	−0.3 / +0.4	−0.4 / +0.4	−0.2 / +0.2	+0.0 / +0.0	−0.3 / −0.8	+0.2 / −0.3	+0.5 / −0.6
	0.25	0.354	+12.0 / −10.8	+2.8 / −2.3	+2.4 / −0.6	−0.2 / +0.2	+0.3 / −0.3	+0.8 / −0.8	+0.0 / +0.0	+0.3 / −1.6	+0.0 / +0.0	+1.0 / −1.2
	0.4	0.146	+18.7 / −16.0	+4.6 / −3.8	+2.7 / −0.2	−0.3 / +0.4	+3.2 / −3.2	−0.8 / +0.8	+0.0 / +0.0	−1.2 / +1.5	+0.0 / +0.0	+0.6 / −1.3
20000	0.25	0.473	+13.1 / −11.8	+6.1 / −3.6	+4.9 / −1.8	−1.5 / +0.2	−2.2 / +2.2	+0.1 / −0.1	+0.0 / +0.0	−0.7 / −0.2	+2.7 / −1.4	+0.6 / −0.5
	0.4	0.193	+22.2 / −18.5	+4.9 / −3.8	+3.6 / −0.0	−0.4 / +0.4	+0.9 / −0.9	+3.0 / −3.0	+0.0 / +0.0	−1.8 / −0.3	+0.0 / +0.0	+1.1 / −1.2
30000	0.4	0.275	+22.7 / −18.8	+6.9 / −5.9	+6.7 / +0.0	−0.2 / +0.3	−0.8 / +0.8	+0.7 / −0.7	+0.0 / +0.0	+0.1 / −4.9	+0.0 / −2.9	+1.3 / −1.3

654

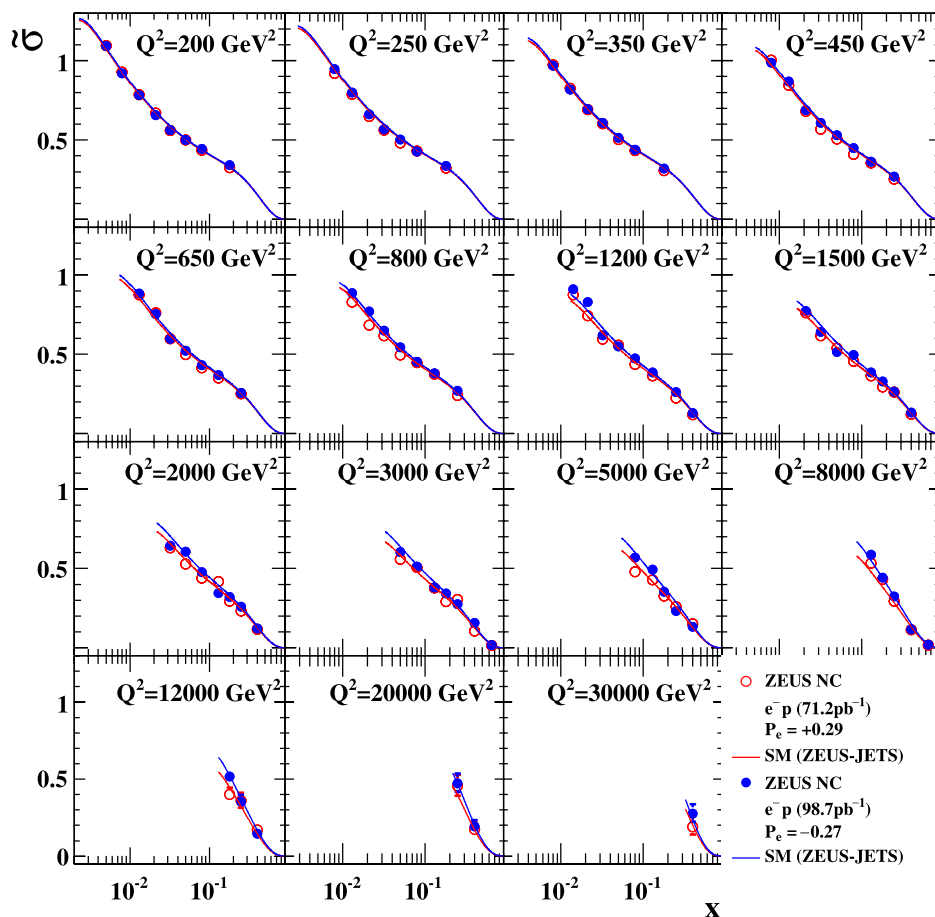Eur. Phys. J. C (2009) 62: 625–658

ZEUS

Fig. 7 The $e^- p$ NC DIS reduced cross section $\tilde{\sigma}$ for positively and negatively polarised beams plotted as a function of x at fixed Q^2. The *closed* (*open*) *circles* represent the ZEUS data for negative (positive) polarisation. The *inner error bars* show the statistical uncertainty while the *outer bars* show the statistical and systematic uncertainties added in quadrature. The *curves* show the predictions of the SM evaluated using the ZEUS-JETS PDFs

ment adds valuable information to the global fits [52, 53] for parton distribution functions.

9.2 Polarised cross sections

At HERA during 2005 and 2006 longitudinal polarisation effects in *ep* DIS become significant at the electroweak scale, where the contributions of both γ and Z exchange to the cross section are comparable. The reduced cross sections for positive and negative longitudinal polarisations, tabulated in Tables 11, 12, 13 and 14, are shown separately in Fig. 7 and are well described by the SM evaluated using the ZEUS-JETS PDFs.

At high Q^2, a difference between the positively and negatively polarised cross sections is predicted. To demonstrate this effect, the single-differential cross-section $d\sigma/dQ^2$ for $y < 0.9$, tabulated in Tables 15 and 16, was measured for positive and negative beam polarisations separately and is

shown in Fig. 8. Both measurements are well described by the SM prediction.

The ratio of measured cross sections for the two different polarisation states are shown in Fig. 9(a). The difference between the two polarisation states is clearly visible at higher Q^2. The asymmetry A^- (see (12)) extracted from these measurements is tabulated in Table 19 and is shown in Fig. 9(b), where only statistical uncertainties are considered. The uncertainty in A^- arising from the relative normalization between data sets was evaluated to be 1.4%. The other systematic uncertainties are assumed to be cancelled. The results compare well to the SM prediction. The deviation of A^- from zero, particularly at high Q^2, shows the difference in the behaviour of the two polarisation states and is clear evidence of parity violation.

The effect of γ/Z interference is quantified by calculating the χ^2 per degree of freedom of A^- with respect both to zero and the SM prediction using the ZEUS-JETS PDFs.

Table 15 The single differential cross section $d\sigma/dQ^2$ ($y < 0.9$) for the reaction $e^- p \rightarrow e^- X$ ($\mathcal{L} = 71.2\,\text{pb}^{-1}$, $P_e = +0.29$). The bin range, bin centre (Q_c^2) and measured cross section corrected to the electroweak Born level are shown. The first (second) error on the cross section corresponds to the statistical (systematic) uncertainties. The number of observed data events (N_{data}) and simulated background events ($N_{\text{bg}}^{\text{MC}}$) are also shown

Q^2 range (GeV^2)	Q_c^2 (GeV^2)	$d\sigma/dQ^2$ (pb/ GeV^2)	N_{data}	$N_{\text{bg}}^{\text{MC}}$
185.0 – 300.0	250	$(1.08 \pm 0.00\,^{+0.01}_{-0.01}) \times 10^1$	74098	105.5
300.0 – 400.0	350	$4.77 \pm 0.03\,^{+0.07}_{-0.05}$	25380	57.6
400.0 – 475.7	440	$2.73 \pm 0.03\,^{+0.05}_{-0.05}$	10769	34.0
475.7 – 565.7	520	$1.78 \pm 0.02\,^{+0.02}_{-0.02}$	7685	30.7
565.7 – 672.7	620	$1.19 \pm 0.02\,^{+0.02}_{-0.01}$	5715	32.6
672.7 – 800.0	730	$(7.77 \pm 0.11\,^{+0.06}_{-0.06}) \times 10^{-1}$	5242	17.8
800.0 – 1050.0	900	$(4.60 \pm 0.06\,^{+0.04}_{-0.04}) \times 10^{-1}$	6873	36.8
1050.0 – 1460.0	1230	$(2.13 \pm 0.03\,^{+0.01}_{-0.02}) \times 10^{-1}$	5558	38.9
1460.0 – 2080.0	1730	$(8.81 \pm 0.15\,^{+0.05}_{-0.05}) \times 10^{-2}$	3551	23.7
2080.0 – 3120.0	2500	$(3.42 \pm 0.07\,^{+0.03}_{-0.02}) \times 10^{-2}$	2269	14.2
3120.0 – 5220.0	3900	$(1.06 \pm 0.03\,^{+0.01}_{-0.01}) \times 10^{-2}$	1363	4.4
5220.0 – 12500.0	7000	$(2.34 \pm 0.08\,^{+0.05}_{-0.01}) \times 10^{-3}$	778	3.7
12500.0 – 51200.0	22400	$(6.24 \pm 0.52\,^{+0.23}_{-0.14}) \times 10^{-5}$	144	1.8

Table 16 Systematic uncertainties with bin-to-bin correlations for $d\sigma/dQ^2$ ($y < 0.9$) for the reaction $e^- p \rightarrow e^- X$ ($\mathcal{L} = 71.2\,\text{pb}^{-1}$, $P_e = +0.29$). The left four columns of the table contain the bin centre (Q_c^2), the measured cross section, the statistical uncertainty and the total systematic uncertainty. The right eight columns of the table list the bin-to-bin correlated systematic uncertainties for δ_1–δ_7, and the total systematic uncertainties summed in quadrature for δ_8–δ_{13}, as defined in Sect. 8. The upper and lower correlated uncertainties correspond to a positive or negative variation of a cut value for example. However, if this is not possible for a particular systematic, the uncertainty is symmetrised

Q_c^2 (GeV^2)	$d\sigma/dQ^2$ (pb/ GeV^2)	stat. (%)	sys. (%)	δ_1 (%)	δ_2 (%)	δ_3 (%)	δ_4 (%)	δ_5 (%)	δ_6 (%)	δ_7 (%)	δ_8–δ_{13} (%)
250	1.08×10^1	± 0.4	$^{+1.2}_{-1.1}$	$^{+0.3}_{-0.0}$	$^{-0.5}_{+0.6}$	$^{+0.5}_{-0.5}$	$^{+0.4}_{-0.4}$	$^{-0.1}_{+0.2}$	$^{-0.0}_{+0.2}$	$^{+0.1}_{-0.1}$	$^{+0.7}_{-0.8}$
350	4.77	± 0.6	$^{+1.5}_{-1.1}$	$^{+0.8}_{-0.0}$	$^{-0.5}_{+0.7}$	$^{+0.5}_{-0.5}$	$^{+0.6}_{-0.6}$	$^{-0.0}_{+0.2}$	$^{-0.2}_{+0.2}$	$^{+0.1}_{-0.1}$	$^{+0.6}_{-0.6}$
440	2.73	± 1.0	$^{+1.8}_{-1.7}$	$^{+0.3}_{-0.0}$	$^{-0.5}_{+0.6}$	$^{+0.5}_{-0.5}$	$^{+1.3}_{-1.3}$	$^{-0.2}_{+0.2}$	$^{-0.4}_{+0.7}$	$^{+0.1}_{-0.1}$	$^{+0.6}_{-0.6}$
520	1.78	± 1.2	$^{+1.3}_{-0.9}$	$^{+0.7}_{-0.1}$	$^{-0.5}_{+0.7}$	$^{+0.0}_{-0.0}$	$^{+0.1}_{-0.1}$	$^{-0.1}_{+0.2}$	$^{-0.2}_{+0.3}$	$^{+0.2}_{-0.2}$	$^{+0.7}_{-0.7}$
620	1.19	± 1.3	$^{+1.4}_{-1.0}$	$^{+0.9}_{-0.1}$	$^{-0.6}_{+0.7}$	$^{+0.2}_{-0.2}$	$^{-0.6}_{+0.6}$	$^{-0.1}_{-0.0}$	$^{+0.1}_{+0.2}$	$^{+0.2}_{-0.2}$	$^{+0.4}_{-0.5}$
730	7.77×10^{-1}	± 1.4	$^{+0.8}_{-0.7}$	$^{+0.0}_{-0.2}$	$^{-0.5}_{+0.6}$	$^{+0.3}_{-0.3}$	$^{+0.1}_{-0.1}$	$^{+0.2}_{+0.1}$	$^{+0.1}_{-0.1}$	$^{+0.1}_{-0.1}$	$^{+0.2}_{-0.3}$
900	4.60×10^{-1}	± 1.2	$^{+0.9}_{-0.8}$	$^{+0.1}_{-0.0}$	$^{-0.4}_{+0.5}$	$^{-0.2}_{+0.2}$	$^{+0.6}_{-0.6}$	$^{+0.1}_{-0.1}$	$^{-0.0}_{-0.0}$	$^{+0.2}_{-0.2}$	$^{+0.3}_{-0.3}$
1230	2.13×10^{-1}	± 1.4	$^{+0.7}_{-0.7}$	$^{+0.1}_{-0.0}$	$^{-0.3}_{+0.4}$	$^{+0.3}_{-0.3}$	$^{-0.1}_{+0.1}$	$^{+0.0}_{+0.1}$	$^{-0.0}_{-0.3}$	$^{+0.3}_{-0.3}$	$^{+0.3}_{-0.4}$
1730	8.81×10^{-2}	± 1.7	$^{+0.6}_{-0.5}$	$^{+0.2}_{-0.0}$	$^{-0.3}_{+0.3}$	$^{+0.1}_{-0.1}$	$^{+0.0}_{-0.0}$	$^{+0.2}_{-0.0}$	$^{-0.2}_{-0.1}$	$^{+0.3}_{-0.3}$	$^{+0.3}_{-0.3}$
2500	3.42×10^{-2}	± 2.1	$^{+0.9}_{-0.6}$	$^{+0.4}_{-0.0}$	$^{-0.2}_{+0.3}$	$^{+0.3}_{-0.3}$	$^{+0.2}_{-0.2}$	$^{-0.1}_{-0.0}$	$^{+0.3}_{+0.1}$	$^{+0.3}_{-0.2}$	$^{+0.3}_{-0.3}$
3900	1.06×10^{-2}	± 2.7	$^{+1.3}_{-0.6}$	$^{+1.2}_{-0.1}$	$^{-0.2}_{+0.3}$	$^{-0.4}_{+0.4}$	$^{-0.1}_{+0.1}$	$^{-0.0}_{-0.0}$	$^{-0.2}_{-0.1}$	$^{+0.1}_{-0.1}$	$^{+0.3}_{-0.3}$
7000	2.34×10^{-3}	± 3.6	$^{+2.3}_{-0.6}$	$^{+2.2}_{-0.0}$	$^{-0.3}_{+0.3}$	$^{-0.0}_{+0.0}$	$^{+0.1}_{-0.1}$	$^{+0.0}_{+0.0}$	$^{-0.3}_{+0.1}$	$^{+0.5}_{-0.2}$	$^{+0.3}_{-0.4}$
22400	6.24×10^{-5}	± 8.4	$^{+3.7}_{-2.3}$	$^{+3.4}_{-0.4}$	$^{-0.7}_{+0.3}$	$^{-1.0}_{+1.0}$	$^{+0.7}_{-0.7}$	$^{+0.0}_{+0.0}$	$^{-1.0}_{-1.6}$	$^{+0.5}_{-0.5}$	$^{+0.6}_{-0.6}$

The $\chi^2/\text{d.o.f.}$ with respect to zero is determined to be 5.5, whereas the $\chi^2/\text{d.o.f.}$ with respect to the SM prediction is 1.5. Thus parity violation in ep NC DIS at very small distances is demonstrated at scales down to $\sim 10^{-18}$ m. At large Q^2 where the u quark dominates the PDF it is expected that $A^- \simeq 2 a_e v_u e_u / e_u^2 \simeq 0.3$. The cross sections obtained from NC DIS measurements can be used to constrain the NC quark couplings within PDF fits [54], and the polarised electron beam data provide sensitivity to quark vector couplings. Therefore, this measurement is a stringent test of the electroweak sector of the Standard Model.

10 Summary

The cross sections for neutral current deep inelastic scattering in $e^- p$ collisions with a longitudinally polarised electron beam have been measured. The measurements are based on a data sample with an integrated luminosity of $169.9\,\text{pb}^{-1}$ collected with the ZEUS detector at HERA from 2005 to 2006 at a centre-of-mass energy of 318 GeV. The accessible range in Q^2 extended to $Q^2 = 50\,000\,\text{GeV}^2$ and has allowed a stringent test of electroweak effects in the Standard Model.

656

Eur. Phys. J. C (2009) 62: 625–658

Fig. 8 The $e^- p$ NC DIS cross section $d\sigma/dQ^2$ for (**a**) positive and (**b**) negative polarisation. The *inset* shows the ratio to the SM prediction. The *closed circles* represent the ZEUS data. The *inner error bars* show the statistical uncertainty while the *outer bars* show the statistical and systematic uncertainties added in quadrature. The *curves* show the predictions of the SM evaluated using the ZEUS-JETS PDFs
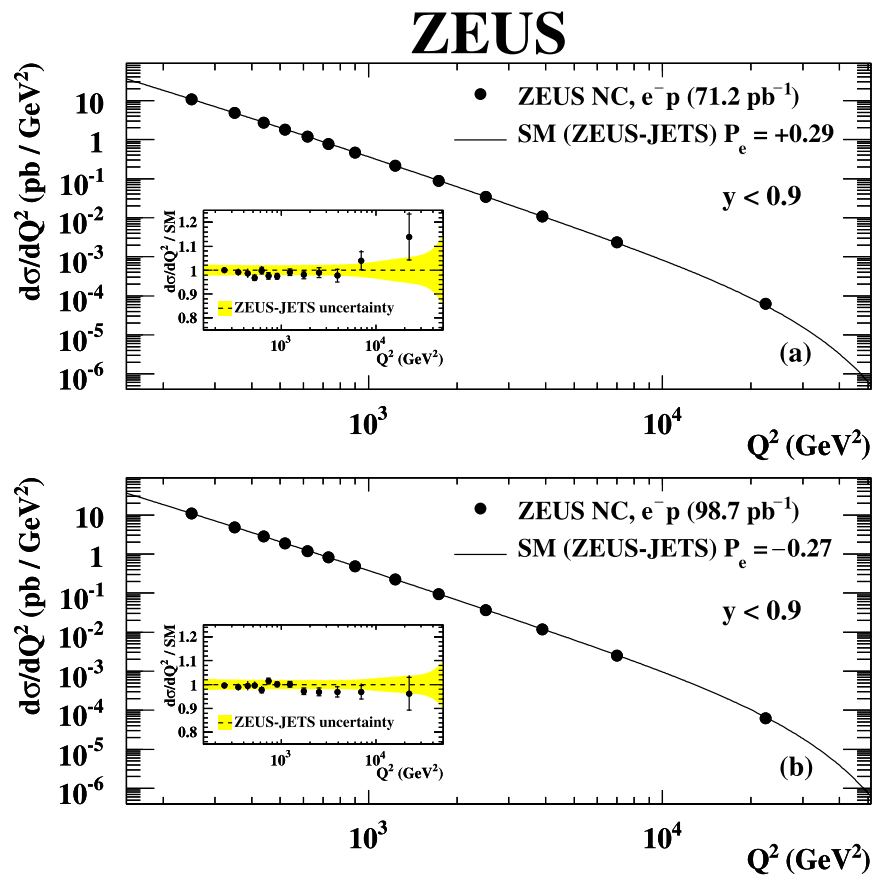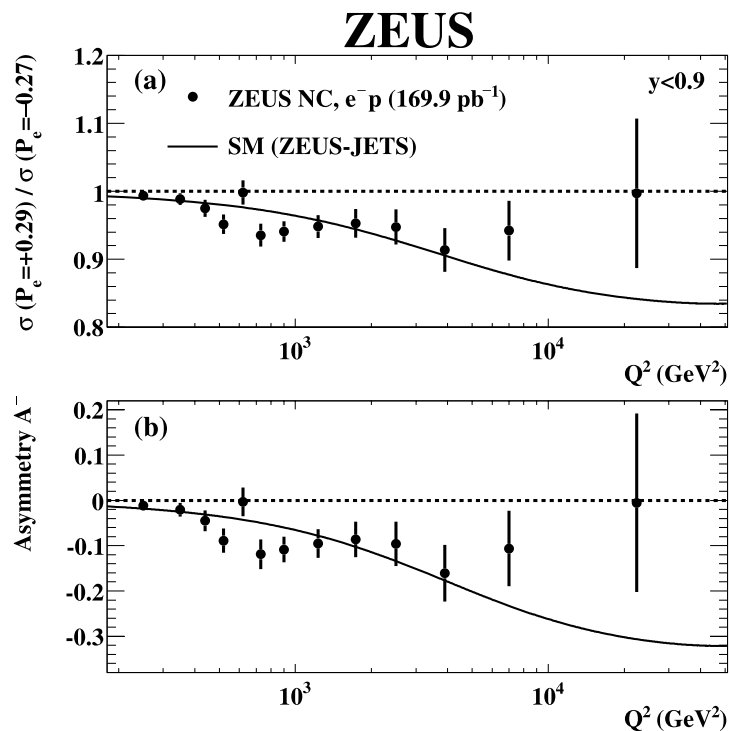

Fig. 9 The ratio of $d\sigma/dQ^2$ using positive and negative polarisation in (**a**), and the polarisation asymmetry A^- as a function of Q^2 in (**b**). The *closed circles* represent ZEUS data. Only statistical uncertainties are considered as the systematic uncertainties are assumed to cancel. The *curves* show the predictions of the SM evaluated using the ZEUS-JETS PDFs

The single-differential cross-sections with respect to Q^2, x and y are presented for $Q^2 > 185\,\text{GeV}^2$ and $y < 0.9$, where the data obtained with negatively and positively po-larised beams are combined. The cross sections $d\sigma/dx$ and $d\sigma/dy$ are also measured for $Q^2 > 3\,000\,\text{GeV}^2$ and $y < 0.9$. The reduced cross sections are measured in the kinematic

Eur. Phys. J. C (2009) 62: 625–658

657

Table 17 The single differential cross section $d\sigma/dQ^2$ ($y < 0.9$) for the reaction $e^-p \rightarrow e^-X$ ($\mathcal{L} = 98.7\,\mathrm{pb}^{-1}$, $P_e = -0.27$). The bin range, bin centre (Q_c^2) and measured cross section corrected to the electroweak Born level are shown. The first (second) error on the cross section corresponds to the statistical (systematic) uncertainties. The number of observed data events (N_{data}) and simulated background events ($N_{\mathrm{bg}}^{\mathrm{MC}}$) are also shown

Q^2 range (GeV^2)	Q_c^2 (GeV^2)	$d\sigma/dQ^2$ (pb/ GeV^2)	N_{data}	$N_{\mathrm{bg}}^{\mathrm{MC}}$
185.0– 300.0	250	$(1.08 \pm 0.00^{+0.01}_{-0.01}) \times 10^1$	103254	146.9
300.0– 400.0	350	$4.83 \pm 0.03^{+0.07}_{-0.06}$	35547	80.0
400.0– 475.7	440	$2.80 \pm 0.02^{+0.05}_{-0.05}$	15291	47.0
475.7– 565.7	520	$1.87 \pm 0.02^{+0.02}_{-0.02}$	11190	42.4
565.7– 672.7	620	$1.19 \pm 0.01^{+0.02}_{-0.01}$	7926	45.0
672.7– 800.0	730	$(8.30 \pm 0.10^{+0.07}_{-0.06}) \times 10^{-1}$	7719	24.7
800.0– 1050.0	900	$(4.89 \pm 0.05^{+0.05}_{-0.04}) \times 10^{-1}$	10094	51.1
1050.0– 1460.0	1230	$(2.25 \pm 0.03^{+0.02}_{-0.02}) \times 10^{-1}$	8111	53.7
1460.0– 2080.0	1730	$(9.25 \pm 0.13^{+0.05}_{-0.05}) \times 10^{-2}$	5158	32.7
2080.0– 3120.0	2500	$(3.61 \pm 0.06^{+0.03}_{-0.02}) \times 10^{-2}$	3314	19.4
3120.0– 5220.0	3900	$(1.16 \pm 0.03^{+0.02}_{-0.01}) \times 10^{-2}$	2065	6.0
5220.0–12500.0	7000	$(2.48 \pm 0.07^{+0.06}_{-0.02}) \times 10^{-3}$	1143	5.0
12500.0–51200.0	22400	$(6.26 \pm 0.45^{+0.23}_{-0.14}) \times 10^{-5}$	200	2.6

Table 18 Systematic uncertainties with bin-to-bin correlations for $d\sigma/dQ^2$ ($y < 0.9$) for the reaction $e^-p \rightarrow e^-X$ ($\mathcal{L} = 98.7\,\mathrm{pb}^{-1}$, $P_e = -0.27$). The left four columns of the table contain the bin centre (Q_c^2), the measured cross section, the statistical uncertainty and the total systematic uncertainty. The right eight columns of the table list the bin-to-bin correlated systematic uncertainties for δ_1–δ_7, and the total systematic uncertainties summed in quadrature for δ_8–δ_{13}, as defined in Sect. 8. The upper and lower correlated uncertainties correspond to a positive or negative variation of a cut value for example. However, if this is not possible for a particular systematic, the uncertainty is symmetrised

Q_c^2 (GeV^2)	$d\sigma/dQ^2$ (pb/ GeV^2)	stat. (%)	sys. (%)	δ_1 (%)	δ_2 (%)	δ_3 (%)	δ_4 (%)	δ_5 (%)	δ_6 (%)	δ_7 (%)	δ_8–δ_{13} (%)
250	1.08×10^1	± 0.3	$^{+1.2}_{-1.1}$	$^{+0.3}_{-0.0}$	$^{-0.5}_{+0.6}$	$^{+0.5}_{-0.5}$	$^{+0.4}_{-0.4}$	$^{-0.1}_{+0.2}$	$^{-0.0}_{+0.2}$	$^{+0.1}_{-0.1}$	$^{+0.7}_{-0.8}$
350	4.83	± 0.6	$^{+1.5}_{-1.1}$	$^{+0.8}_{-0.0}$	$^{-0.5}_{+0.7}$	$^{+0.5}_{-0.5}$	$^{+0.6}_{-0.6}$	$^{-0.0}_{+0.2}$	$^{-0.2}_{+0.2}$	$^{+0.1}_{-0.1}$	$^{+0.6}_{-0.6}$
440	2.80	± 0.8	$^{+1.8}_{-1.7}$	$^{+0.3}_{-0.0}$	$^{-0.5}_{+0.6}$	$^{+0.5}_{-0.5}$	$^{+1.3}_{-1.3}$	$^{-0.2}_{+0.2}$	$^{-0.4}_{+0.7}$	$^{+0.1}_{-0.1}$	$^{+0.6}_{-0.6}$
520	1.87	± 1.0	$^{+1.3}_{-0.9}$	$^{+0.7}_{-0.1}$	$^{-0.5}_{+0.7}$	$^{+0.0}_{-0.0}$	$^{+0.1}_{-0.1}$	$^{-0.1}_{+0.2}$	$^{-0.2}_{+0.3}$	$^{+0.2}_{-0.2}$	$^{+0.7}_{-0.7}$
620	1.19	± 1.1	$^{+1.4}_{-1.0}$	$^{+0.9}_{-0.1}$	$^{-0.6}_{+0.7}$	$^{+0.2}_{-0.2}$	$^{-0.6}_{+0.6}$	$^{-0.1}_{-0.0}$	$^{+0.1}_{+0.2}$	$^{+0.2}_{-0.2}$	$^{+0.4}_{-0.5}$
730	8.30×10^{-1}	± 1.2	$^{+0.8}_{-0.7}$	$^{+0.0}_{-0.2}$	$^{-0.5}_{+0.6}$	$^{+0.3}_{-0.3}$	$^{+0.1}_{-0.1}$	$^{+0.2}_{+0.1}$	$^{+0.1}_{-0.1}$	$^{+0.1}_{-0.1}$	$^{+0.2}_{-0.3}$
900	4.89×10^{-1}	± 1.0	$^{+0.9}_{-0.8}$	$^{+0.1}_{-0.0}$	$^{-0.4}_{+0.5}$	$^{-0.2}_{+0.2}$	$^{+0.6}_{-0.6}$	$^{+0.1}_{-0.1}$	$^{-0.0}_{-0.0}$	$^{+0.2}_{-0.2}$	$^{+0.3}_{-0.3}$
1230	2.25×10^{-1}	± 1.1	$^{+0.7}_{-0.7}$	$^{+0.1}_{-0.0}$	$^{-0.3}_{+0.4}$	$^{+0.3}_{-0.3}$	$^{-0.1}_{+0.1}$	$^{+0.0}_{+0.1}$	$^{-0.0}_{-0.3}$	$^{+0.3}_{-0.3}$	$^{+0.3}_{-0.4}$
1730	9.25×10^{-2}	± 1.4	$^{+0.6}_{-0.5}$	$^{+0.2}_{-0.0}$	$^{-0.3}_{+0.3}$	$^{+0.1}_{-0.1}$	$^{+0.0}_{-0.0}$	$^{+0.2}_{-0.0}$	$^{-0.2}_{-0.1}$	$^{+0.3}_{-0.3}$	$^{+0.3}_{-0.3}$
2500	3.61×10^{-2}	± 1.8	$^{+0.9}_{-0.6}$	$^{+0.4}_{-0.0}$	$^{-0.2}_{+0.3}$	$^{+0.3}_{-0.3}$	$^{+0.2}_{-0.2}$	$^{-0.1}_{-0.0}$	$^{+0.3}_{+0.1}$	$^{+0.3}_{-0.2}$	$^{+0.3}_{-0.3}$
3900	1.16×10^{-2}	± 2.2	$^{+1.3}_{-0.6}$	$^{+1.2}_{-0.1}$	$^{-0.2}_{+0.3}$	$^{-0.4}_{+0.4}$	$^{-0.1}_{+0.1}$	$^{-0.0}_{-0.0}$	$^{-0.2}_{-0.1}$	$^{+0.1}_{-0.1}$	$^{+0.3}_{-0.3}$
7000	2.48×10^{-3}	± 3.0	$^{+2.3}_{-0.6}$	$^{+2.2}_{-0.0}$	$^{-0.3}_{+0.3}$	$^{-0.0}_{+0.0}$	$^{+0.1}_{-0.1}$	$^{+0.0}_{+0.0}$	$^{-0.3}_{+0.1}$	$^{+0.5}_{-0.2}$	$^{+0.3}_{-0.4}$
22400	6.26×10^{-5}	± 7.2	$^{+3.7}_{-2.3}$	$^{+3.4}_{-0.4}$	$^{-0.7}_{+0.3}$	$^{-1.0}_{+1.0}$	$^{+0.7}_{-0.7}$	$^{+0.0}_{+0.0}$	$^{-1.0}_{-1.6}$	$^{+0.5}_{-0.5}$	$^{+0.6}_{-0.6}$

range $200 < Q^2 < 30\,000\,\mathrm{GeV}^2$ and $0.005 < x < 0.65$ at zero polarisation by correcting the residual polarisation of the combined data sample. These measurements are combined with previously measured e^+p neutral current cross sections to extract $x\tilde{F}_3$. In addition, the interference structure function $xF_3^{\gamma Z}$ is extracted at an average value of $Q^2 = 5\,000\,\mathrm{GeV}^2$.

The reduced cross-sections and the single-differential cross-section $d\sigma/dQ^2$ have also been measured separately for positive and negative values of the longitudinal polarisation of the electron beam. Parity violation is observed through the polarisation asymmetry A^-. The measured cross sections confirm the predictions of the Standard Model and provide strong constraints at the electroweak scale.

Table 19 The polarisation asymmetry measured using positively and negatively polarised e^-p beams ($\mathcal{L} = 71.2\,\text{pb}^{-1}$, $P_e = +0.29$ and $\mathcal{L} = 98.7\,\text{pb}^{-1}$, $P_e = -0.27$, respectively). The bin range, bin centre (Q_c^2) and measured Asymmetry A^- are shown. Only the statistical uncertainties on the measurement are shown as systematic uncertainties are assumed to cancel

Q^2 range (GeV^2)	Q_c^2 (GeV^2)	Asymmetry $A^- \times 10$
185.0– 300.0	250	-0.11 ± 0.09
300.0– 400.0	350	-0.21 ± 0.15
400.0– 475.7	440	-0.45 ± 0.23
475.7– 565.7	520	-0.89 ± 0.27
565.7– 672.7	620	-0.03 ± 0.32
672.7– 800.0	730	-1.19 ± 0.32
800.0– 1050.0	900	-1.09 ± 0.28
1050.0– 1460.0	1230	-0.95 ± 0.32
1460.0– 2080.0	1730	-0.86 ± 0.39
2080.0– 3120.0	2500	-0.96 ± 0.49
3120.0– 5220.0	3900	-1.61 ± 0.63
5220.0–12500.0	7000	-1.06 ± 0.83
12500.0–51200.0	22400	-0.06 ± 1.97

References

1. J. Breitweg et al. (ZEUS Collaboration), Eur. Phys. J. C **11**, 427 (1999)
2. S. Chekanov et al. (ZEUS Collaboration), Eur. Phys. J. C **21**, 443 (2001)
3. S. Chekanov et al. (ZEUS Collaboration), Eur. Phys. J. C **28**, 175 (2003)
4. S. Chekanov et al. (ZEUS Collaboration), Phys. Rev. D **70**, 052001 (2004)
5. S. Aid et al. (H1 Collaboration), Nucl. Phys. B **470**, 3 (1996)
6. C. Adloff et al. (H1 Collaboration), Nucl. Phys. B **497**, 3 (1997)
7. C. Adloff et al. (H1 Collaboration), Eur. Phys. J. C **13**, 609 (2000)
8. C. Adloff et al. (H1 Collaboration), Eur. Phys. J. C **21**, 33 (2001)
9. C. Adloff et al. (H1 Collaboration), Eur. Phys. J. C **19**, 269 (2001)
10. C. Adloff et al. (H1 Collaboration), Eur. Phys. J. C **30**, 1 (2003)
11. S. Chekanov et al. (ZEUS Collaboration), Phys. Lett. B **637**, 210 (2006)
12. R. Devenish, A. Cooper-Sarkar, *Deep Inelastic Scattering* (Oxford University Press, Oxford, 2003)
13. M. Klein, T. Riemann, Z. Phys. C **24**, 151 (1984)
14. E. Rizvi, T. Sloan, Eur. Phys. J. C Direct C **2**, 1 (2001). doi:10.1007/s1010501c00N2
15. U. Holm, (ZEUS Collaboration), (eds.), The ZEUS Detector. Status Report (unpublished), DESY, 1993. Available on http://www-zeus.desy.de/bluebook/bluebook.html
16. N. Harnew et al., Nucl. Instrum. Methods A **279**, 290 (1989)
17. B. Foster et al., Nucl. Phys. Proc. Suppl. B **32**, 181 (1993)
18. B. Foster et al., Nucl. Instrum. Methods A **338**, 254 (1994)
19. A. Polini et al., Nucl. Instrum. Methods A **581**, 656 (2007)
20. M. Derrick et al., Nucl. Instrum. Methods A **309**, 77 (1991)
21. A. Andersen et al., Nucl. Instrum. Methods A **309**, 101 (1991)
22. A. Caldwell et al., Nucl. Instrum. Methods A **321**, 356 (1992)
23. A. Bernstein et al., Nucl. Instrum. Methods A **336**, 23 (1993)
24. H. Abramowicz et al., Nucl. Instrum. Methods A **313**, 126 (1992)
25. G. Abbiendi et al., Nucl. Instrum. Methods A **333**, 342 (1993)
26. A.A. Sokolov, I.M. Ternov, Sov. Phys. Dokl. **8**, 1203 (1964)
27. V.N. Baier, V.A. Khoze, Sov. J. Nucl. Phys. **238** (1969)
28. D.P. Barber et al., Nucl. Instrum. Methods A **329**, 79 (1993)
29. M. Beckmann et al., Nucl. Instrum. Methods A **479**, 334 (2002)
30. A. Kwiatkowski, H. Spiesberger, H.-J. Möhring, Comp. Phys. Comm. **69**, 155 (1992). Also in *Proc. Workshop Physics at HERA*, ed. by W. Buchmüller, G. Ingelman (DESY, Hamburg, 1991)
31. G.A. Schuler, H. Spiesberger, in *Proc. Workshop on Physics at HERA*, ed. by W. Buchmüller, G. Ingelman, vol. 3 (DESY, Hamburg, 1991), p. 1419
32. H. Spiesberger, HERACLES and DJANGOH: Event Generation of *ep* Interactions at HERA Including Radiative Processes, 2005. Available on http://wwwthep.physik.uni-mainz.de/~hspiesb/djangoh/djangoh.html
33. H.L. Lai et al. (CTEQ Collaboration), Eur. Phys. J. C **12**, 375 (2000)
34. L. Lönnblad, Comput. Phys. Commun. **71**, 15 (1992)
35. G. Ingelman, A. Edin, J. Rathsman, Comput. Phys. Commun. **101**, 108 (1997)
36. T. Sjöstrand, Comput. Phys. Commun. **39**, 347 (1986)
37. T. Sjöstrand, M. Bengtsson, Comput. Phys. Commun. **43**, 367 (1987)
38. T. Sjöstrand, Comput. Phys. Commun. **82**, 74 (1994)
39. H. Jung, Comput. Phys. Commun. **86**, 147 (1995)
40. G. Marchesini et al., Comput. Phys. Commun. **67**, 465 (1992)
41. R. Brun et al., GEANT3, Technical Report CERN-DD/EE/84-1, CERN, 1987
42. S.U. Noor, Measurement of neutral current electron-proton cross sections with longitudinally polarised electrons using the ZEUS detector. PhD thesis, York University, 2007. Available on http://www-zeus.desy.de/physics/exo/ZEUS_PUBLIC/theses.php
43. S. Bentvelsen, J. Engelen, P. Kooijman, in *Proc. Workshop on Physics at HERA*, vol. 1 ed. by W. Buchmüller, G. Ingelman, (DESY, Hamburg, 1992), p. 23
44. K.C. Höger, in *Proc. Workshop on Physics at HERA*, ed. by W. Buchmüller, G. Ingelman, vol. 1 (DESY, Hamburg, 1992), p. 43
45. F. Jacquet, A. Blondel, in *Proceedings of the Study for an ep Facility for Europe*, ed. by U. Amaldi, (Hamburg, 1979) p. 391. Also in preprint DESY 79/48
46. W.H. Smith, K. Tokushuku, L.W. Wiggers, in *Proc. Computing in High-Energy Physics (CHEP), Annecy, France, Sept. 1992*, ed. by C. Verkerk, W. Wojcik (CERN, Geneva, 1992), p. 222. Also in preprint DESY 92-150B
47. P. Allfrey et al., Nucl. Instrum. Methods A **580**, 1257 (2007)
48. D.E. Groom et al. (Particle Data Group), Eur. Phys. J. C **15**, 1 (2000)
49. H. Abramowicz, A. Caldwell, R. Sinkus, Nucl. Instrum. Methods A **365**, 508 (1995)
50. S. Chekanov et al. (ZEUS Collaboration), Eur. Phys. J. C **42**, 1 (2005)
51. A. Argento et al. (BCDMS Collaboration), Phys. Lett. B **140**, 142 (1984)
52. P.M. Nadolsky et al., Phys. Rev. D **78**, 013004 (2008)
53. A.D. Martin et al., hep-ph/090100002
54. S. Shimizu, in *Proc. 14th Int. Workshop on Deep Inelastic Scattering (DIS2006)*, Tsukuba, Japan, April 2006, ed. by M. Kuze, K. Nagano, K. Tokushuku (World Scientific, Singapore, 2006), pp. 145–148